

Romanian Journal of MINERAL DEPOSITS

continuation of

DARI DE SEAMA ALE SEDINTELOR INSTITUTULUI DE GEOLOGIE SI GEOFIZICA
COMPTES RENDUS DES SÉANCES DE L'INSTITUT DE GÉOLOGIE ET GÉOPHYSIQUE
(2. Zacaminte)

Founded 1910 by the Geological Institute of Romania

ISSN 1220-5648

VOL. 92
No. 1-2

CONTENT

	<i>page</i>
Paulo A. ARANHA, Adolf H. HORN, Wallace M. TRINDADE GPR supported sampling for environmental purposes. Examples from the Rio São Francisco marginal lagoons, Minas Gerais, Brazil	1
Ioan PINTEA, Sorin Silviu UDUBAŞA, Elena Luisa IATAN, Ion BERBELEAC, Daniel BÎRGĂOANU, Oana Claudia CIOBOTEA-BARBU, Eduard GHINESCU Microthermometry and Raman spectroscopy of fluid and melt inclusions in the alpine porphyry copper deposits from Romania: insights on micrometallogeny	9
Iulia NEGREA, Gheorghe C. POPESCU, Monica MACOVEI, Eduard GHINESCU Spherulites from Letea beach ridge – Danube Delta, preliminary data	33
Robert SZABO, Gheorghe C. POPESCU, Eduard GHINESCU Contributions to the mineralogy of the „purple” metamorphic rocks from the north-west flank of Vâlcan Mountains	41
Safaa Abdulhadi Khudhair ALSHAWI, Gheorghe C. POPESCU, Daniela DIMOFTE, Antonela NEACŞU The quantitative and qualitative preliminary evaluation for the heavy minerals of the sand quaternary deposits from the southeastern Iraq region	49
Safaa Abdulhadi Khudhair ALSHAWI, Gheorghe C. POPESCU, Daniela DIMOFTE Overview of heavy minerals study in the south and southwest of Iraq	59



Geological Institute of Romania
Society of Economic Geology of Romania
Bucureşti – 2019



DIRECTORS OF THE JOURNAL

Dr. Ștefan Marincea, General Director of the Geological Institute of Romania

Prof. Dr. Gheorghe Damian, President of the Society of Economic Geology of Romania

Editor in Chief: Sorin Silviu Udubașa (University of Bucharest).

Editorial Secretary: Monica Macovei (University of Bucharest)

Editorial board

Peter Andráš, Matej Bel University, Banská Bystrica, Slovakia

Anne-Sylvie Andre-Mayer, Université de Lorraine, Nancy, France

Andrei Ionut Apopei, "Alexandru Ioan Cuza" University, Iași

Essaid Bilal, Ecole des Mines, Saint Etienne, France

Grigore Buia, University of Petrosani

Andrei Buzatu, "Alexandru Ioan Cuza" University, Iași

Nicolae Buzgar, "Alexandru Ioan Cuza" University, Iași

Georgios Christofides, Aristotle University of Thessaloniki, Greece

Floarea Damian, Technical Univ. Cluj-Napoca – North Center Baia Mare

Gheorghe Damian, Technical Univ. Cluj-Napoca – North Center Baia Mare,

János Földessy, Miskolc University, Hungary

Ovidiu Gabriel Iancu, "Alexandru Ioan Cuza" University, Iași

Gheorghe Ilinca, University of Bucharest

Marian Lupulescu, New York State Museum, USA

Mihai Marinescu, University of Bucharest

Marcel Mărunțiu, Geological Institute of Romania

Vasilios Melfos, Aristotle University of Thessaloniki, Greece

Ferenc Molnar, Geological Survey of Finland

Marian Munteanu, Geological Institute of Romania

Antonela Neacsu, University of Bucharest

Bogdan Niculescu, University of Bucharest

M.S. Pandian, Pondicherry University, India

Lucian Petrescu, University of Bucharest

Ioan Pintea, Geological Institute of Romania

Gheorghe C. Popescu, University of Bucharest

Relu Roban, University of Bucharest

Ioan Seghedi, Institute of Geodynamics of the Romanian Academy, Bucharest

Dan Stumbea, "Alexandru Ioan Cuza" University, Iași

Călin Tămaș, Babeș-Bolyai University, Cluj-Napoca

George Tudor, Geological Institute of Romania

Mircea Țicleanu, Geological Institute of Romania

Sorin Silviu Udubașa, University of Bucharest

Rom. J. Mineral Deposits is also the Bulletin of the **Society of Economic Geology of Romania**.

The authors are responsible for the ideas presented in the papers.

ISSN 1220-5648



Geological Institute of Romania
Society of Economic Geology of Romania



Romanian Journal of MINERAL DEPOSITS

ISSN 1220-5648

VOL. 92
No. 1-2

2019

CONTENT

- Paulo A. ARANHA, Adolf H. HORN, Wallace M. TRINDADE**
GPR supported sampling for environmental purposes. Examples from the Rio São Francisco marginal lagoons, Minas Gerais, Brazil 1
- Ioan PINTEA, Sorin Silviu UDUBAȘA, Elena Luisa IATAN, Ion BERBELEAC, Daniel BÎRGĂOANU, Oana Claudia CIOBOTEA-BARBU, Eduard GHINESCU**
Microthermometry and Raman spectroscopy of fluid and melt inclusions in the alpine porphyry copper deposits from Romania: insights on micrometallogeny 9
- Iulia NEGREA, Gheorghe C. POPESCU, Monica MACOVEI, Eduard GHINESCU**
Spherulites from Letea beach ridge – Danube Delta, preliminary data 33
- Robert SZABO, Gheorghe C. POPESCU, Eduard GHINESCU**
Contributions to the mineralogy of the „purple” metamorphic rocks from the north-west flank of Vâlcan Mountains 41
- Safaa Abdulhadi Khudhair ALSHAWI, Gheorghe C. POPESCU, Daniela DIMOFTE, Antonela NEACȘU**
The quantitative and qualitative preliminary evaluation for the heavy minerals of the sand quaternary deposits from the southeastern Iraq region 49
- Safaa Abdulhadi Khudhair ALSHAWI, Gheorghe C. POPESCU, Daniela DIMOFTE**
Overview of heavy minerals study in the south and southwest of Iraq 59

GPR SUPPORTED SAMPLING FOR ENVIRONMENTAL PURPOSES. EXAMPLES FROM THE RIO SÃO FRANCISCO MARGINAL LAGOONS, MINAS GERAIS, BRAZIL

Paulo A. ARANHA¹, Adolf H. HORN^{1*}, Wallace M. TRINDADE²

¹Federal University of Minas Gerais; Belo Horizonte, Brazil; *aranha1941@gmail.com*

¹Federal University of Minas Gerais; Belo Horizonte, Brazil; **hahorn@ufmg.br*; Tel.: +55 31 34417505; Fax: +55 31 3409 5410

²Federal Institute of Minas Gerais, Pirapora, Brazil; *wallace.trindade@ifmg.edu.br*

Abstract: The human occupation of the San Francisco basin results in an increase of the impacts. Marginal lagoons are filled during the flooding of the river, together with wind transport, rain washout and interaction with subsurface water with sedimental material. Therefore, marginal lagoons are important for the knowledge of the evolution of a river system. To obtain representative profile sampling it is necessary to know the geological and dynamical situation of the lagoons. To obtain information about sediment distribution and structures, GPR-profiles on the lagoons are an adequate technique for rapid and exact results and permit to find easily appropriate locations for sampling. The obtained samples show a very good correlation with GPR results and permit an evaluation of the history of the lagoons. It was able to obtain information about climate variations, like rainfall, wind directions, insolation and temperature evolution, and anthropogenic influence shown by chemical alteration of the sediment composition permitting to determine the evolution of different sources, industrial or agronomical.

Keywords: GPR, San Francisco River, marginal lagoons, anthropogenic influence, contamination.

1. Introduction

Marginal lagoons are lake environments of periodic or permanent flooding resulting from the overflow of the rivers, which receive contributions from direct rainfall or underground water (Junk, 1989). These lagoons are considered wetlands and are playing an important ecological and hydrodynamic role in a river basin system.

In the upper to middle course of the San Francisco River Basin (Patrus et al., 2001), these lagoons are responsible for breeding and restocking of migratory fish (Pompeu, 1997; Pompeu and Godinho, 2003). From a hydrodynamic point of view, these marginal lagoons are elongated depressions usually towards the river channel that, like the flood plains, reduce the kinetic energy of the flood pulses, acting as areas of sediment deposition and retention (Wolman and Leopold 1957; Junk, 1989; Gama, 2006).

The particle size and mineral composition, the stratigraphic organization and the chemical composition of these sediments deposited in lagoons are important records of river hydrodynamics, climate changes and the entry of contaminants in drainage area (Godoy et al., 1998; Argollo, 2001; Nery, 2009).

Agricultural activities and industrial processes are using a growing number of chemical compounds to enhance the quality and quantity of production in various industrial processes or as micronutrients and pesticides in agriculture. Many of them have elevated toxicity in excess and their cumulative effects might affect the quality of natural resources and human health (Malavolta 1989; Duffus 2002).

To evaluate this contamination, its changes in quality and quantity, representative sampling is absolutely necessary. To see how the marginal lagoons reflect the chemical and environmental evolution of a basin, we need to find the best place for sampling. The use of ground-penetrating radar (GPR) is a good method to find the localities with the greatest amount of sediments and with the best properties for analyses.

This work will show the connection between GPR profiles and the data which can be extracted from the drill samples, localized by this geophysical method.

2. Regional setting

The study area is located in the surroundings of Pirapora city in the upper to middle course of São Francisco River, in the Northern part of Minas Gerais State (Fig. 1).

In this area of the basin, a large number of marginal lagoons exists in the floodplain, where the São Francisco River in the periods of floods reaches an average width of 4 km. Some of these marginal lagoons were selected for this study (Fig. 2).

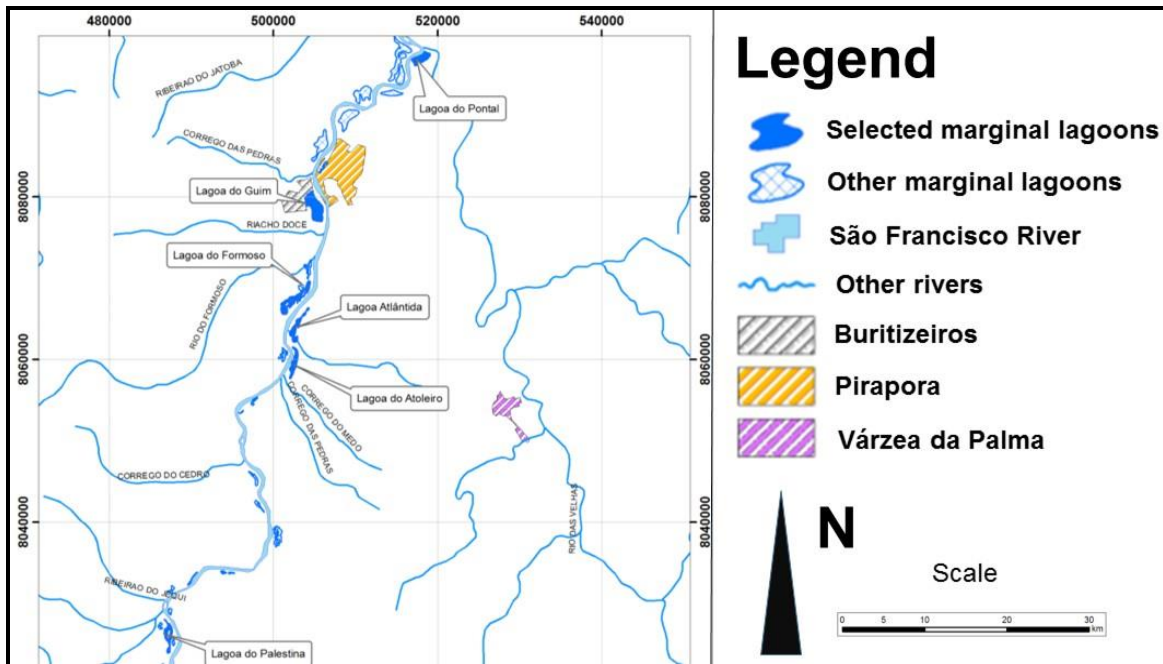


Fig. 1. Location map of the studied area with the selected lagoons.

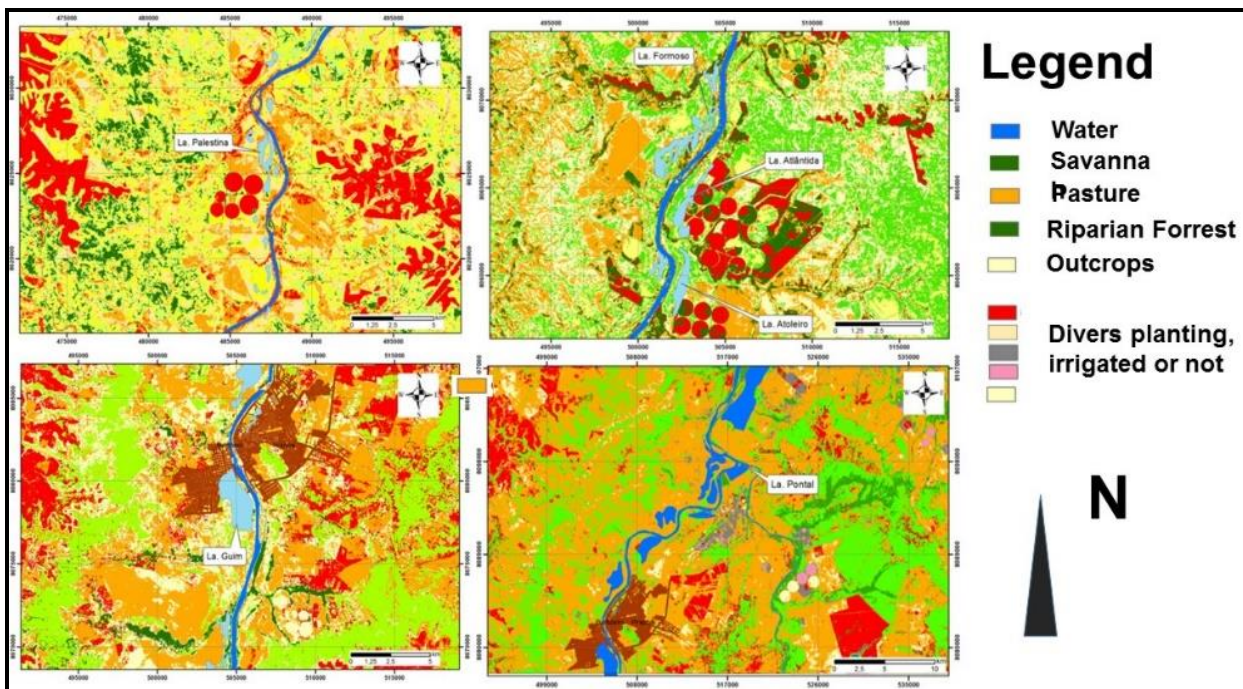


Fig.2. Geological situation of the investigated lagoons.

3. Situation of the studied area

The study area belongs to the Sanfranciscana basin of Neoproterozoic age, formed by Três Marias Formation of the Bambuí Group, and covered by Mesozoic and Cenozoic sediments, composed by conglomerates, iron-rich lateritic deposits and other clastic sediments.

In the river plain, dystrophic alics soils mainly occur from the borders, in the form of alicic or fluvic neosols, poorly developed eutrophic, and not discriminated planosols (Baggio, 2002).

Semi deciduous seasonal-, semi deciduous permanent forests, savannas, pioneer formations, sometimes substituted by anthropogenic forests and the agricultural systems can be observed, according to IEF (2005).

Based on the Köppen classification, the climate is of Aw- type, tropical rainy, hot, humid with dry winter and rainy summer. It is characterized by the average temperature of the coldest month always higher than 18°C (CPRM, 2001; Patrus et al., 2001).

The natural landscape has been greatly modified by the replacement of native vegetation, and the installation of the industry in urban centers. From the Decade of 1970, there was a significant increase in the urban population. From 1990 a diversification and intensification of the land use and occupation were registered with the introduction of the monocultures of soy, corn and coffee in rural areas and the arrival of the textile industries in the industrial district of Pirapora (Baggio, 2002), causing an increase of contaminants in the water and sediments of the basin (Ribeiro et al., 2012).

4. Material and methods

4.1. Sampling and preparation

The selected marginal lagoons were investigated (Fig. 2), geographically separated and associated with different land uses and occupations. These are located upstream and downstream of the Pirapora city.

4.1.2. GPR profiling

The GPR profiles were obtained using a Mala/Ramac equipment with antennas of 100 MHz and the following parameters: common offset, horizontal steps: 0,1m; stacks: 8; time window: 400ns. All profiles were obtained perpendicular to the lagoon direction.

These profiles were processed using the program Gradix (DOS version), and the sections were plotted on EPS extension. The velocity was obtained by a CMP profile acquired in each area. We interpreted the radargrams based on the reflection patterns, the continuity and interruptions of the reflector (Fig. 3).

4.1.3. Sample drilling

The samples were collected from the boreholes along profiles oriented by GPR results, using a percussion-coring rig, which allowed the extraction of the control sample with good preservation of the sedimentary layers (Fig. 3).

In the Lagoon I, for example, the sampling reached a depth of 350 cm and was subdivided into 14 layers. The material was sealed in plastic bags and transported in coolers under low-temperature conditions. The samples were stored at 4°C until analyzed. Then the samples were dried at 120°C, sieved, and the particle size fraction <0.164µm was used for chemical analyses.

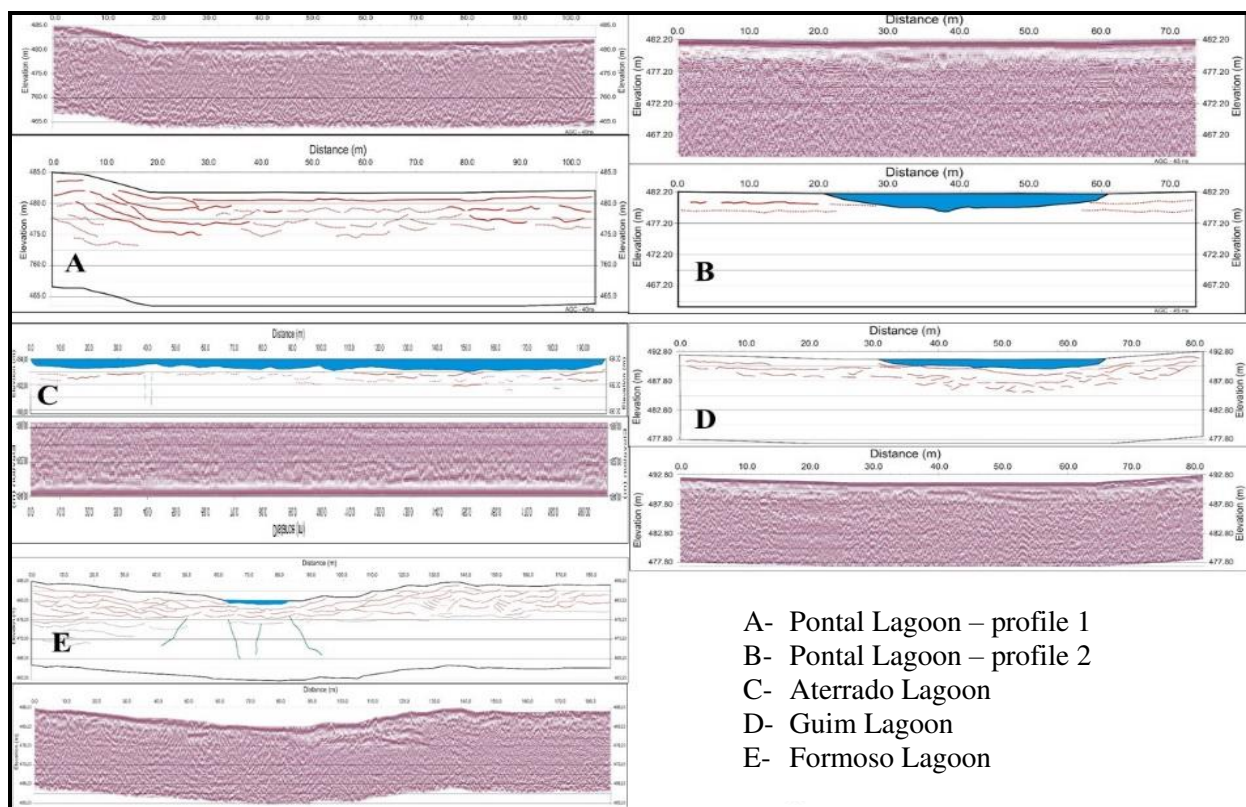


Fig. 3. GPR-profiles executed at the best localities in every marginal lagoon.

4.2. Analytical Methods

4.2.1. Granulometric investigations

The granulometric fraction <0,2 mm of each layer was examined in a particle Analyzer Sympatec Laser System-Partikel-Technik H2387 model using the method of X-ray diffractometry with detection ranges between 0.2 and 2000 μm and classified according to the scale of Wentworth (1922). The samples were dried at 120°C, sieved, and the particle size fraction <0.164 μm was used for chemical analyses.

The results of particle size distribution and elemental concentrations were organized in profiles, using the STRATER 3.0 software, correlated with GPR profiles, and evaluated using the STATPLUS pro 9.0 software for calculating minimum, maximum, average, mean and standard deviation.

4.2.2. Chemical investigations

Analytical investigation of the selected elements (Cr, Ni, Cu, Zn, Cd, Pb, Co and As) were done by using XRF, ICP-OES techniques. The overall composition of these sediments was done by XRF analyzes of the fine material.

The fine sediment (0.063 mm) was subjected to acid digestion in MARS-CEM microwave, following the method SW-846-3051 – US EPA (US Environmental Protection Agency, 1998). About 0.50 g of the fine fraction of the sediment was digested with 10 ml of concentrated nitric acid (HNO_3) for 10 minutes (ramp time) and temperature stabilization at 180°C and pressure (350 psi) for 4'30" (hold time). The samples were then filtered by cellulose filter (0.45 μm) and analyzed by ICP-OES (Spectroflame from Spectro Analytical Instruments).

5. Results

The GPR investigations executed on selected profiles show for all lagoon different depth of sediment deposition (Fig. 3). With exception of the do Formoso and Aterrado lagoons profiles, no tectonic influence is visible.

The interpretation of the GPR data has shown a chaotic system of deposition and erosion, probably caused by the different events of water transport in the principal riverbed and the contributions from torrential surface water input alternating with dry periods. In the upper part, due to the influence of the Três Marias Lake, the sediment deposition seems to be more homogeneous.

The depth of the profile shows the difference between deposition at the Rio São Francisco and at the confluence between Rio São Francisco and das Velhas River (Fig. 4). At the Guim Lagoon, the particle distribution indicates sedimentation with principally silt and clay due to the regulatory effects of the Três Marias Lake, which retains the sand fraction (after SP02-C14 to SP02-C12).

In the Pontal Lagoon, which is influenced by the two rivers, the sandy fraction early than SP07-C11 was much higher, indicating the lack of regulation of the two rivers and the extensive use of irrigation, which transported fine material to the rivers. The sediment changes before SP07-C11 may indicate changes in the rain volume from the source areas of the rivers (Fig. 4).

The mineral distribution is concordant with the rocks eroded by the rivers (Fig. 4), formed principally by alteration minerals from gneissic-granitic rocks and the arenitic-siltic-clay rocks of the sediment series (Bambuí Group s.l.). The assessment of minerals and the grain size distribution in the sediment profiles can indicate variations in river transport energy (silt and clay), agricultural activities and water level changes (Fig. 4).

The variations in the distribution of selected main and trace elements (Fig. 5) together with mineral distribution and the granulometry profiles allowed to estimate a correlation with natural and anthropogenic events in the basin.

The distribution of the main elements is nearby the same in the two lagoons and reflects the mineralogical composition of the sediments, and high arenite (SiO_2) rich part together with the mica fractions (Fig. 5). The iron oxide shows the oxidant environment of the transport system. Also visible are the changes in chemical composition before SP02-C14. The high TiO_2 tenor is probably a function of the gneissic-granitic basement rich in rutile, anatase, titanite and titanomagnetite.

The profiles show a distribution of the selected element decreasing with profile depth (Fig. 6) and deposition time (Fig. 7). Zn shows a correlation with the fine fraction (Fig. 6) and an increase of values with the industrial activity (Fig. 7). Arsenic may be connected to the period with intensive forestation in the basin and the use of fungicides (Fig. 6 A, B) and industrial production and the increase of the urban region along the Velhas River (Fig. 6 B). The element peaks between SP07-C14 and SP07-C19 are coincident with the building of steel and Si-facilities near Varzeá da Palma and Pirapora.

The generally increased values of the elements, like Cr, Ni, Cu, Cd, Co and As, are correlated with the increase of agricultural activities and the use of fertilizer and with defensives (pesticides).

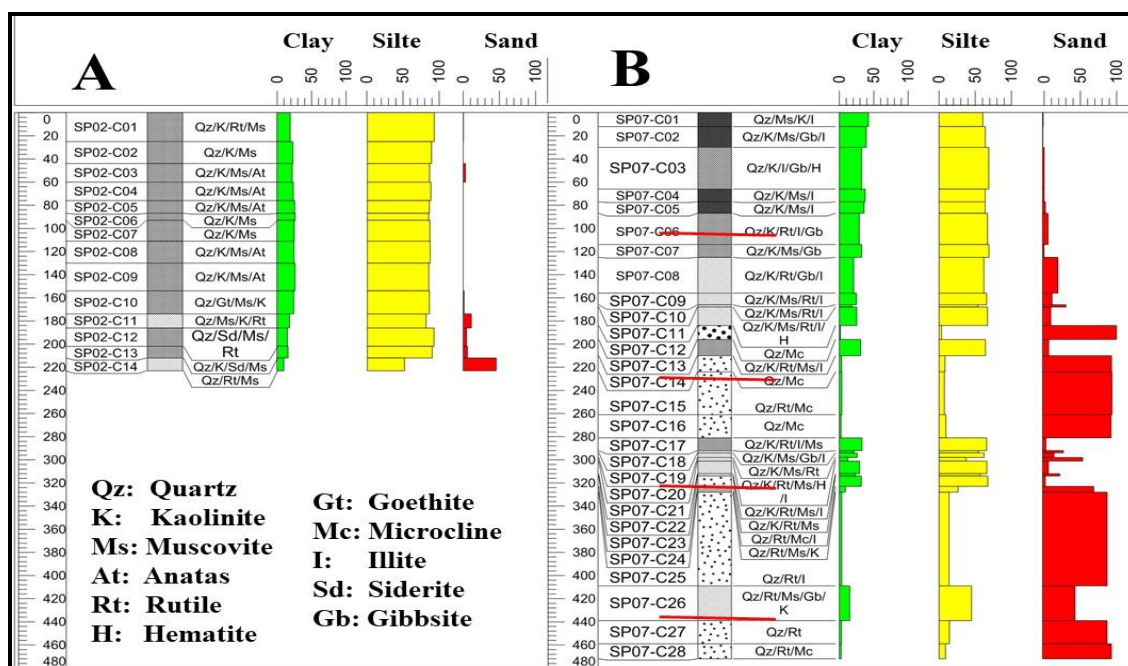


Fig. 4. Mineral and granulometric distribution in the two lagoons and the distribution of high (sand; gravel) and low energy deposition (clay, silt), indicating changes between wet and dry periods. A. Guim Lagoon; B. Pontal Lagoon.

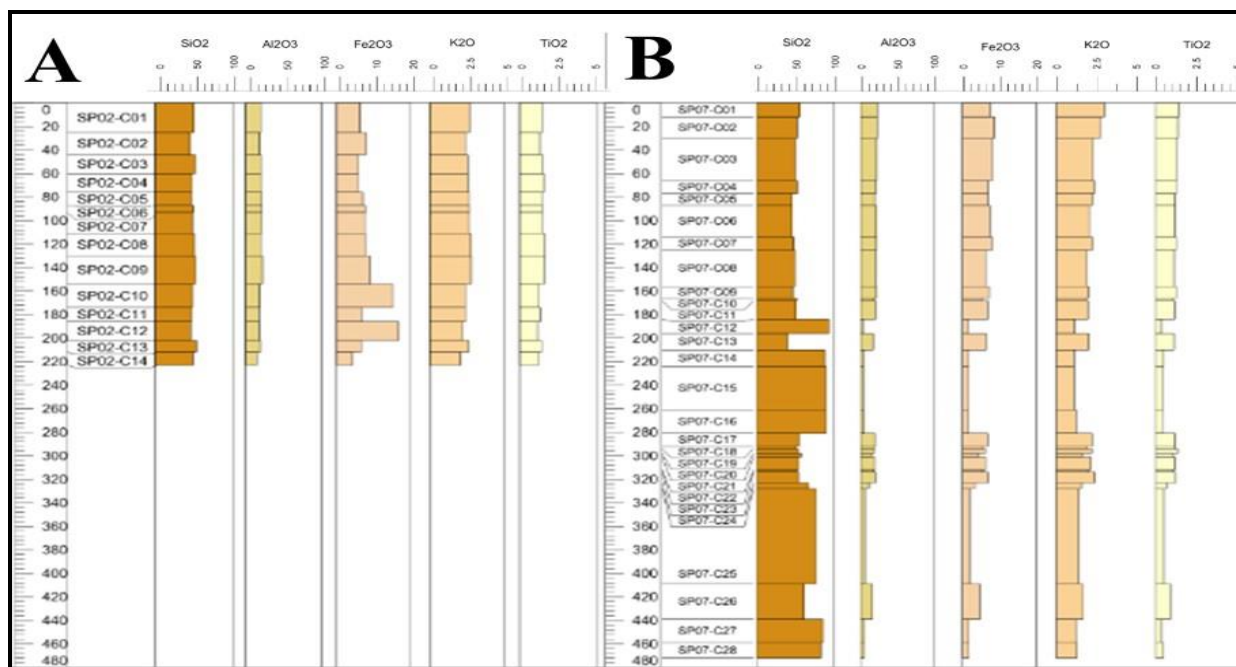


Fig. 5. Main elements distribution in the profiles. A. Guim Lagoon; B. Pontal Lagoon.

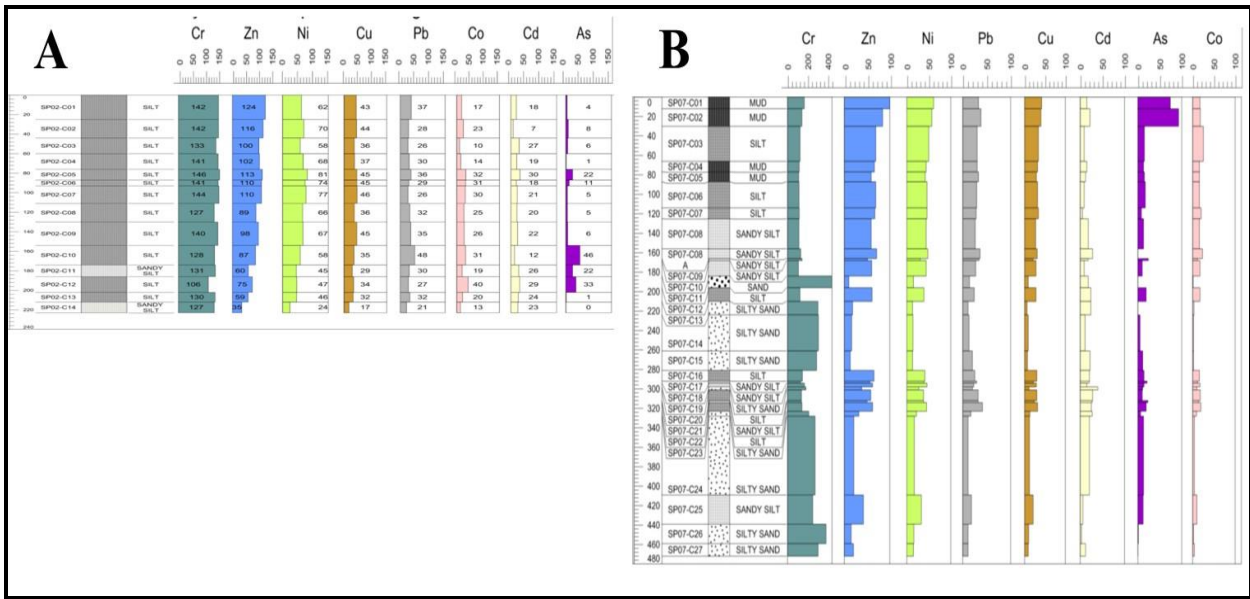


Fig. 6. Trace element distribution in the profiles. A. Guim Lagoon; B. Pontal Lagoon.

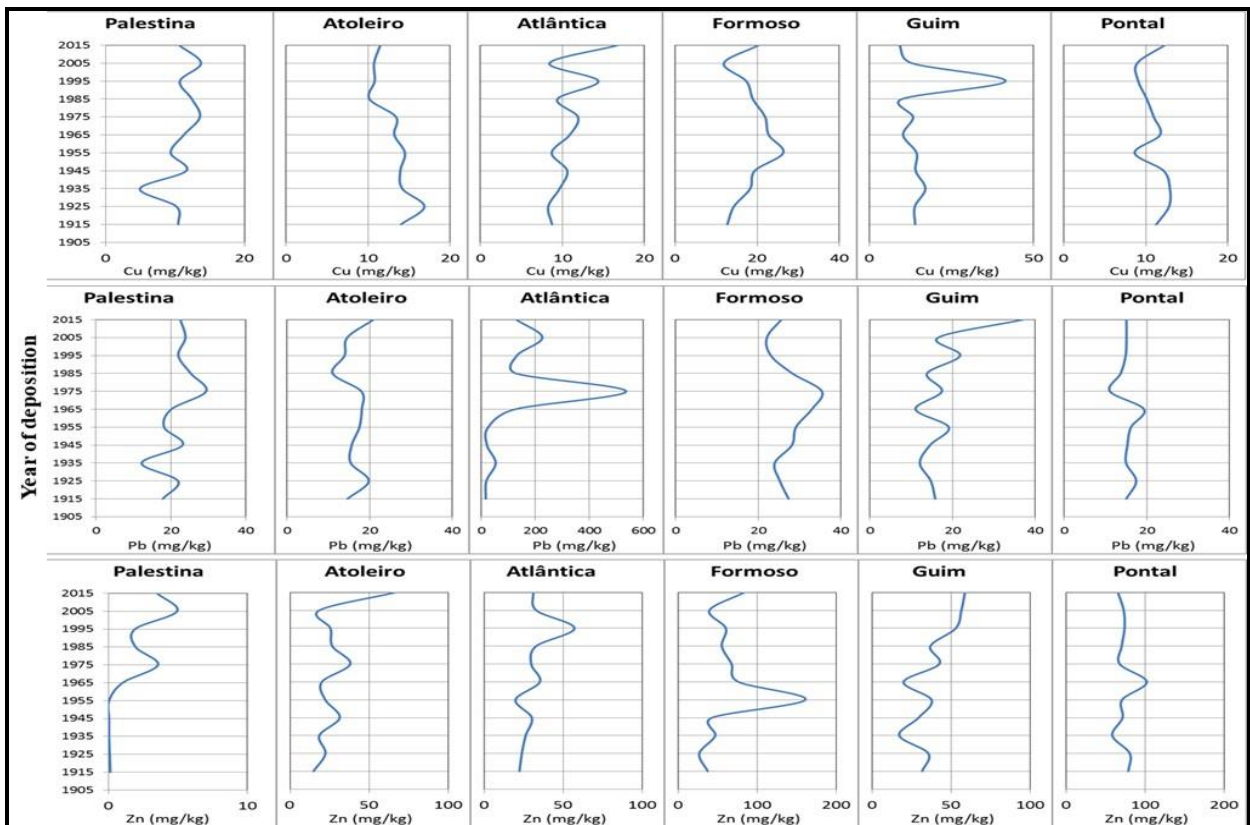


Fig. 7. Impact interpretation based on GPR-mineralogical and chemical data in the profiles.

In Fig. 7 is shown the correlation between the selected element distribution and the age of sediment deposition. The profiles show a variation of the element distribution, which can be correlated with impact events, and changes in basin occupation and human activities.

The Zn distribution shows high concentration from S to N connected to two events caused by the liberation of Zn from the Três Marias industrial complex.

Pb and Cu are connected to the use of agricultural beginning in 1945 and reducing the contribution after 1975 with changes in quantity and types of supplies.

The sediment distribution marks well the downstream transport compartment.

The variation of chemical parameters is clearly related to the human occupation and the increase of its activities like industry, farming and foresting (Figs. 5, 6 and 7).

6. Conclusions

The use of geophysical methods to obtain the sediment distribution in the lagoons permitted us to find the best places for drill sampling. It is an easy, rapid and cheap method for application in dry and humid areas, even with open watersheds.

The application of X-ray Fluorescence together with laser particle size analysis in lake profiles has proved to be a fast and effective technique in sediment characterization. It has shown the occurrences of mineral areas of heavy metals in-depth and the existence of distinct deep-water depositional patterns.

The results showed that the highest concentrations of heavy metals in the marginal lagoons are strongly associated with fine sediments typical of low-energy environments, demonstrating the importance of these systems for spatial-temporal evaluation of environmental quality.

The use of a geochronological tracer may support the time distribution of the contamination and help to follow the contamination profile in time and space.

7. Acknowledgements

We thank FAPEMIG, CNPq, and CAPES for financial support and UFMG, UNIMONTES, and local farmers for logistic support.

8. References

- Argollo R. M. (2001) Cronologias de sedimentação recente e de deposição de metais pesados na baía de Todos os Santos usando ^{210}Pb e ^{137}Cs . Tese (Doutorado em Geofísica) - Instituto de Geociências, Universidade Federal da Bahia, Salvador, 104 p.
- Baggio H.F. (2002) Alterações na paisagem natural e agrícola do município de Buritizeiro – MG: implicações do plantio generalizado de pinus e eucaliptos no meio ambiente físico, biológico e socioeconômico. Dissertação (Mestrado em Geografia) - Instituto de Geociências-IGC/UFMG, Belo Horizonte, 149 p.
- CPRM - Companhia de Pesquisa de Recursos Minerais (2001) Análise de Consistência de dados. Companhia de Pesquisa de Recursos Minerais. Belo Horizonte, 125p.
- Duffus J.H. (2002) Heavy metals - a meaningless term? Pure Applied Chemical, p. 793 - 807.
- Gama M.G.C. (2006) Água, vereda, veredeiro: um estudo sobre as agriculturas camponesa e comercial, nas cabeceiras do rio Formoso, em Buritizeiro-MG. Dissertação (Mestrado em Geografia) - Instituto de Geografia, Universidade Federal de Uberlândia, Uberlândia, 115 p.
- Godoy J. M., Moreira I., Wanderley C., Simões Filho F. F., Mozeto A. A. (1998) An alternative method for the determination of excess ^{210}Pb in sediments. Radiation Protection Dosimetry. v. 75, n. 1-4, p. 111-115.
- Junk W. (1989) The flood pulse concept in River-floodplains System. Can. J. Fish. Aquat. Sci. 106, p. 110-127.
- Malavolta E. (1989) Fertilizantes e seu impacto ambiental: micronutrientes e metais pesados, mitos, mistificações e fatos. Sao Paulo: ProduQuimica, p. 153.
- Nery, J.R.C. (2009) Determinação da taxa de sedimentação na foz do rio. Tese de Doutorado em Geologia. Instituto de Geociências e Ciências Exatas, Universidade Estadual Paulista - UNESP. Rio Claro-SP. 158 p.
- Patrus L.R.A., Santos A.C.S., Figueiredo V.L.S., Matos A.R., Menezes I.C.R. (2001) Parcela mineira da Bacia do São Francisco: caracterização hidro climática e avaliação dos recursos hídricos de superfície. In: Pinto C.P. and Martins-Neto M. (eds.) Bacia do São Francisco: geologia e recursos naturais. SBG-MG, Belo Horizonte, p. 285-326.

- Pompeu P. S. (1997) Efeitos das estações seca e chuvosa e da ausência de cheias nas comunidades de peixes de três lagoas marginais do médio São Francisco. Dissertação de Mestrado. Instituto de Ciências Biológicas, Universidade Federal de Minas Gerais - UFMG, Belo Horizonte-MG. 72p.
- Pompeu P. S., Godinho H. P. (2003) Ictiofauna de três lagoas marginais do médio São Francisco. In: Godinho, H. P. and Godinho, A. L. (eds.). Águas, peixes e pescadores do São Francisco das Minas Gerais. Belo Horizonte: PUC Minas, p. 167-181.
- Ribeiro E.V, Magalhaes A.P. Jr., Horn A.H., Trindade W.M. (2012) Metais pesados e qualidade da água do Rio São Francisco no segmento entre Três Marias e Pirapora-MG: índice de contaminação. Geonomos, p. 49 - 63.
- Wolman M.G., Leopold L.B. (1957) Rivers flood plains: some observations on their formation. Professional Paper, United States Geological Survey, 283 C., p. 87-107.

MICROTHERMOMETRY AND RAMAN SPECTROSCOPY OF FLUID AND MELT INCLUSIONS IN THE ALPINE PORPHYRY COPPER DEPOSITS FROM ROMANIA: INSIGHTS ON MICROMETALLOGENY

Ioan PINTEA^{1*}, Sorin Silviu UDUBAȘA², Elena Luisa IATAN³, Ion BERBELEAC³, Daniel BÎRGĂOANU¹, Oana Claudia CIOBOTEA-BARBU¹, Eduard GHINESCU¹

¹Geological Institute of Romania, 1, Caransebeș Str., 012271 Bucharest, Romania;

²Univ. of Bucharest, 1, N. Bălcescu Blv., 010041 Bucharest, Romania;

³Institute of Geodynamics of Romanian Academy, 19-21, J.-L. Calderon Str., 020032 Bucharest, Romania.

* ipinteafllncs@yahoo.com

Abstract: The paper presents complementary analyses of Raman spectroscopy and high-temperature microthermometry on fluid/melt inclusions from alpine porphyry copper and associated epithermal and skarn deposits from Romania. It reveals a complex phase association and multistage evolution during the magmatic-to-hydrothermal processes underlying the deep-seated MASH zones of the related subduction factories. Important differences in P-T-X properties were found for the main mineralizing processes between the two porphyry copper deposit clusters, one in the Banat region of the South Carpathians (Upper Cretaceous) and other in the Metaliferi Mountains of the South Apuseni Mountains (Miocene). These differences ranged up to 300°C in temperature, more than 1-3 kbar of pressure and 20-30 wt% NaCl eq. salinity. Although the magmatic-hydrothermal transitions are characterized by melt-melt-fluid immiscibility at high P-T conditions in both regions.

Detailed complementary microthermometry and Raman spectroscopy show regularity during heating/quenching cycles indicating successive phase transitions of multiple daughter minerals in hydrosaline melt inclusions. Complex hydrous saline phases, including javorieite-like, halite, anhydrite, magnetite, hematite and sulfide as triangular chalcopyrite (identified before and after microthermometry by Raman spectroscopy) behaved as true daughter minerals precipitated from the hydrosilicate liquid inside the trapped singular or coeval silicate-hydrosaline melt inclusions starting from about 1085°C, the estimated trapping temperature by microthermometry. The same successive phase transitions are envisaged to proceed during the formation of the alteration-mineralization assemblages characteristic to typical porphyry copper genesis.

Keywords: hydrosaline melt inclusions, microthermometry, Raman spectroscopy, porphyry copper deposits, Carpathians, Romania

1. Introduction

Fluid-melt evolution and ore elements transport and deposition during the formation of porphyry copper systems is a complex process involving fluid phase separation from various magma compositions and batches situated at different depths above the subduction zones from Upper Cretaceous and Miocene environments in the Carpathian regions from Romania. These processes took place over large P-T-X conditions from orthomagmatic to multiple hydrothermal episodes starting above 1000°C and frequently finished under 100°C, from more than 2kb to less than 100bar, and salinity from less than 10 wt% NaCl eq. to more than 80 wt% NaCl eq. (Pintea, 2014 and references therein). Magmatic immiscibility between hydrosilicate melt, hydrosaline melt, sulfate ± carbonate ± phosphate ± chloride ± fluoride vapor-rich “melt”, sulfide and oxide melt took place during first and secondary boiling in potassic and phyllic assemblages, followed by successive boiling episodes which deposited ore minerals in the argillic and propylitic alteration zones. The ore elements are redistributed amongst various solid phases, which generally could be identified as daughter mineral phases in silicate, hydrosaline and aqueous inclusions from ubiquitous quartz in characteristic veinlets in the stockworks structures of the porphyry copper systems. This study uses microthermometry and Raman spectroscopy to provide useful insights on micrometallogeny from the behavior of the included phases after trapping suggesting that similar characteristics generally apply to porphyry Cu-(Au)-(Mo) formation.

1.1. Materials and methods

Doubly polished quartz thin sections and wafers were used for petrography, microthermometry and Raman spectroscopy. Microthermometry of silicate melt-hydrosaline melt inclusions were measured in a “home-made” heating stage up to 1100°C under the microscope. The heating stage was calibrated with K₂Cr₂O₇ (398°C), α-β quartz transition temperature (573°C), NaCl (801°C), gold (1064°C). A kanthal heating element was used for heating, and maximum quenching was simply done by cutting off the electrical power. The heating rate ranged from 5° to 100°/min in variable combination steps and quenching rate by 50° to 200°C/min. The duration of a complete heating-cooling cycle in hydrosaline melt

inclusions ranged between 10 min to more than 1.5 hours. The relative accuracy of phase change measurements ranged between 86-99.5%. Calculated P-T-X data were based upon the SoWat software (Driesner and Heinrich, 2007; Driesner, 2007). It is worth noting that when entrapment of the fluid phases is heterogeneous, i.e. two or more fluid phases were trapped together in the same cavity, the recorded P-V-T-X-properties are not representative of the initial formation conditions of the complex silicate-hydrosaline melt inclusions but the microthermometry could be used to characterize the nature of included phases and their physical (immiscibility) chemical (ore element partitioning) inter-relationships.

Vibrational Raman spectra of solid daughter phases (transparent and opaque) from both porphyry copper provinces were performed at the Geological Institute of Romania on a Raman Renishaw spectrometer equipped with a Leica DM 2700M microscope and 50x objective lenses. Excitation was provided by two laser types with 532 nm with grating of 1200 grooves/mm and 1800 grooves/mm and 785 nm with grating of 1200 grooves/mm, respectively. The spectral resolution was +/- (1-2) cm^{-1} and laser exposure ranged between 5 to 15 sec with spectral accumulations from 1 to 55.

Decrepitated mound analysis is a complementary method used to estimate the chemical and mineralogical composition of thermally decrepitated fluid inclusion and successfully used, especially in exploration targets. There are several papers published in the literature which deal with sample analysis procedure starting with sample collection in the field, fluid inclusion selection for decrepitation study, analytical protocols on SEM-EDS and electron microprobe (Haynes et al., 1988; Heinrich and Cousens, 1989; Kontak, 2004; Kontak, 2013; Tweedale et al., 2015). The decrepitated mounds of the brine inclusions formed accidentally during microthermometry in the same assemblages such as those used in recorded phase transition were also analyzed tentatively by Raman spectroscopy. To prevent atmospheric hydration, the used quartz section fragments were immediately sealed in aluminum foil. During analysis, the laser was focused on several points of the concentrically deposited mound including the former cavity bottom.

2. Geological setting

There are two main regions of porphyry copper and related epithermal and skarn deposits occurrences in Romania:

1. The Late Cretaceous Banatitic (Laramide) province in the Banat region which belongs to the 1500 km - long of Apuseni – Banat – Timok – Srednogorie magmatic-metallogenetic belt in the Carpathian-Balkan orogen formed on the European margin during the closure of the Neotethys Ocean (Ciobanu et al., 2002; Zimmerman et al., 2008; Ilinca et al., 2011; Gallhofer, 2015). The magmatic arc was active for ~25 Myr (~92-67 Myr – Gallhofer, 2015).

2. The Miocene porphyry copper cluster from the “Golden Quadrangle” in the Metaliferi Mountains, which includes around 20 porphyry-epithermal Cu-Au(Mo) and related magmatic-hydrothermal deposits/prospects of the Hălmagiu - Brad - Săcărâmb, Zlatna - Stănița, Bucium - Roșia Montană - Baia de Arieș volcano-tectonic basins, with extension in Zarand (Tălagiu) and Poiana Ruscă Mountains (Deva) (Udubașa et al., 2001; Roșu et al., 2004; Berbelec et al., 2014).

Additionally, possible prospective areas include the Eastern Carpathian from Baia Mare mining district (e.g. Nistru; Oaș, SE-Gutâi Mountains and Țibleș massif,) and Călimani-Gurghiu-Harghita volcanic chain (e.g. tourmaline indicative mineral in the South Harghita region) – Pinteș et al. (1999), Damian (2003), Pinteș and Laczko (2005), Vlad (2011), Pinteș (2016).

The porphyry copper deposits consist of small-sized, intrusive stocks with concentric alteration zones which exhibit similarities with the Lowell and Guilbert (1970) model during Laramian times and with the Hollister (1975) diorite model during Miocene times.

The spatial distribution of the porphyry ore bodies seems to be controlled by N-S Laramian tectono-magmatic alignments (Banat) and NW trending Neogene basins controlled by crustal faults (Metaliferi Mountains). The Laramian porphyry Cu mineralizations are intimately associated with intrusive bodies and skarn deposits and Neogene ores with volcanic structures (Ianovici et al., 1977).

2.1. Upper Cretaceous porphyry Cu-Mo (Au) deposits in the Banat Mountains metallogenetic sub-belt

The Romanian sector of the Late Cretaceous Banatitic Magmatic and Metallogenetic belt contains plutons (granitoids), volcano-plutonic complexes and related dikes (calc-alkaline, I-type granitoids), with related ores and shoshonitic plutons that lack economic interest (Fig. 1). Cu (Mo) ores in skarn/porphyry deposits are related to plutonic apophyses along a major N-S Oravița-Ciclova-Sasca-Moldova Nouă alignment of the South Banat Mts (Vlad and Berza, 2003). Mineral deposits within the

Cretaceous Banatitic Magmatic and Metallogenic belt are strongly differentiated with respect to the host rock types and depth of magma emplacement. Copper and base metal skarn deposits form the most widespread metal accumulations. Porphyry copper ores with Cu ± Au, Ag, Mo are hosted by shallower hypabyssal bodies: e.g., Moldova Nouă. Subeconomic porphyry copper (± Mo) accumulations are also present at Oravița, but the hydrothermal alteration is far less pervasive than at Moldova Nouă. Large shallow porphyry-style systems with pyrite halos (and/or skarn halos) extend only south of Poiana Ruscă but they lack economic mineralization. Some occurrences are set apart by prominent Fe metallogeny (e.g., Ocna de Fier, Mașca Băișoara) (Ilinca, 2012).

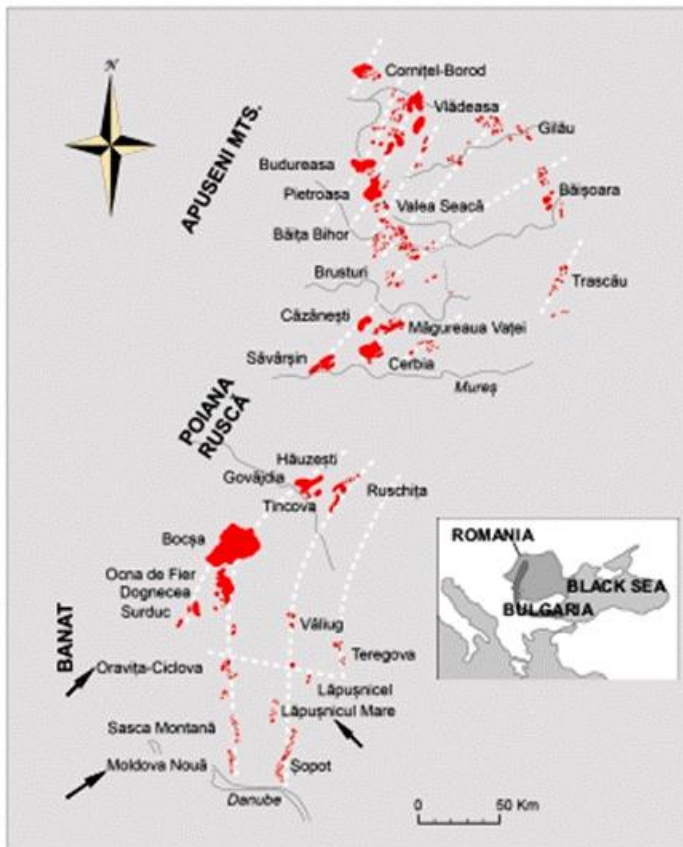


Fig.1. The banatitic belt from Romania with petrogenetic alignments and banatitic massif containing the porphyry Cu-Au-Mo deposit in the Banat region (arrows) – modified from Ilinca et al. (2011).

2.2. Miocene porphyry Cu-Au (Mo) deposits in the Apuseni Mountains

The porphyry copper deposits from the Apuseni Mountains are associated with the Miocene magmatism and metallogenic activity (Fig. 2). Magmatic-volcanic products' geochemistry reflects a gradual evolution, from normal (14.8-11 Myr) and "adakitic-like" calc-alkaline products (12.6-7.4 Myr), to the latest magmatic products having alkaline features (Roșu et al., 2004).

Porphyry-epithermal hydrothermal systems are centered on the volcanic structures, being genetically related to porphyritic, andesite-microdiorite subvolcanic bodies. The porphyry copper deposits from Apuseni Mountains can be divided into three types: Cu-Mo (Au) type (Deva, Rosia Poieni), Cu-Au type (Valea Morii, Bolcana, Rovina, Voia, Talagiu, Larga, Trâmpoiele, Valea Tisei, Tarnita) and Au-Cu porphyry type (Colnic, Ciresata) (Cioacă and Munteanu 2012).

3. Mineralization- alteration characteristics

3.1. Upper Cretaceous

Skarn mineralizations occur commonly as lenses and irregular bodies with branching apophyses in the vicinity of igneous apices and display no striking mineral zoning. The Cu ores consist commonly of chalcopyrite + pyrite + molybdenite (Bozovici), pyrite + chalcopyrite + molybdenite + magnetite + tetrahedrite (Moldova Nouă), pyrite + chalcopyrite + molybdenite + scheelite + gold (Oravița), pyrite + chalcopyrite + scheelite (Ciclova), (Table 1). Dissemination is dominant in the potassic zone while fracture filling is the most important in the phyllic zone (Ianovici et al., 1977).

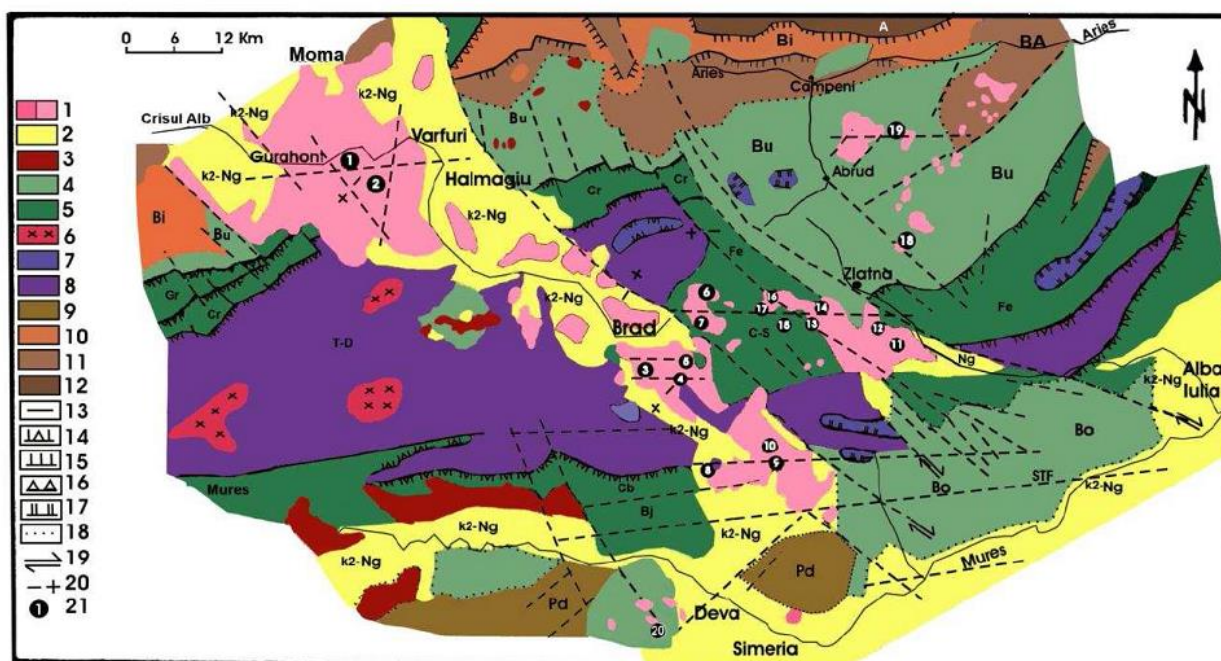


Fig. 2. Sketch map of the South Apuseni Mountains with the location of porphyry epithermal Cu - Au (Mo) and epigenetic hydrothermal deposits/prospects (simplified after the Geological Map of Romania edited by Geological Institute of Romania, scale 1: 50,000, Abrud, Zlatna, Geoagiu, Deva, Brad, sheets; modified by Berbeleac et al., 2005). 1. Tertiary volcanic rocks: a. Neogene and b. undifferentiated volcanics (Uroi trahyandesite rocks); 2. K₂-Ng: Fața Băii Fm. - Upper Cretaceous-Neogene sedimentary deposits; 3. K₂-Pg: Banatitic rocks undifferentiated; Late Cretaceous Fm. (dominantly Bucium Unit); 5. Early Cretaceous Fm. (dominantly Feneș nappe); 6. Jurassic granitoides; 7. Ardeu nappe and others; 8. Jurassic ophiolite (Drocea-Techereu nappe); 9. Padeș crystalline schists (Pz); 10. Biharia nappe system - shear zone; 11. Baia de Arieș series (Pcb); 12. Feniș-Gîrda nappe; 13. geological boundary; 14. K₂-Pg nappes; 15. Pre-Gossau nappes; 16. Variscan nappes; 17. Mesocretaceous nappes; 18. Unconformity; 19. Thrust faults; 20. Normal fault and block movement; 21. Ore deposits/prospects. A- Feniș Gîrda nappe, Bo- Bozeș nappe, Bu- Bucium nappe, Bi- Biharia nappe, Ba- Baia de Arieș nappe, Bj- Bejani nappe, Cb- Căbesti nappe, T-D- Techereu-Drocea, Cr- Criș, Gr- Groși, C-S- Curechiu-Stănița, STF- South Transylvania Fault. Ore deposits/prospects: 1. Tălagiu North, 2. Tălagiu Central South, 3. Musariu, 4. Valea Morii Nouă, 5. Cireșata, 6. Remetea, 7. Colnic, 8. Bolcana, 9. Voia, 10. Voia North, 11. Fața-Băii - Larga, 12. Trâmpoiele, 13. Muncăceasca Vest, 14. Popa-Stănița, 15. Măgura Poieni, 16. Valea Tisei, 17. Runculeț, 18. Bucium Târnița, 19. Roșia Poieni, 20. Deva. Modified from Berbeleac et al. (2014). Metaliferi Mountains: Lat. 46°18'(46.3°) N and Long. 22°50'(22.8333°) E, from <http://map.carta.com/>.

Table 1. Main geologic features of the Upper Cretaceous porphyry Cu-(Mo)-Au deposits from Banat region (Southwestern Romania).

Deposit, Elements	Mineralization type, Host Rock	Alteration	Ore mineralogy	Ore deposit morphology
Lapusnicu Mare Cu	skarn, quartz monzodiorite	propylitic, argillic	cpy, py, po, mo, hem, mgt, sph	impregnations
Moldova Noua Cu	skarn, porphyritic granodiorite, monzodiorite, diorite, carbonate sedimentary (J-K age)	potassic, phillitic, propylitic	mgt, ccp, py, sph, mo, ttr, bn, gn	impregnations, disseminations, veinlets
Ciclova Montana Cu-Mo (W)	skarn, granodiorite, carbonate sedimentary (J age)	phillitic, argillic, propylitic	py, ccp, gn, sph, mo, mgt, hem, ttr, bis, schl	stockworks, lenses, impregnations
Oravita Cu (Mo, W, Bi)	skarn, granodiorite, diorite, gabbro, paleozoic pelites, carbonate sedimentary (J-K age)	phillitic, argillic, propylitic	ccp, py, mgt, hem, bn, mo, po, sph, ttr, schl	stockworks, lenses, impregnations

Mineral abbreviations: cpy - chalcopyrite, py - pyrite, po - pyrrotite, mo - molybdenite, hem - hematite, mgt - magnetite, sph - sphalerite, ttr - tetrahedrite, bn - bornite, gn - galena, bis - bismuthinite, schl - scheelite.

In relation to the degree of alteration, porphyry copper deposits show a spatial zonation of ore minerals. In the central parts of the mineralized body, the phyllic alteration is dominant (sericite-quartz ± chlorite) where magnetite, hematite, pyrite, chalcopyrite, ± bornite, ± molybdenite and secondary Cu minerals are present (Fig. 3). Peripheral, the propylitic alteration is associated with other alteration types such as the argillic zone, with variations in the upper part of the structure (quartz, argillic minerals,

alunite, anhydrite, chlorite, albite) where pyrite, marcasite, \pm sulfides are present. The main by-products of this type of ores are: Mo, Au, Fe, Ti, Pb, Zn, Cd, In, etc. (Cioacă and Munteanu, 2012).

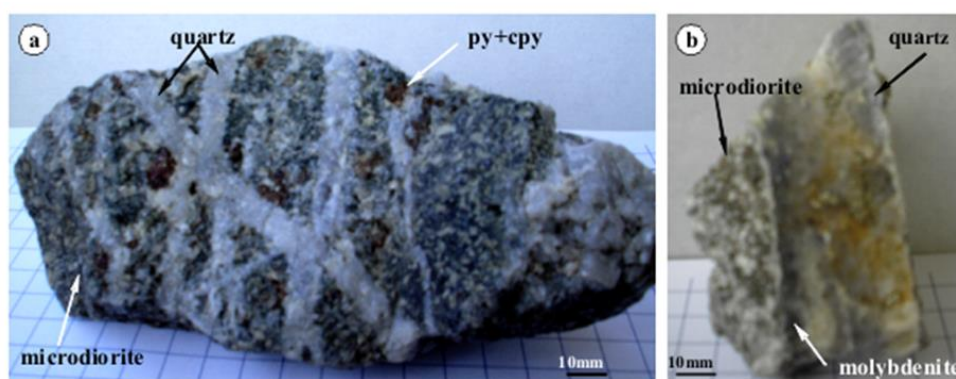


Fig. 3. Characteristic quartz veinlets in the porphyry Upper Cretaceous Cu-Au-Mo deposits from **a.** Lăpușnicu Mare and **b.** Moldova Nouă in the Banat region (South Carpathians); py - pyrite, cpy - chalcopyrite.

3.2. Miocene

Miocene porphyry copper deposits of the Apuseni Mountains show affinities towards the dioritic model. They contain pervasive potassic alteration with disseminated grains, veins and veinlets of pyrite + chalcopyrite (Tarnița, Rovina, Valea Morii, Bolcana), pyrite + chalcopyrite + molybdenite (Roșia Poieni) and quartz + bornite + chalcopyrite \pm calcite \pm fluorite (Deva), (Table 2), surrounded by the argillic zone (Fig.4). In some places, a larger scale zonality is provided by the axial setting of porphyry copper-bearing subvolcanoes surrounded and even cut by base metal veins connected with adjacent volcanic structures (e.g. Valea Morii - Ianovici et al., 1977; Kouzmanov et al., 2010).

Porphyry copper ores of the Apuseni Mountains show an evolution from acid to neutral regimes, highlighted by the mineral association with Fe oxides.

Table 2. The main characteristics of the Miocene porphyry Cu-Au-Mo deposit from the Metaliferi Mountains (South Apuseni Mountains, Western Romania).

Deposit Elements	Host Rock	Alteration	Ore mineralogy	Ore deposit morphology
Rosia Poieni Cu-Au (\pm Mo)	qtz andesite, amph-andesite, microdiorite	potassic, phyllic, propylitic, advanced argillic	py, cpy, bn, mgt, mo, hem, ttr, tenn, po, sph, gn, en, Au, Ag, cc, cv, anh, alu, dg, tld, ru, viv	impregnations, disseminations breccias, veins, veinlets
Tarnita Cu-Au (\pm Mo)	amph-andesite, microdiorite	potassic, phyllic, propylitic, argillic	py, cpy, mgt, bn, mo, hem, ttr, po, sph, gn, Au, cc, cv, anh, alu, dg, ru, viv	impregnations, veins, breccias
Bolcana Cu-Au (\pm Mo)	microdiorite, amph-andesite	potassic, phyllic, propylitic, argillic	cpy, py, mgt, hem, bn, Au, cv, cc, ttr, sph, gn, po, mo, ru, alu, anh	impregnations, veins, breccias
Valea Morii Cu-Au (\pm Mo)	andesite, qtz-diorite, amph-px microdiorite	potassic, phyllic, propylitic, argillic	cpy, py, mt, mo, bn, sph, gn, Au, ru, alu, anh	stockwork, veinlets, veins
Deva Cu-Au (\pm Mo)	andesite, microdiorite, granodiorite	potassic, phyllic, propylitic, argillic	bn, cpy, mgt, py, cv, hem, Au, mo	impregnations, veins, breccias
Talagiu Cu-Au (\pm Mo)	andesite, microdiorite	potassic, phyllic, propylitic, argillic	py, cpy, bn, mgt, hem, Au, Ag, sph, tld, alu, anh, ru, gy	impregnations, veins, breccias

Mineral abbreviations: py – pyrite, cpy - chalcopyrite, bn – bornite, mgt – magnetite, mo – molybdenite, hem – hematite, ttr – tetrahedrite, tenn – tennantite, po – pyrrhotite, sph – sphalerite, gn – galena, en – enargite, Au – native gold, Ag – native silver, cc – chalcocite, cv – covellite, anh – anhydrite, alu – alunite, dg – digenite, tld – tellurides, ru – rutile, viv – vivianite, gy – gypsum.

4. Fluid and melt inclusion study

In this paper, we intend to complement the extended review paper published by the first author (Pintea, 2014) with some new microthermometric experiments on silicate melt-hydrosaline melt inclusions in quartz from both porphyry Cu-(Au)-(Mo) districts from Romania by adding specific information about the microthermometric behavior of halite, anhydrite, magnetite/hematite and

chalcopyrite daughter minerals from specific brine inclusion assemblages. Many of these microthermometric measurements were preceded and/or postdated by Raman microspectroscopy for solid species identification in the same or similar inclusions. In the next step of this study, we intended to record the individual Raman spectra for each above-mentioned phase during heating and quenching. This is based upon the idea that the named phases are true daughter minerals precipitated from a complex hydrosilicate–hydrosaline mixture forming primary isolated or consistent microfissure healing assemblages. Moreover, it is presumed that the majority of ore elements are partitioned amongst silicate and hydrosaline phases following a fractionation descent line starting from orthomagmatic stages and finishing at epithermal ones.

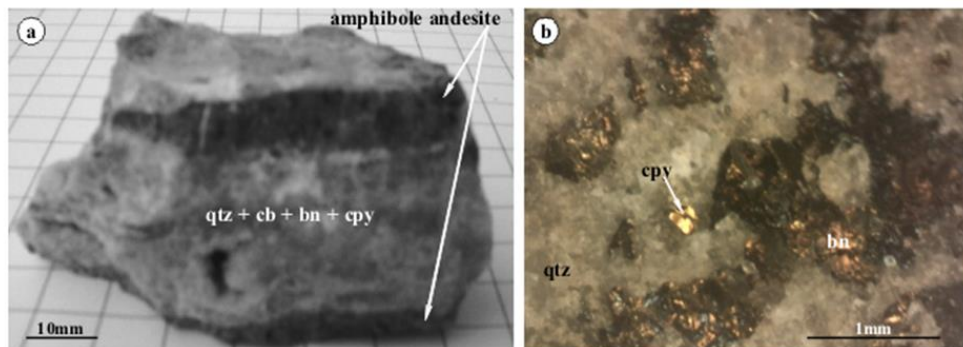


Fig. 4. Quartz-carbonate-bornite-chalcopyrite veinlet from Deva porphyry Cu-Au-Mo deposit (Miocene), **a.** transversal section, and **b.** longitudinal section; qtz - quartz, cb – calcite, cpy - chalcopyrite, bn - bornite.

4.1.1. Silicate melt - hydrosaline melt immiscibility in porphyry copper systems

Heterogeneous silicate-hydrosaline-sulfide/oxide assemblage was first described in Romania at the Miocene Deva porphyry Cu-Au (Mo) by Pintea (1993) followed by the evidence that this is a common process during magmatic-hydrothermal transition in all the porphyry deposits and occurrences from the Miocene in the Metaliferi Mountains and Eastern Carpathians, and also in the Upper Cretaceous in the Southern Carpathians, especially at Moldova Nouă and Oravița mining prospects from the Banat region in Romania. Preliminary data on the microthermometry of glass and hydrosaline melt inclusions from these deposits were presented in an unpublished Romanian Geological Institute report (Pintea in Roșu et al., 2002) and a published extended abstract (Pintea, 2002; Fig.5). It was evident that there are important differences regarding the content and microthermometric behavior of silicate-hydrosaline phases from the two mentioned regions during the main stages of mineralization, i.e. Miocene vs. Upper Cretaceous. Firstly, homogenization temperatures and halite dissolution temperatures in the Upper Cretaceous are up to 150°-300°C less than in the Miocene porphyry deposits, and also the salinity shows differences of about 20-30 wt% NaCl eq. Secondly, the homogenization temperatures in complex silicate-hydrosaline inclusions show lower values of around 300°C and less than 1-3 kb pressure in the Upper Cretaceous samples. One possible explanation of these differences was emphasized for the Miocene prospects from the Metaliferi Mountains (Pintea, 2014) with respect to the tectonomagmatic events related to the orientation of the subduction plane and asthenospheric thermal regime in the mantle wedge. More information based upon geodynamic models and magmatic-hydrothermal controls on porphyry systems especially Cu(-Mo-Au) deposits in the last decades can be found in some recently published papers (e.g. Udubașa et al., 2001; Richards, 2009; Harris et al., 2013; Gallhofer, 2015; Audétat and Simon, 2012; Kouzmanov and Pokrovski, 2012, and references therein).

During the heating procedure under the microscope stage, the complex, nearly crystalline silicate glass-hydrosaline melt, together with the opaque phase, become an emulsion containing two globules of salt melt floating in the hydrosilicate liquid phase at high temperature (Fig.6). The two opaque particles, one triangular and another globular (at room temperature) still remain undissolved at the bubble homogenization temperature (892°C) and both of them seem to be in the liquid state at this temperature. On further heating one of them (probably hematite) melted completely at 912°C (20°C after the bubble homogenization temperature). The remaining opaque liquid globule is still there at 988°C (Fig.6-j), and is probably a liquid sulfide. In other similar inclusion the opaque liquid globule remained up to 1037°C, and probably turned into copper chloride at such high temperature (e.g. Hack and Mavrogenes, 2006). On quenching, the vapor bubble appeared first suddenly, perhaps with an attached solid oxidic phase.

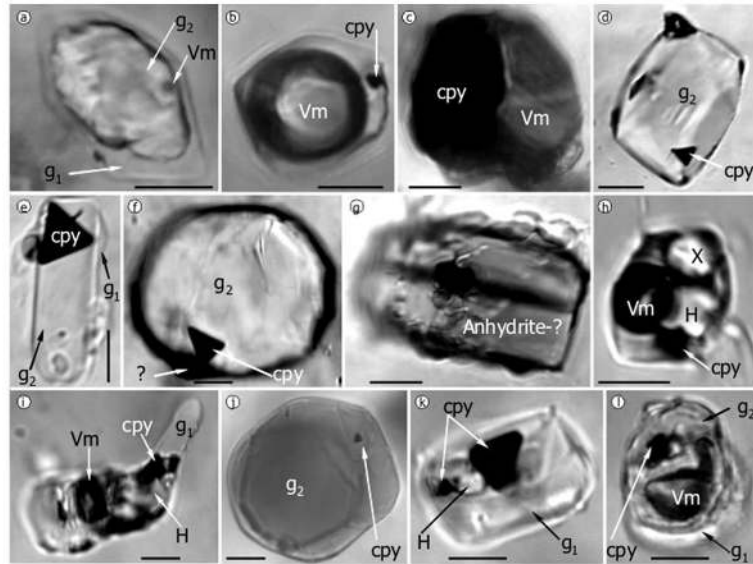


Fig. 5. Fluid and melt inclusions types in Upper Cretaceous porphyry copper deposits from the Banat metallogenic sub-belt. Notations: g1, g2- glass; Vm- vapor-"melt", cpy- chalcopyrite, H- halite, X – unidentified crystal; Scale bar: 10µm.

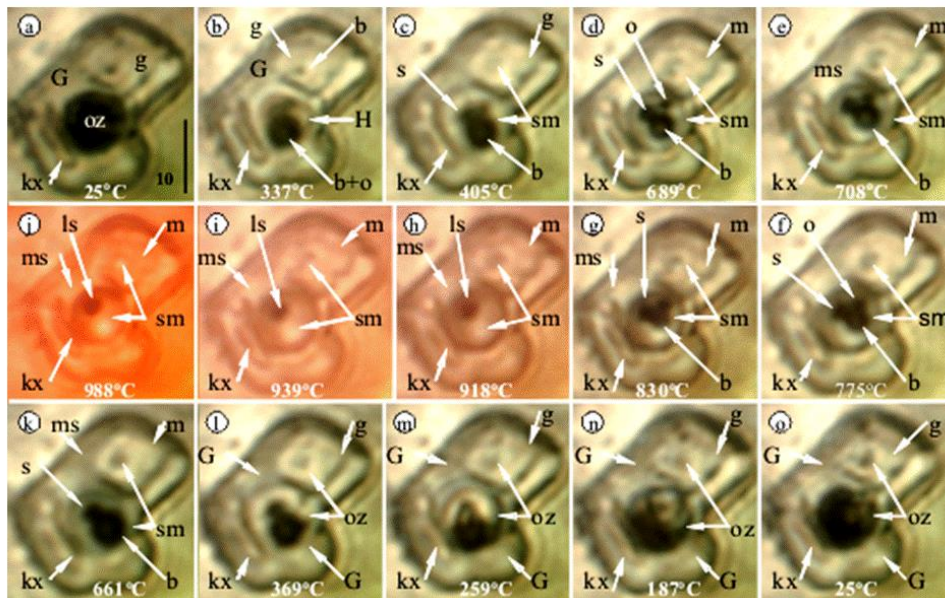


Fig. 6. Silicate melt - salt melt microthermometry showing immiscibility in a glassy inclusion from coarse grain quartz from Oravița porphyry Cu-Mo-(Au) prospect (Nicolae adit). Notations: G- glass, g- another glass, kx- anhydrite, H- halite, b- bubble, o- opaque, sm- salt melt, m- another melt, ms- silicate melt, s- sulfide (chalcopyrite), ls- liquid sulfide, oz- ore fluid (bubble+halite+opaque+other phases). Scale bar: 10µm.

Then the sulfide liquid solidified and turned into a triangular shape (probably chalcopyrite) and also remained in contact with the bubble assemblage. The main two salt globules remain rounded but are developed around some elongated grains inside the hydrosilicate liquid above 600°C. These elongated phases are perhaps sulfate or carbonate phases and do not melt completely during heating. On further quenching, the halite renucleated more evidently in the bigger salt globule. The hydrosilicate liquid solidified as amorphous silicate glass, around 500°C, or less. Calculated values by SoWat program for halite dissolution temperature $T_{mH}=401^{\circ}\text{C}$ and $T_{\text{bubble}}=892^{\circ}\text{C}$ give a pressure of $P=1784.59$ bar, salinity $W_s=47.2345$ wt% NaCl eq., density $d=0.831571$ g/ccm, with molar NaCl fraction $x=0.21$, and originally trapped fluid was in the V+L phase state.

The hydrosilicate melt phase in these inclusions has shown an uncommon complex composition suggesting the presence of a "clathrasil" compound (hydrosilicate of K,Na, Ca, etc), or a "zeolitic" melt framework (e.g. Momma, 2014). Generally, the silicate glass phase seems to contain carbonate, sulfate and phosphate radicals as the Raman spectra suggested (Fig. 7).

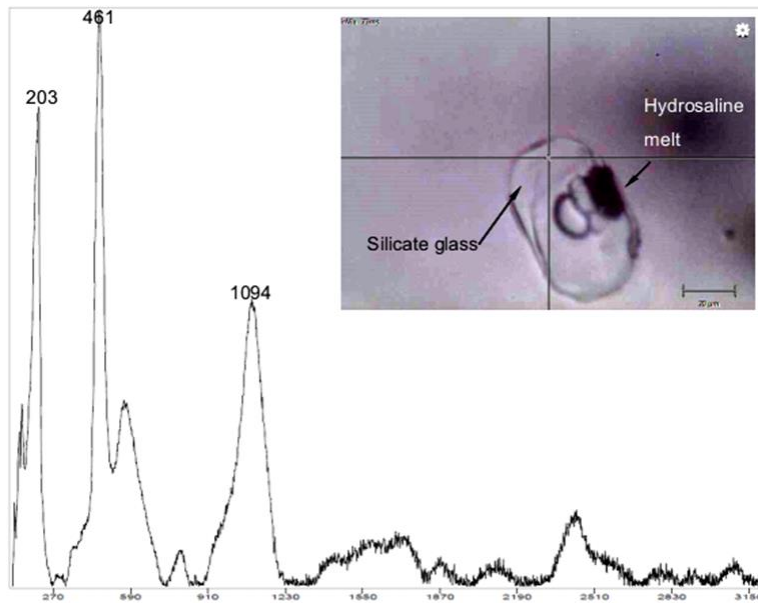


Fig. 7. Raman spectra of silicate glass component in complex silicate-hydrosaline melt inclusion in quartz from Oravița porphyry Cu-Mo-Au prospect (Upper Cretaceous, Banat region). This is indicative of the presence of CO_3^{2-} stretching line at 1094 cm^{-1} ; 203 and 461 cm^{-1} being the significant peaks of hosting quartz (Frezzotti et al., 2012). Scale bar: $20 \mu\text{m}$.

Ultimately, minuscule salt daughter phases solidified too under quenching (they melted first during the heating cycle), probably zeolites (see Stefanova et al., 2014). This kind of microthermometric behavior suggests that all the non-silicate phases were segregated from the main hydrosilicate liquid as temperature decreased, resulting in a complex melt-melt-fluid immiscibility.

Fluid inclusion studies in the porphyry copper system from Banat region (Upper Cretaceous) were done at Moldova Nouă prospect (Gheorghiiță, 1975), Lapușnicul Mare area by Pomârleanu and Întorsureanu (1985) and by Pintea, in an unpublished IGR report (Roșu et al., 2002). It was noticed that there are many types of fluid and melt inclusions especially in the characteristic quartz veinlets (some types in Fig.5) and their P-T-X-properties ranged widely between magmatic-to-epithermal (and skarn) stages (Pintea, 2002, and unpublished report - 2002) from $\geq 980^\circ\text{C}$ - 1100°C , 1 - 1.5 kb , 60 - $87 \text{ wt}\%$ NaCl eq. and 4 - $5 \text{ wt}\%$ H_2O where silicate melt, hydrosaline melt, volatile species and around $30 \text{ vol}\%$ of crystallized phases are present; the porphyry copper formation started during the magmatic to hydrothermal transition at $\leq 980^\circ\text{C}$ - 450°C , 0.3 - 1.0 kb and 40 - $70 \text{ wt}\%$ NaCl eq. to ≤ 35 - $40 \text{ wt}\%$ NaCl eq. and 450°C - 200°C and $<1.0 \text{ kb}$, which is the main stage of mineralization formation (Fig. 8); the final stages were characterized by low salinity fluids ($<5 \text{ wt}\%$ NaCl eq.) where aqueous liquid solution and low-density vapor phase are coexistent.

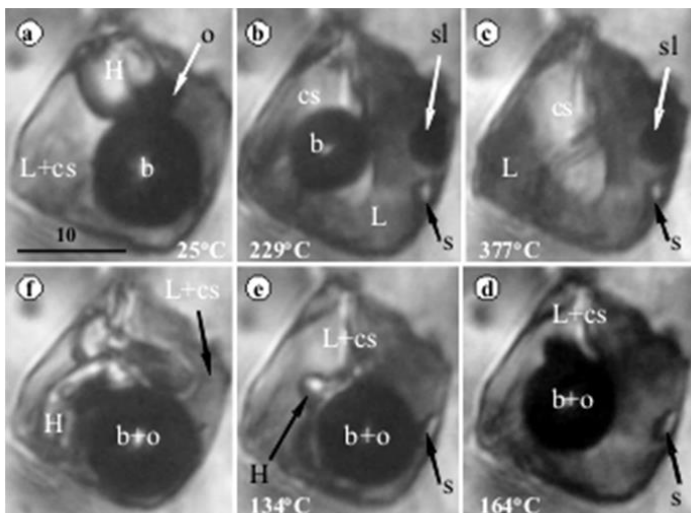


Fig. 8. Typical brine inclusion microthermometry in quartz from the main stage of mineralization of the Moldova Nouă porphyry Cu-Mo-(Au). Notations: L-liquid, H- halite, cs- clathrasil, b- vapor bubble, o- opaque (chalcopyrite?), sl- liquid sulfide globule, s- unknown solid, Tm- melting temperature, Th- homogenization temperature, Tn- renucleation temperature. Scale bar: $10 \mu\text{m}$.

During microthermometry, the brine inclusion type, as an example, is presented in successive microphotographs in Fig. 8. The first phase melting is around 100°-150°C; the halite melted around 250°-350°C and partial homogenization by bubble disappearance rarely exceeded 400°-450°C for the main stage of mineralization. The opaque phase is presumed to be chalcopyrite and becomes rounded at about halite melting temperature but still remains as an opaque liquid globule after vapor bubble homogenization temperature. On quenching, the vapor bubble renucleated first with some opaque phase (oxide) attached to it. Shortly after, the opaque sulfide starts to form as a triangular opaque but still remained attached to the vapor bubble. An unknown white solid phase (perhaps a clathrasil compound, precipitated immediately after sealing, but never remelted) remains unchanged in shape and volume. Halite renucleated as several particles, which immediately start to coagulate by Ostwald ripening. After several microthermometric cycles, the composition does not seem to be changed and all phases melted and renucleated in the same order. SoWat calculated values, for $T_{mH}=298^{\circ}\text{C}$ and $T_{hbubble}=363^{\circ}\text{C}$, are: pressure, $P=136.265$ bar, salinity, $W_s=37.5702$ wt% NaCl eq., density, $d=1.02705$ g/ccm, with NaCl molar fraction $x=0.16$, and the original trapped fluid was a single-phase state. On quenching, the bubble renucleated suddenly at 352°C , and halite at 137°C . It is worth noting that after the second microthermometric cycle in the same inclusion the homogenization temperature slightly increased, so it is better to avoid multiple cycling, but even so the renucleation of the melted phases still remains in the same reversed order.

4.1.2. Immiscibility in the Miocene deposits from the Metaliferi Mountains

The best example of multiple immiscibility at high temperature and various pressure conditions is represented by the complex silicate glass-hydrosaline melt inclusions from Deva porphyry Cu-Au-(Mo) prospect in the Metaliferi Mountains from the South Apuseni region in western Romania (Fig. 2). Moreover, they are also coexistent with a sulfide-rich phase represented especially by bornite and chalcopyrite (Pintea, 1993; 1995; 1996a, b; 2014; Fig. 4). In these veinlets, multiple melt inclusion types which delineate specific assemblages as primary random silicate melt, salt melt, hydrosaline melt and vapor-rich inclusions, some of them showing very high and uncommon homogenization temperatures, up to around 1400°C , were described (Pintea, 2014, and reference therein). Recently similar observations were reported at Grasberg porphyry Cu-Au from the Late Pliocene Ertsberg-Grasberg porphyry-skarn Cu-Au-(Mo) district in the Papua province in eastern Indonesia (Mernagh and Mavrogenes, 2019, and references therein).

During more than 25 years of investigations, various forms of immiscibility have been found in each of the Miocene porphyry copper systems from the Metaliferi Mountains (Pintea, 2014). One simple example is presented in Fig. 9 where ore fluids (vapor, salt and an opaque) are dispersed as globules of various sizes inside the hydrosilicate liquid phase. At the highest temperature (i.e. Fig. 9; 1049°C) a liquid phase surrounds both the vapor bubble and the opaque phase in the hydrosaline globule. When halite dissolution temperature can be recorded, the salinity ranged around 60wt% NaCl eq, calculated at the highest temperature in the stage, but these values are indicative because the final homogenization temperature was not achieved. Obviously, these inclusions cannot be homogenized even at very high temperatures (see Pintea, 2014) but the immiscibility is evident because the hydrosilicate glass is completely melted at such high temperatures, and SoWat program suggested heterogeneous entrapment of (V+L) phase at those temperatures.

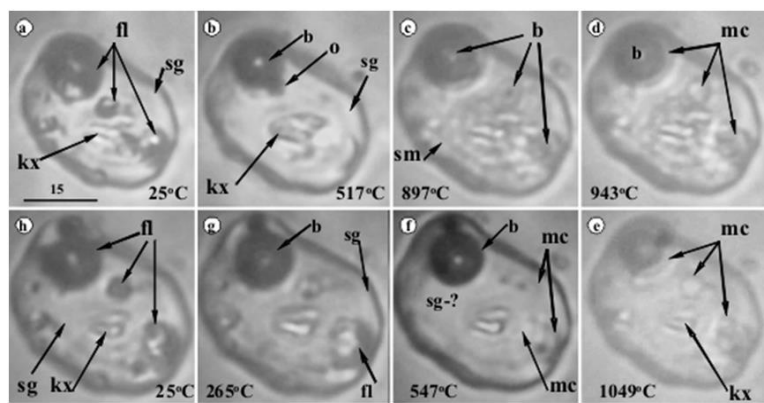


Fig. 9. Immiscibility between silicate melt and ore fluid in reheated glass inclusion in quartz from Bolcana ore deposit. Notations: of- ore fluid (bubble+halite+opaque+other phase), kx- solid, sg- silicate glass, sm- silicate melt, mc- salt melt, b- bubble, o- opaque. Scale bar: 15µm.

As it was already mentioned (Pintea, 2014) the hydrosilicate-hydrosaline-(Fe-S-O) melt immiscibility is the most prominent genesis process of porphyry copper systems from the Metaliferi Mountains and controls the entire fluid-melt evolution of the transition from magmatic-to-hydrothermal stages. The common trapping temperature in the magmatic stage (first and secondary boiling) was estimated during microthermometry by a pair of silicate melt and hydrosaline melt inclusions, based upon the beginning of silicate liquid formation in hydrosaline melt inclusion and salt melt exsolution in the contemporaneous silicate melt inclusion in the same assemblage, around 1085°C (i.e. Pintea, 1996a; 2009; 2012; 2014), which agrees with the main orthomagmatic-hydrothermal process in the Burnham model (Burnham, 1979; Bodnar, 1995; Campos et al., 2002; Drew, 2006; Becker, 2007; Bodnar, 2010). This process is perhaps completed by endogeneous auto-metasomatic gas-solid reaction (e.g. Blundy et al., 2015; Henley et al., 2017) which could be recognized based upon microtextural features (Pintea, 2010; 2014) of the quartz veinlets assemblage and cross-cutting relations (Kouzmanov et al., 2010; Silito, 2010). So, these are subsolidus reactions and took place especially between 550° and 850°C (60-80 wt % NaCl eq.; 1-2 kbar or more), characterizing the main porphyry ore stage formation process (potassic and phyllic alteration zones). At lower P-T-X conditions there are successive fluid events characteristic to the argillic and propylitic stages at <200°C, <23 wt % NaCl eq., and less than 100-300 bar. There are multiple mineral generations of apatite, rutile, ilmenite, quartz, anhydrite, calcite and ore minerals mainly magnetite, hematite, chalcopyrite, many of them being also formed as daughter minerals in the various melt and fluid inclusions types mentioned above. Most of these minerals can be found within a single hydrosaline inclusion suggesting that they form from a single generation of fluid flow (Mernagh, 2019, personal communication). The ore elements, especially Cu, Au and Mo, were partitioned between these melt-melt-fluid assemblages and their precipitation as economic mineralization was directly related to specific geodynamic conditions (e.g. Gallhofer, 2015).

5. Brine inclusions (hydrosaline melt) microthermometry

If all, or almost all, the solid microphases inside the hydrosaline melt inclusions or brine inclusions (see Kouzmanov and Pokrovski, 2012, for multiple term definitions), are daughter minerals then each of them should be in equilibrium with a complex hydrosilicate-saline solution (or melt) at specific P-T-X conditions until the content of the inclusions becomes homogeneous or heterogeneous function of trapping conditions. In this respect, we made a separate study of microthermometry coupled with Raman spectroscopy for the main daughter minerals such as halite, magnetite, hematite, anhydrite and triangular chalcopyrite. An interesting fact is the presence of javorieite – KFeCl_3 (Koděra et al., 2017) which seems to behave almost as a daughter phase (Kozák et al., 2017). A similar phase was noted frequently during microthermometry in several porphyry copper deposits in the Metaliferi Mountains (e.g. Pintea, 2014) and it was recorded as the first sharp melting point before halite dissolution between 256°-461°C and also tentatively indicated by a weak Raman shift at 64 cm^{-1} in the Bolcana Fe-rich porphyry Cu-Au-(Mo) deposit. The first melting points in hydrosaline melt inclusions between 88°-271°C (Pintea, 2014) are indicative for other hydrated salt complexes, sometimes the KCl daughter phase is used to estimate salinity in KCl-NaCl-H₂O system. They constantly renucleated as the last solid phases during the quenching cycle after heating by microthermometry, even around 70°C. A range of homogenization measurements have shown P-T-X data on a large scale of Th between 420° to 1300°C, 31-89 wt% NaCl eq. for salinity and 0.1 to 12.8 kbars for pressure trapping conditions (e.g. Pintea, 2012; 2014), suggesting various depth sources, fluid-phase immiscibility and/or heterogeneous trapping.

5.1. Halite microthermometry

Heterogeneous trapping involves the entrapment of several fluid and/or solid phases in one cavity, and their microthermometric behavior could be very complex and final homogenization temperature can be recorded only in the commercial high-temperature stages such as Linkam TS 1500 (Pintea, 1996). But in this case, is still possible to estimate salinity if we consider this temperature as a minimum homogenization value. As an example, in Fig. 10, the SoWat program estimated, for $T_{mH}=612^\circ\text{C}$ and $T_{h_{bubble}} \gg 1037^\circ\text{C}$, a pressure of 1312.53 bar, salinity of 75.9472 wt% NaCl eq., density of the liquid phase = 1.102 g/ccm with NaCl molar fraction $x_{\text{NaCl}}=0.5$. The original fluid was in the (V+L) phase state as it was precluded initially by visual estimation (i.e. bubble about 40-50% volume). In the same inclusion, the opaque phase melted at 786°C, another opaque melted at 1000°C, and a meniscus was formed during heating between a silicate film and the chloride-rich phase at 1000°C, suggesting immiscibility. Sulfide renucleated at 574°C (probably chalcopyrite). During heating, these complex brine inclusions (e.g. Fig. 10) homogenize at very uncommonly high temperatures (e.g. Pintea, 1996a, b; 2014;

Mernagh and Mavrogenes, 2019, and references therein), although these high-temperature values could be related to some specific geodynamic conditions as mentioned above (e.g. Pintea, 2014; Gallhofer, 2015). Nevertheless, the new data concerning the evolution of a vapor rich fluid at low pressure and high temperature in the Banska Štiavnica stratovolcano complex (e.g. Koděra et al., 2014) indicate that such fluid/melt complexes, related to the H₂O-NaCl-KCl-FeCl₂ system, could be responsible for the formation of a new porphyry Au deposit type (Kozák et al., 2017). If so, perhaps the highest homogenization temperature recorded at Deva porphyry Cu-Au-Mo deposit (e.g. Pintea, 2014) is representative for the boiling points of the common chloride salt, NaCl (1440°C) and KCl (1411°C), representing an internal artifact of the hydrosaline melt phase without any geological meaning in that context.

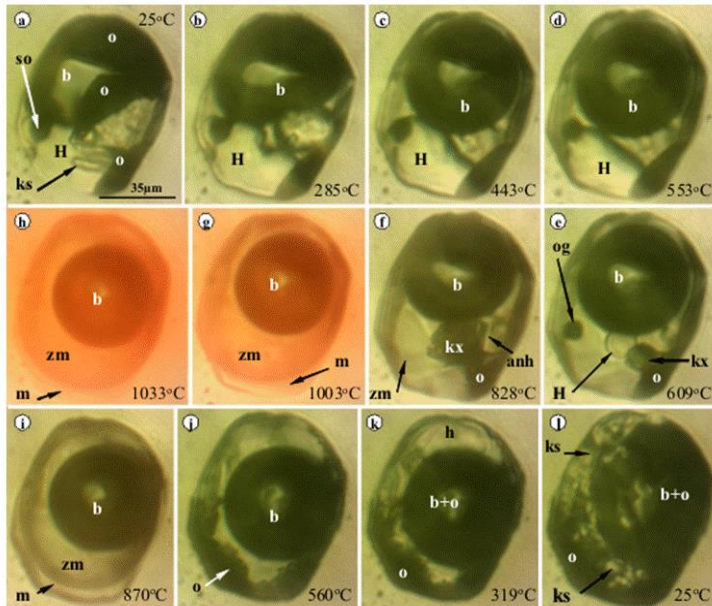


Fig. 10. Microthermometry of halite in a presumed heterogeneous hydrosaline melt inclusion from Valea Morii porphyry Cu-Au (Mo) deposit. Notations: so- solid opaque, H- halite, o- another opaque, b- bubble, ks- soluble minerals, og- globular opaque (liquid), anh- anhydrite, zm- hydrosilicate liquid, m- silicate melt. Scale bar: 35µm.

Homogeneous trapping is characteristic of hydrosaline melt inclusions which become “single-phase state” at vapor bubble homogenization and could be representative for a specific homogeneous population of inclusions or a part of a heterogeneous brine inclusion assemblage which trapped various proportion of fluid/melt phases. As an example, in Fig. 11 a homogeneous hydrosaline melt inclusions indicated $T_{mH} = 554^\circ\text{C}$, and $T_{bubble} = 889^\circ\text{C}$. The SoWat calculated pressure is $P = 1246.21$ bar, salinity is $W_s = 67.5962$ wt% NaCl eq., and density $d = 0.773078$ g/ccm, and the fluid is in the single-phase state (homogeneous). The vapor bubble renucleated at $T_{bubble} = 778^\circ\text{C}$, halite suddenly formed at $T_{nH} = 538^\circ\text{C}$ and ultimate phases renucleated at $T_n = 207^\circ\text{C}$, suggesting the presence of a zeolite phase as the final product of hydrosilicate fractionation, as it could be seen in the quartz-hosted microvein system, mentioned by Stefanova et al. (2014) at Elatsite porphyry Cu-Au deposit in Bulgaria.

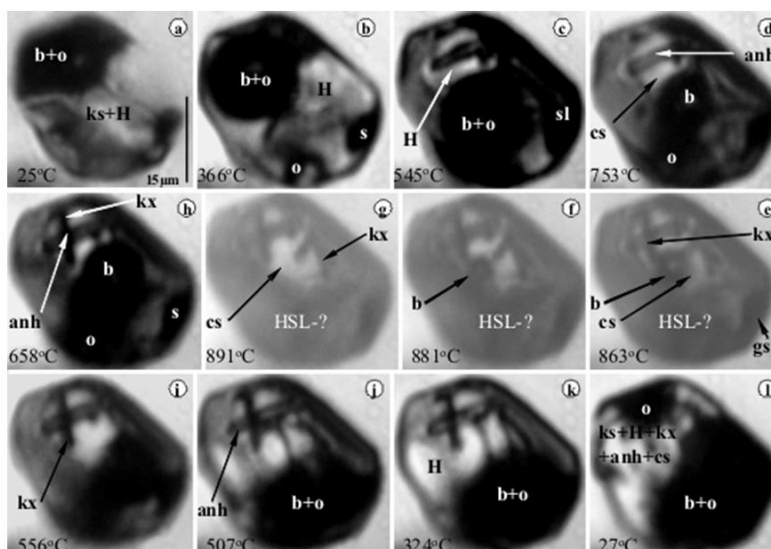


Fig. 11. Microthermometric sequences in homogeneous hydrosaline melt inclusions in quartz from Valea Morii porphyry Cu-Au (Mo) deposit. Notations: b+O- bubble+opaque, ks- saline daughter phases, s- sulfide, sl- liquid sulfide, anh- anhydrite, kx- unknown phase, cs- clathrasil (?), gs- globular sulfide. Scale bar: 15µm.

Generally, all daughter minerals melted in the presence of the vapor bubble, although frequently, some solid grains remain undissolved at the bubble homogenization temperature probably because of modifications after entrapment. It is worth noting that, at high temperatures, the final fluid is not only a simple saline mixture but rather a hydrosilicate complex liquid probably as a colloidal solution from which the melted phases renucleated due to the contraction of the silicate gel (silicothermal fluid) during quenching (Pirajno, 2009). It is assumed by experimental evidence that a separate SiO₂-rich clathrasil complex (Momma, 2014) or “a coarsened solid phase” is formed after trapping (Kotel’nikova and Kotel’nikov, 2010), and never remelted again during microthermometry, suggesting that the initial composition of the hydrosilicate liquid is now drastically changed. As a primary consequence, it is obvious that the H₂O-NaCl is only a good proxy for the complex hydrosilicate phase, which would be better characterized in the SiO₂-H₂O-NaCl system (Bodnar et al., 1985) or even better with Na₂SO₄-H₂O-SiO₂ (Kotel’nikova and Kotel’nikov, 2010), if we consider anhydrite as a real daughter phase and the presence of silicate compound as clathrasil, indicating oversaturated hydrosilicate-chloride rich phase, and indeed some of the last renucleated phases in hydrosilicate melt inclusions are zeolite-like. Probably, the same process took place in the veinlets fissure or pockets generating alteration-mineralization assemblages in the potassic and phyllic zones (see also Stefanova et al., 2014). The white coarsened solid component (i.e. clathrasil) is a ubiquitous “relic” in the Miocene porphyry Cu-(Au-Mo) system from Metaliferi Mountains but is also in the Upper Cretaceous porphyry Cu-(Mo-Au) in the Banat region and in pegmatites from Vlădeasa granite in the North Apuseni Mountains.

It has been known for a long time (e.g. Cloke and Kesler, 1979; Sterner and Bodnar, 1987; Campbell et al., 2001; Becker et al., 2008; Lecumberri-Sanchez- et al., 2012) that in many natural and synthetic compositions of the H₂O-NaCl system, the halite dissolution temperature is higher than the vapor bubble homogenization temperature (Fig. 12) or sometimes these are equal. In Fig. 12 the vapor bubble disappeared before halite dissolution in complex hydrosaline melt inclusion from Talagiu porphyry Cu-Au-Mo deposit from Metaliferi Mountains (Miocene) in South Apuseni Mountains (western Romania). SoWat calculates, for final halite homogenization temperature T_{mH}= 599°C and bubble disappearance temperature T_{hbubble}= 512°C, a pressure of P= 1628.25 bar, salinity W_s= 72.5583 wt% NaCl eq., and density d= 1.33906 g/ccm, with NaCl molecular fraction x= 0.4; the fluid is “single-phase state”.

Such microthermometric behavior leads to various theoretical and practical explanations such as the following: 1. these inclusions are accurate geobarometers (e.g. Roedder and Bodnar, 1980), or 2. their microthermometry is influenced by the entrapment mode which includes, by textural evidence, that halite was trapped together with the liquid phase as a heterogeneous suspension leading to “the potential to overestimate the fluid inclusion salinity” (Campbell et al., 2001). Moreover, “it appears that much of the published data for fluid inclusions that homogenize by halite dissolution represent inclusions that have either trapped a halite crystal along with the liquid or have reequilibrated by necking and/or stretching” (Becker et al., 2008). An interesting issue in this context is the “salting out” effect (Hovland et al., 2014) which preclude that halite particle forms at the supercritical condition at around 400°C or more function of the salinity of the H₂O-NaCl system, and they could easily be trapped as solid particle together with some liquid phase in the inclusion cavity.

5.2. Anhydrite microthermometry

Anhydrite is another common daughter solid phase present in almost all hydrosaline melt inclusions from the porphyry copper and pegmatites from Metaliferi Mountains (Miocene), Banat region and North Apuseni Mountains (Upper Cretaceous), respectively. It appears in short or longer prisms (baguette) with high birefringence and characterized by a large range of melting temperatures, depending on the global composition of the hydrosaline melt inclusion. Despite the fact that it is so common in porphyry copper systems, there are few data on anhydrite microthermometry mainly because of the complexity of brine inclusions making it hard to be observed directly under the microscope heating stage.

During heating, generally, anhydrite is more easily visible after the halite dissolution (see also Braxton, 2007) when it appears as long prismatic, baguette, next to the vapor bubble, and sometimes a silicate phase (mica) and one or more opaque grains (sulfide and oxide) are present too. On further heating, it disappeared before vapor bubble homogenization (e.g. Fig. 13) and their melting temperature almost fits the experimental data in the Albite-Quartz-Anhydrite-H₂O system (Ducea et al., 1999). In Fig. 13 the melting temperatures are the followings: T_{m1}= 66-238°C, T_{mH}= 543°C, T_{m anh}= 723°C, vapor bubble disappearance temperature in the presence of liquid opaque phase at T_{hbubble}= 770°C. It is shown that at T_{max}= 1062°C in the stage the opaque liquid is still there but his diameter decreased substantially.

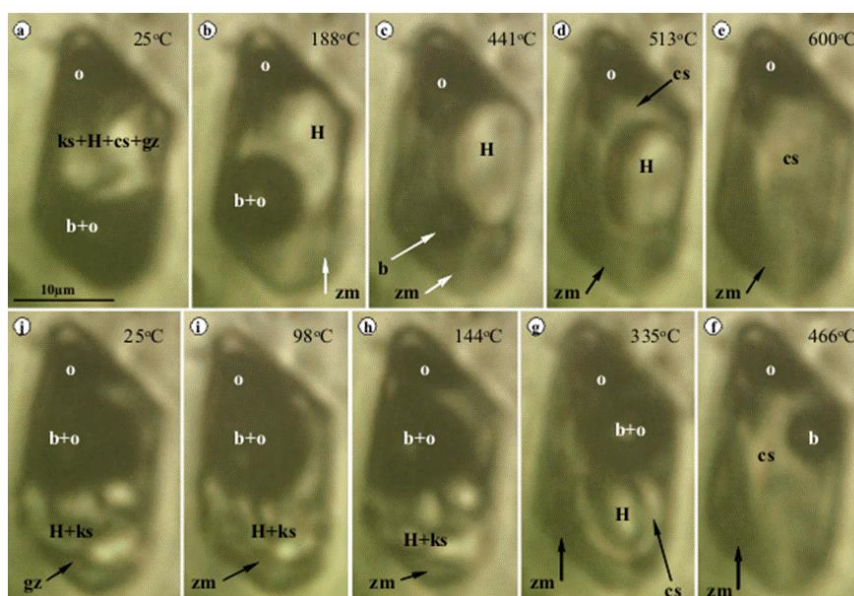


Fig. 12. Brine inclusion microthermometry by halite homogenization in quartz from Tălagiu porphyry Cu-Au (-Mo) deposit. Notations: ks- soluble salt, H- halite, cs- clathrasil, b- bubble, o- opaque, zm- hydrosilicate liquid (melt), gz- transparent glassy coverage. Scale bar: 10µm.

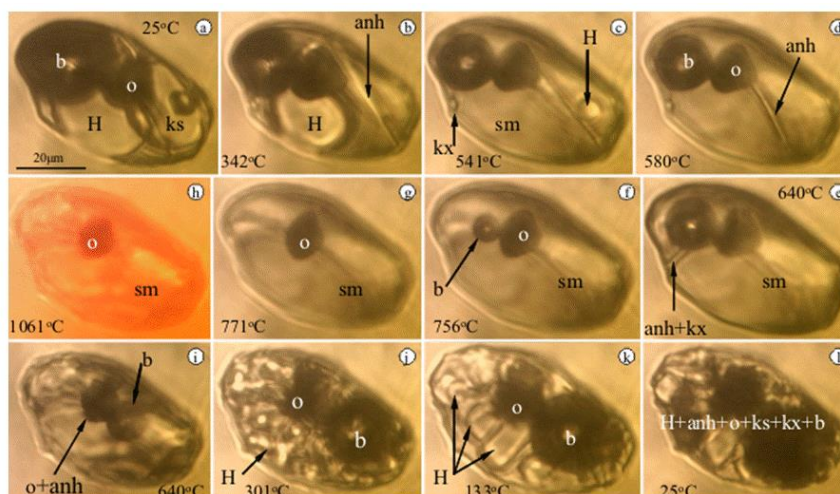


Fig. 13. Anhydrite microthermometry in a homogeneous hydrosaline melt inclusion in quartz from Roşia Poieni. Notations: b- bubble, o- opaque, H- halite, ks- other salt daughter minerals, anh- anhydrite, kx- unidentified phase. Scale bar: 20µm.

Trapping conditions calculated by SoWat at 770°C, give: pressure, $P=907.48$ bar, salinity, $W_s=66.0109$ wt % NaCl eq., and density, $d=1.064$ at NaCl mole fraction, $x=0.4$. Originally the fluid is in the “single-phase state”. On quenching, anhydrite renucleated after the vapor bubble and before halite renucleation. Generally, the microthermometric cycles were reproducible. Although, for example in a batch of hydrosaline melt inclusions ($n=102$) from Valea Morii porphyry Cu-(Au)-(Mo) deposit (Pintea, unpublished data) even though anhydrite was always present, only in 23 cases from 102 microthermometric analyses (as an example), anhydrite melting temperature was recorded between 803°-1063°C. During quenching, anhydrite renucleated between 658°-793°C, but the process is very difficult to be recorded and, unfortunately, this could only be observed in 4 microthermometric analyses of the same batch of measurements. Nevertheless, many repeated microthermometric analyses from the batch samples mentioned above, have shown again, after quenching, the presence of anhydrite, so it is a matter of optical microscopy determination of the tiny anhydrite microcrysts rather than the absence of anhydrite daughter phase. Perhaps by coupling Raman spectroscopy during microthermometry the anhydrite could be better evidenced, as it is presumed after several cycles of the same inclusion from Fig. 13, by the characteristic peak at 983 cm^{-1} which is indicative for the presence of (SO_4^{2-}) by very strong molecular vibrational stretching (e.g. Arcanite – K_2SO_4 , Frezzotti et al., 2012, in Fig. 14).

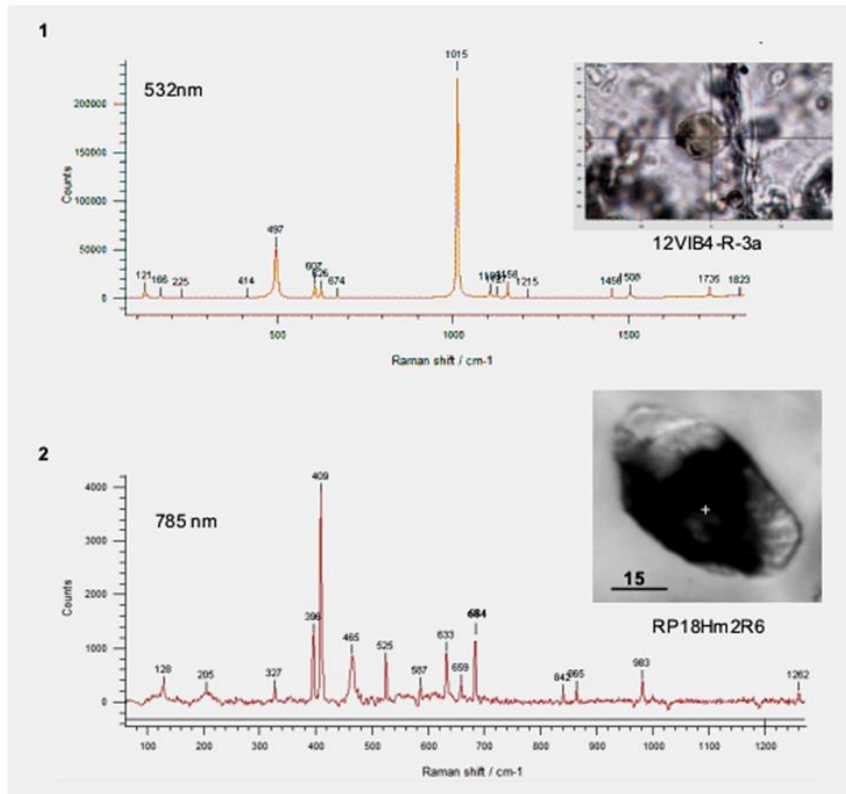


Fig. 14. Solid inclusion (glassy) in quartz from Voia porphyry Cu-Au-Mo deposit before microthermometry indicating the vibrational stretching of anhydrite at 1015-1016 cm^{-1} (Burke, 1994), in (1), and the Raman spectra in the same inclusion from Fig. 13 after microthermometry (scale bar: 15 μm). The Raman shift peaks are indicative for sulphate (983 cm^{-1}), carbonate (1081 cm^{-1}), hematite (409 cm^{-1}), ilmenite 684 cm^{-1} , sulfide (<400 cm^{-1}), in (2).

5.3. Opaque phases microthermometry

The alteration-mineralization stages in porphyry copper genesis are composed mainly by the veinlets and brecciated zones dominated by magnetite, hematite (specularite), chalcocopyrite, pyrrhotite, sulfosalts, pyrite, marcasite, all of which are associated with quartz, anhydrite, gypsum, calcite, and sometimes fluorite and alunite. Many of these minerals were also formed in hydrosaline melt inclusions after sealing in the host minerals (mostly studied in quartz).

One of the most important observations is that after (sometimes before) halite dissolution, the opaque minerals (oxides, sulfides) become globular most probably in the liquid state and most probably turning into chloride compounds before they were homogenized in the hydrosilicate-salt liquid. Moreover, some of these (typically oxides) are attached to the vapor bubble until they are completely melted around the bubble disappearance temperature. That is, at high temperature, magnetite is floating together with the vapor phase in the hydrosaline melt inclusions.

5.3.1. Magnetite/hematite

Magnetite is one of the common opaques in hydrosaline melt inclusions and generally, during heating, a sudden transition was observed above 650°-700°C changing them to transparent platelets of hematite or FeCl_2 (Pintea, 2009). On further heating, these new phases become rounded and are perhaps in a liquid state as iron chloride, dissolving at very high temperatures (Pintea, 2014).

It was noted that during the heating/quenching microthermometric cycles, the oxide minerals and even sulfides are in very close relationship with the vapor bubble evolving together during temperature variations. This phenomenon is very common at the large scale in the subvolcanic-magmatic system where during degassing, sulfides and magnetite are attached to the vapor bubble and transported despite gravity forces at the surface and precipitated as individual layers (Edmonds, 2015; Mungall et al., 2015; Knipping et al., 2019). In Fig. 15 the microthermometry indicates that the halite melted at $T_{\text{mh}} = 464^\circ\text{C}$ and the homogenization temperature is more than 1081°C. The SoWat estimated a pressure of $P = 2331.66$ bar, the salinity, $W_s = 55.0043$ wt% NaCl eq., and density, $d = 0.883646$ g/ccm with NaCl molar fraction, $x = 0.27$. As it is confirmed, the fluid is in the (V+L) state, because the homogenization temperature cannot be reached in our microthermometric stage. So, probably the initial state of the fluid was

homogeneous above 1081°C. An unknown transparent phase melted at $T_{\text{mds}} = 716^\circ\text{C}$, the opaque melted between 936°C - 1025°C , which renucleated at 644°C . The unknown transparent phase (ds) renucleated at 609°C . Anhydrite melted above 936°C . In 16 out of 102 microthermometric analyses of hydrosaline melt inclusions at Valea Morii deposit, as mentioned above, the opaque phase is presumed to be a magnetite/hematite daughter phase, and the melting temperature ranged between 786°C - 1068°C . The renucleation process showed the formation of similar opaque phases but they are difficult to be microscopically identified even by Raman spectroscopy. Anyhow, the high melting temperatures indicate that magnetite/hematite has formed inside the hydrosaline melt or hydrosilicate melt inclusions after trapping, indicating a magmatic or hydrothermal origin as it was demonstrated by silicate melt inclusion in magnetite microthermometry (Knipping et al., 2015) and by exsolution from iron-rich melt at the El Laco magnetite lava flows (Tornos et al., 2016).

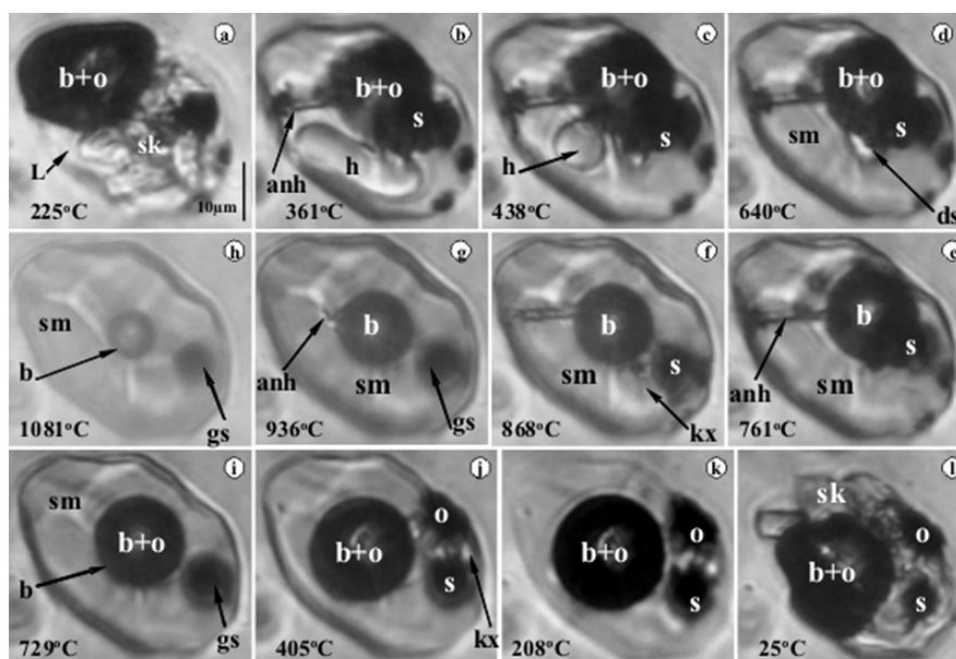


Fig. 15. Microthermometric sequence in heterogeneous hydrosaline melt inclusion in quartz from Bolcana porphyry Cu-Au (Mo) deposit. Notations: sk- salt crystals, b- bubble, ds- unknown solid phase, anh- anhydrite, o- oxide (magnetite and/or hematite), sm- salt melt, gs- globular liquid sulfide, kx- unknow solid. Scale bar: $10\mu\text{m}$.

5.3.2. Triangular chalcopyrite microthermometry

Besides optical microscopy, SEM-EDS, PIXE, or direct chemical analysis, the presence of triangular chalcopyrite as a truly daughter phase can be proved by coupling microthermometry with Raman spectroscopy (Fig. 16 and Fig. 17). It is well known that chalcopyrite is consistently present in hydrosaline melt inclusions from porphyry copper deposits since the fluid and melt inclusion assemblages of these deposits have been extensively investigated (e.g. Roedder, 1971, 1984; Nash, 1976; Eastoe, 1978; Ramboz, 1979; Lowenstern, 1993; Damman et al., 1996; Redmond et al., 2004; Heinrich et al., 2005; Kouzmanov and Pokrovski, 2012).

It is also observed that chalcopyrite obviously doesn't melt during heating in low salinity vapor-rich inclusions, mainly because of the H_2 moving in or out after entrapment (Mavrogenes and Bodnar, 1994; Spencer et al., 2015). Moreover, some recent experimental work demonstrated that several elements such as Cu, Ag, Na can diffuse out or in, inducing important modification of the initial fluid and melt inclusion content (Li et al., 2009; Lerchbaumer and Audétat, 2012; Seo and Heinrich, 2013). Nevertheless, "Sterner and Bodnar (1984) showed that by adding a large excess of powdered chalcopyrite to capsules containing 10 wt% NaCl solution, inclusions containing chalcopyrite daughter mineral were produced. When these inclusions are heated, the chalcopyrite completely dissolves and reprecipitates when the inclusions are cooled" (Bodnar and Sterner, 1987). The same successful chalcopyrite microthermometry was achieved by using the hydrogenation technique proposed by Mavrogenes and Bodnar (1984), which was perfected recently by Spencer et al. (2015). In both experimental studies, chalcopyrite proved to be a real daughter phase by specific melting and renucleation behavior during heating/quenching cycles.

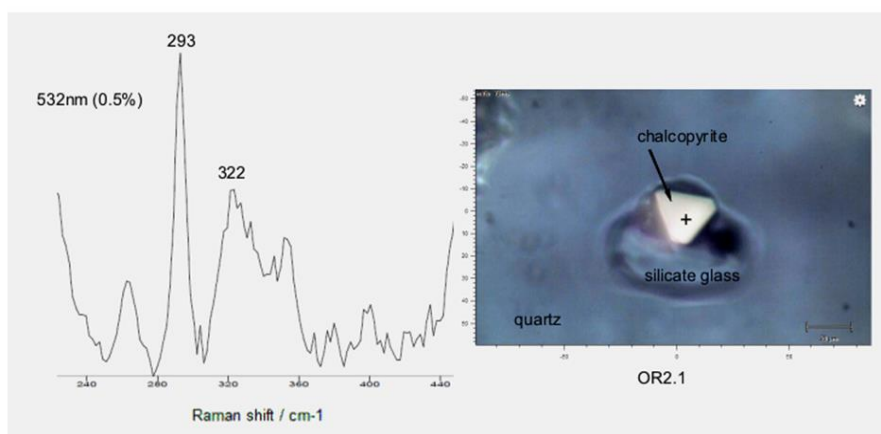


Fig. 16. Raman spectra of chalcopyrite daughter mineral in hydrosilicate melt inclusion in quartz from Oravița porphyry Cu-Mo-Au deposit (Upper Cretaceous). Chalcopyrite has a very strong peak at 293 cm^{-1} , and some weaker peaks at 322 cm^{-1} , 352 cm^{-1} and 378 cm^{-1} (Frezzotti et al., 2012). Scale bar: $25\mu\text{m}$.

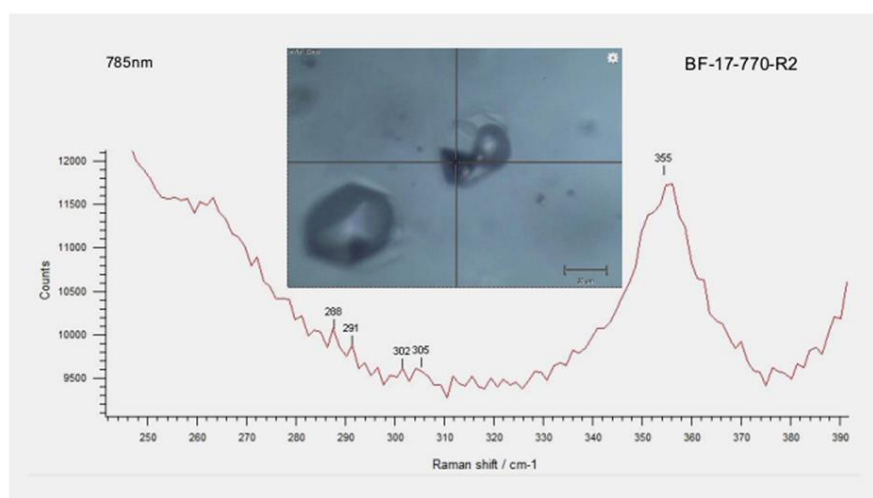


Fig. 17. Raman spectra of triangular chalcopyrite daughter mineral in hydrosaline melt inclusion of quartz from Bolcana porphyry Cu-Au-Mo deposit (Miocene). Common Raman shifts peaks between $291\text{--}293\text{ cm}^{-1}$, $320\text{--}323\text{ cm}^{-1}$, depending on laser line power and position of the inclusion in the host quartz. Scale bar: $20\mu\text{m}$.

During heating of hydrosaline melt inclusions (here as an example) the first melting temperature is given by dissolution of an intermediate complex such as iron hydrate sulfate and/or carbonate (or zeolite), together with the thin amorphous hydrosilicatic film (Pintea et al., 2018) followed by another complex phase such as javorieite (KFeCl_3) or other similar phases (e.g. Kozák et al., 2017) until halite melted sharply at 611°C , as shown in Fig. 18. At that temperature, the remaining phases are the vapor bubble and two opaque grains, one attached to the bubble and other somewhere nearby, together with a transparent baguette presumed to be anhydrite. The opaque globule attached to the vapor bubble turned to an opaque liquid globule and stayed attached until high temperature, and then it suddenly separated from the vapor bubble. At this temperature (i.e. 1050°C), an opaque globule and a vapor bubble are floating in the hydrosaline-silicate liquid. After the heating was stopped, the liquid globule immediately moved back towards the vapor bubble and started to crystallize as a thin opaque plate from inside the bubble. On further quenching, another opaque phase renucleated (oxide) together with the transparent baguette (anhydrite). The sulfide became more triangular in shape, suggesting chalcopyrite, as also revealed by the Raman shift at 291 cm^{-1} , measured several months after the microthermometry. The halite renucleated suddenly as several separate grains, which coagulated by Ostwald ripening. The last formed solid phases filled up the interstitial space between vapor, halite and the opaque phase, perhaps as a solid fragile amorphous hydrosilicatic crust (Pintea et al., 2018). Repeated microthermometric cycles followed almost the same phase transition succession and the data in Fig. 18 are compiled from them, as follows: halite melt at $T_{\text{mH}} = 611^\circ\text{C}$, the opaque phase at $T_{\text{mO}} = 1017^\circ\text{C}$, and final homogenization temperature around $T_{\text{h}} \geq 1052^\circ\text{C}$. Anhydrite melting temperature was recorded only in the second cycle, at 987°C . An unknown solid phase melted around 1040°C , and if the temperature of formation is estimated at 1052°C ,

the SoWat estimated pressure is $P= 1364.37$ bar, salinity is $W_s= 75.8046$ wt% NaCl eq., and density $d= 1.09793$, with NaCl molar fraction $x= 0.5$. The original fluid was in the “single-phase state” even if in reality the final homogenization temperature was not recorded in this case. During quenching, the opaque (chalcopyrite) renucleated at $T_{no}= 657^\circ\text{C}$ and halite renucleated at $T_{nH}= 495^\circ\text{C}$. Anyhow, the cycles are not completely reproducible due to post-entrapment modifications but because the content and number of phase transitions are almost the same in the repeated cycles it is assumed that the complex salt phase, halite, anhydrite, magnetite/hematite, chalcopyrite are daughter minerals and were precipitated from a complex hydrosaline-silicate liquid, as hydrosilicate gel or silicothermal fluid.

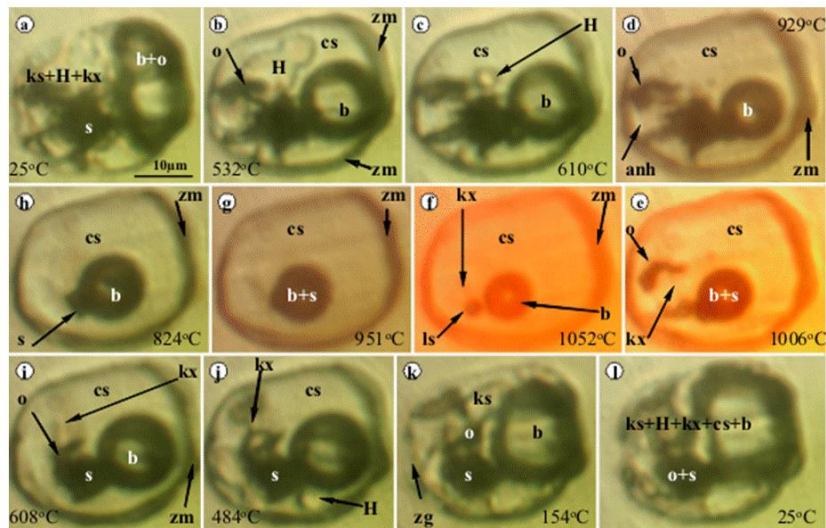


Fig. 18. Chalcopyrite melting and renucleation in homogeneous hydrosaline melt inclusion from Valea Morii porphyry Cu-Au (Mo) deposit. Notations: s- sulfide (chalcopyrite?), ls- liquid sulfide, H- halite, ks- other salts, b- bubble, cs- clathrasil (?), zg- hydrosilicate glass, o- opaque. Scale bar: 10µm.

6. Characterization of the decrepitated mound by Raman spectroscopy

During microthermometric cycles of a quartz sample, many of the hydrosaline melt inclusions decrepitated and liberated the highly concentrated liquid melt outside microcavities wetting the surface of the host mineral (i.e. quartz). These fluids precipitated obviously in a concentric microtexture with oxide/sulfide close to the micro-pit, then silicate melt and salt to the rim. So, the content of exploded inclusion is almost completely saved in this process and can be qualitatively analyzed by Raman spectroscopy. Some examples of Raman spectra are shown in Fig. 19 and Fig. 20, suggesting the presence of the main silicate, sulfide/oxide and salt minerals in inclusions before decrepitation. In fact, only the vapor phase is missing from the initial chemical composition. We also emphasized that some of the components suffered chemical modification after decrepitation caused by decompression and changing temperature, but they give important clues about the chemistry of the included fluid or melt phases. The Raman spectra show that these precipitated assemblages contain halite ($353\text{-}355\text{ cm}^{-1}$), silicate glass ($628\text{-}633\text{ cm}^{-1}$), hematite (409 cm^{-1}), chalcopyrite ($291\text{-}293\text{ cm}^{-1}$), magnetite (654 cm^{-1}), other sulfides ($<500\text{ cm}^{-1}$), sulfate (983 cm^{-1}), carbonate ($1028\text{-}1081\text{ cm}^{-1}$) and phosphate ($916\text{-}1000\text{ cm}^{-1}$) ions, comparative to the data from RRuff Raman database, Frezzotti et al. (2012) and Hurai et al. (2015). The concentric deposition of the precipitate is interesting, suggesting immiscibility even during quenching at the surface of the host-quartz sample. Anyhow, there are some notable variations, as a function of the inclusion types suggesting that each micro-pit contains its specific initial chemical composition, and perhaps other unknown causes, and the Raman spectra of this study should be interpreted only as qualitative and informative.

7. Discussion

Based upon several hundreds of microthermometric measurements on hydrosaline melt inclusions from the Miocene of the Metaliferi Mountains, Eastern Carpathians and the Upper Cretaceous porphyry Cu-(Mo)-(Au) deposits in the Banat region and pegmatites from Vlădeasa granite massif in the North Apuseni Mountains, Pinteá (1993; 1997; 2002; 2009; 2012; 2014) it has been shown that there are at least four types of partial homogenization to one or more liquids as follows: **1.** complex silicate melt - hydrosaline melt inclusions showing silicate melt-salt melt assemblages at partial homogenization

temperature $T_{hp} = 1100^\circ$ to $> 1300^\circ\text{C}$ by vapor bubble homogenization in the salt melt fraction; **2.** hydrosaline melt inclusions without visible liquid solution at room temperature conditions, forming a salt melt and silicate melt immiscible mixture between 1000° to $>1200^\circ\text{C}$ by bubble disappearance in the salt melt globule; **3.** hydrosaline melt inclusions with some aqueous liquid fraction generating salt melt \pm silicate melt rim \pm unmelted solid phases after vapor bubble homogenization between 700° to 1000°C ; and **4.** brine inclusions with a larger aqueous liquid fraction homogenizing by vapor bubble or halite disappearance at temperatures between 450°C (or lower especially in the Upper Cretaceous samples) to less than 700°C - 800°C .

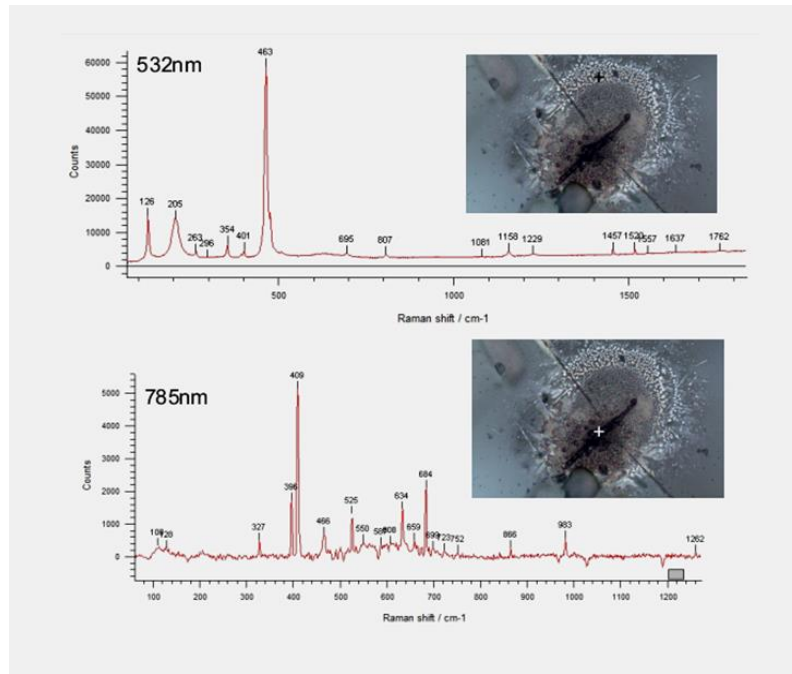


Fig. 19. Raman spectra of the decrepitated mound precipitated concentrically around the former hydrosaline melt inclusion in quartz from Roşia Poieni porphyry Cu-Au-(Mo) deposit. (see text for explanations).

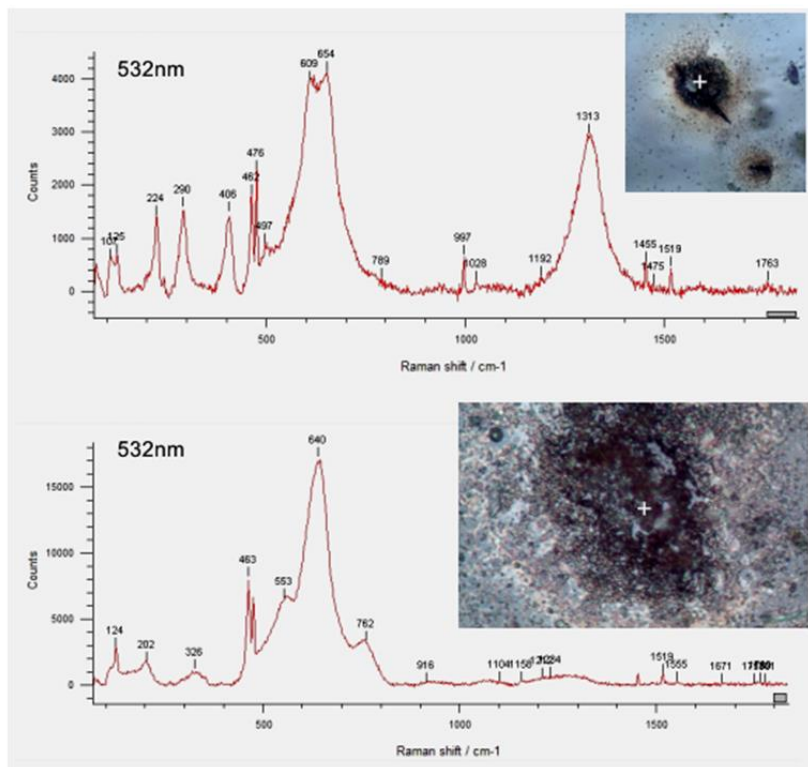


Fig. 20. Raman spectra of decrepitated mound precipitated around the former hydrosaline melt inclusion in quartz from Bolcana porphyry Cu-Au-(Mo) deposit (see text for explanations).

By fixing the formation temperature at around 1085°C based upon the beginning of the silicate liquid formation in hydrosaline melt inclusions and salt melt exsolution in the contemporaneous silicate melt inclusions in the same assemblage (Pintea, 1995, 1996b, 2007, 2009, 2014), it is rational to compare these entrapment conditions to the Burnham model (1979) of granodioritic magma crystallization as a primary source of fluid and ore elements (protore) in porphyry copper genesis (Bodnar, 1995; Becker, 2008, Bodnar, 2010). That is a dynamic fluid-melt system sourced at the bottom of the magma chamber by successive basic influxes especially with a volatile-rich front interacting with felsic mushes above. The main porphyry stock formation contains representative quartz veinlets in successive cross-cutting relationships with potassic and phyllic mineralization–alteration facies (e.g. Sillitoe, 2010). This means that the melting/renucleation temperatures of the solid daughter phases determined by microthermometry coupled with Raman spectroscopy in this study suggest successive fluid-melt fractionation during decompression and changing temperature. This happens during the transition from the magmatic to hydrothermal stages in the presence of a hydrous silicate melt (silicothermal fluid) which segregates chlorides, sulfides, sulfates, oxide phases, and partitions the ore elements by immiscibility and boiling episodes.

Similar results were published recently by Mernagh and Mavrogenes (2019) for the Grasberg porphyry Cu-Au deposit, especially the case of their defined B2 hydrosaline melt inclusion in quartz paragenesis, which is similar to the hydrosaline inclusions in porphyry copper systems in Romania (e.g. Pintea, 2014). By coupling microthermometry with LA-ICP-MS, their study has shown the chemical complexity of these high-temperature inclusions containing Na (20-60 wt%), K (20-40 wt%, occasionally up to 70 wt%) and Fe (20-50 wt%) as major elements and lower amounts of Li, Mg, Al, S, Ca, Ti, Cu, As, Se, Rb, Sr, Y, Mo, Cs, Ce, Yb and Pb. The majority of these components are transported initially as chloride and sulfide/oxide complexes and they melted and recrystallized “in situ” during heating/quenching microthermometric cycles.

There is now important evidence on the presence of FeCl₂-KCl-NaCl in hydrosaline melt inclusions and other fluid inclusion types (Koděra et al., 2014; Mernagh and Mavrogenes, 2019) together with H₂O-NaCl (Bodnar et al., 1985), H₂O-CaSO₄ (Kotel'nikova and Kotel'nikov, 2010, 2016), H₂O-CaCO₃ (Kotel'nikova and Kotel'nikov, 2011) evolving from a hydrosilicate liquid (Smirnov et al., 2017) in various P-V-T-X conditions. In our study, they form at temperatures of about 1085°C, the pressure ranges from less than 100 bar up to more than 2kb, and the salinity from 30 wt% to more than 70-80 wt% NaCl eq. It is worth mentioning that hydrosilicate liquid behaves as a colloidal solution or silicothermal fluid-melt emulsion (e.g. Pirajno, 2009; Wilkinson et al, 1996; 2015; Thomas and Davidson, 2016; Pintea et al., 2018) from which chloride melt, sulfide and oxide segregated by immiscibility and successive boiling episodes during decompression and temperature changes. Around 100 Raman spectra on hydrosaline and vapor-rich melt inclusions from porphyry Cu-Au-Mo deposit in both regions mentioned above, suggest the presence of CO₂, CO₃²⁻, HCO₃⁻, SO₄²⁻, PO₄³⁻, and the molecular vibration modes of S-H, C-H and O-H could be assigned to H₂S, CH₄, CO₂ and H₂O as main volatile phases partitioned between silicate melt and aqueous fluid. The latest ones were already measured quantitatively by Gas Chromatography – Mass Spectrometry in the Miocene porphyry Cu-Au deposit from the Metaliferi Mountains (Pintea, 1996; Cuna et al., 2001);

8. Conclusions

Complementary microthermometry and Raman spectroscopy data in this study on silicate melt and hydrosaline melt inclusions from Upper Cretaceous and Miocene porphyry Cu-(Au)-(Mo) deposits from the Banat region and the South Apuseni Mountains (Metaliferi Mountains) confirmed the previously published data and observations (Pintea, 2014, and references therein), indicating the complexity of the PVTX trapping conditions in these deposits. Many of the included phases are truly daughter mineral phases formed from a complex hydrosilicate liquid mainly by fluid-melt immiscibility.

The most important successive phase transitions are the following:

A. Heating melting temperatures:

1. Hydrous compounds or other solid complexes including sylvite (~70°-300°C);
2. The second melting points (~300°-350°) of solid complexes such as javorieite (KFeCl₃ - Koděra et al., 2017);
3. Halite melting temperature (468°-662°C), the main T_m reference for salinity estimation;
4. Magnetite and/or hematite turning to hematite and/or FeCl₂ or an opaque liquid phase, respectively (786°-1068°C);
5. Anhydrite final dissolution temperature (723°-1063°C) in hydrous salt-silicate melt association;

6. Vapor-rich “melt” bubble (Vm) dissolution temperature at the final homogenization temperature (Th) or sulfide-salt-silicate immiscible final phase state (682°-1426°C, Pintea, 2014).

B. Main quenching temperatures are the following:

1. Sudden Vm (i.e. vapor-rich “melt”) renucleation (1284°-659°C, Pintea, 2014);

2. Opaque phase recrystallization (845°-681°C);

3. Anhydrite renucleation (658-793°);

4. Chalcopyrite precipitation (650°-500°C);

5. Halite renucleation (574°-255°C);

6. Another opaque and transparent phase formation (less than 200°C).

It is worth noting that during heating/quenching cycles the opaque phases and other saline/silicate/sulfate compounds remain in a liquid state over a large temperature interval. However, the microthermometry cycles are not always reproducible mainly because of “in-situ” modifications, during heating-cooling especially for chalcopyrite (see also Spencer et al., 2015). Anyhow, the high-temperature microthermometry in silicate-, and hydrosaline melt inclusions coupled with Raman spectroscopy give the following valuable information on P-T-X properties of the initial enclosed fluid/melt phases:

- during the heating procedure at least two (or three) liquid (melt) phases are coexistent around the proposed entrapment temperature suggesting immiscibility and/or heterogeneous trapping;
- on quenching, a vapor-rich “melt” is suddenly renucleated followed by the recrystallization of sulfates, oxides, silicates, sulfides and saline daughter microphases. Frequently, a coarsened solid phase, presumably a “clathrasil” compound, is precipitated after trapping and never remelts during additional microthermometry. Its presence suggests that initially the hydrosaline melt inclusions were more silica-rich and they were obviously heterogeneously trapped;
- the Raman spectroscopy suggests the presence of CO₂, CO₃²⁻, HCO₃⁻, SO₄²⁻, PO₄³⁻, and the molecular vibration modes of S-H, C-H and O-H could be assigned to H₂S, CH₄, CO₂ and H₂O as main volatile phases partitioned between silicate melt and aqueous fluid;
- the complex fluid phase assemblages exsolved from deep MASH zones, where the parental melt originated and mixed again at shallow levels with silicate crystal mushes, are the precursors of mineralized high temperature potassic and phyllic alteration zones in Alpine porphyry Cu-(Au)-(Mo) deposits from Romania.

Acknowledgements. The study has been partially supported by the Research Projects no. PN19-45-01-02 financed by the Romanian Ministry of Research and Innovation, and no. 29 PCCDI/2018 “GEORES” and PN-III-P4-ID-PCCF-2016-4-0014 “CUTE” financed by UEFISCDI, Romania. Many thanks to Dr. T. Mernagh for valuable criticism improving substantially the manuscript.

References

- Audétat A., Simon A.C. (2012) Magmatic controls on porphyry copper genesis. *Soc. Econ. Geol., Inc., Spec. publ.*, 16, p. 553-572.
- Bakker R.J. (2003) Package FLUIDS 1. Computer programs for analysis of fluid inclusion data and for modelling bulk fluid properties. *Chem. Geol.*, 194, p. 3-23.
- Becker S.P. (2007) Fluid inclusion characteristics in magmatic-hydrothermal ore deposits. PhD thesis, Virginia Polytechnic Inst. and State Univ., Blacksburg, VA, USA, 138p.
- Becker S.P., Fall A., Bodnar R.J. (2008) Synthetic fluid inclusions. XVII. PVTX properties of high salinity H₂O-NaCl solutions >30 wt% NaCl: application to fluid inclusions that homogenize by halite disappearance from porphyry copper and other hydrothermal ore deposits. *Econ. Geol.* 103, p. 539–554.
- Berbeleac I., Udubaşa S.S., Iatan E.L., Vişan M. (2014) Geological and structural constraints on the localization of Neogene porphyry-epithermal related Cu-(Au)-(Mo), and epigenetic hydrothermal deposits/prospects from South Apuseni Mts., Romania. *Rom. J. Miner. Deposits*, 87/1, p. 47-52.
- Blundy J., Mavrogenes J., Tattitch J.B., Sparks S., Gilmer A. (2015) Generation of porphyry copper deposits by gas-brine reaction in volcanic arcs. *Nature Geosci.* 8, p. 235-240.
- Bodnar R.J. (1995) Fluid inclusion evidence for a magmatic source for metals in porphyry copper deposits. *Mineralogical Association of Canada, Short Course Volume 23*, p. 139–152.
- Bodnar R.J. (2003) Introduction to aqueous-electrolyte fluid inclusions. In: Samson I., Anderson A., Marshall D. (eds.) *Fluid Inclusions: Analysis and Interpretation*. Mineralogical Association of Canada Short Course, 32, p. 81-100, Québec.
- Bodnar R.J. (2010) Magmatic fluid evolution associated with epizonal silicic plutons. *ACROFI & TBG XIV*, Novosibirsk, Russia, *Abstr. Vol.*, p. 30-31.

- Bodnar, R.J., Burnham, C.W., Sterner, S.M. (1985) Synthetic fluid inclusions in natural quartz. III. Determination of phase equilibrium properties in the system H₂O-NaCl to 1000°C and 1500 bars. *Geochim. et Cosmochim. Acta*, 49, p. 1861–1873.
- Bodnar R.J., Sterner S.M. (1987) Synthetic fluid inclusions. In: Ulmer G.C. and Barnes H.L. (eds.) *Hydrothermal experimental techniques*. New York, Wiley-Interscience, p. 423–457.
- Bodnar R.J., Vityk, M.O. (1994) Interpretation of microthermometric data for H₂O-NaCl fluid inclusions. In: De Vivo B. and Frezzotti M.L. (eds.) *Fluid Inclusions in Minerals: Methods and Applications*. Virginia Tech, Blacksburg, VA, p. 117-130.
- Braxton D.P. (2007) Bayongan and Bayugo porphyry gold deposits NE Mindanao, Philippines: geology, geochemistry, and tectonic evolution. PhD thesis, Univ. of Tasmania, 277p.
- Burke E.A.J. (1994) Raman microspectrometry of fluid inclusions: the daily practice. In: De Vivo B. and Frezzotti M. L. (eds.) *Fluid Inclusions in Minerals: Methods and Applications*. Virginia Tech., Blacksburg, VA, p. 25-44.
- Burnham C.W. (1979) Magmas and hydrothermal fluids. In: Barnes H.L. (ed.) *Geochemistry of Hydrothermal ore deposits*. 2nd Ed. John Wiley, New York, p. 71–136.
- Campbell A.R., Lundberg S.A.W., Dunbar N.W. (2001) Solid inclusions of halite in quartz: evidence for the halite trend. *Chem. Geol.*, 173, p. 179-191.
- Campos E., Touret J.L.R., Nikogosian I., Delgado J. (2002) Overheated, Cu-bearing magmas in the Zaldívar porphyry-Cu deposit, Northern Chile. *Geodynamic consequences*. *Tectonophysics*, 345, p. 229-251.
- Cioacă M, Munteanu M. (2012) The present state of knowledge on the high technology elements in porphyry copper deposit from Romania. EGU General Assembly 2012, Geophysical Research Abstracts, Vol. 14, EGU2012-4402.
- Ciobanu C.L., Cook N.J., Stein H. (2002) Regional setting and geochronology of the Late Cretaceous Banatitic Magmatic and Metallogenic Belt. *Miner Deposita*, 37, p. 541-567.
- Cloke P.L., Kesler S.E. (1979) The halite trend in hydrothermal solutions. *Econ. Geol.*, 74, 8, p. 1823-1831.
- Cuna S., Palibroda N., Cuna C., Pintea I. (2001) The mass spectrometric method for analysis of volatile species from fluid inclusions. ABCD-GEODE Workshop, Vața Băi, Romania. *Rom. J. Miner. Deposits*, 79, suppl 2., p. 48-49.
- Damian F. (2003) The Mineralogical Characteristics and the Zoning of the Hydrothermal Types Alteration from Nistru Ore Deposit, Baia Mare Metallogenic District. *Studia Univ. "Babeș-Bolyai", Geol.*, XLVIII, 1, p. 101-112.
- Damman A.H., Kars S.M., Touret J.L.R., Rieffe E.C., Kramer J.A.L.M., Vis R.D., Pintea I. (1996) PIXE and SEM analysis of fluid inclusions in quartz crystals from the K-alteration zone of the Rosia Poieni porphyry Cu deposit, Apuseni Mountains, Rumania. *Eur. J. Mineral*, 8, p. 1081-1096, Stuttgart. Germany.
- Drew L.J. (2006) A tectonic model for the spatial occurrence of porphyry copper and polymetallic vein deposits - applications to Central Europe. U.S. Geological Survey Scientific Investigations Report 2005–5272, 36 p.
- Driesner T., Heinrich C. A. (2007) The System H₂O–NaCl. Part I: correlation formulae for phase relations in temperature-pressure-composition space from 0 to 1000°C, 0 to 5000 bar, and 0 to 1 X_{NaCl}. *Geochim. et Cosmochim. Acta* 71 (20), p. 4880–4901.
- Driesner T. (2007) The System H₂O–NaCl. II. Correlations for molar volume, enthalpy, and isobaric heat capacity from 0 to 1000 degrees C, 1 to 5000 bar, and 0 to 1 X_{NaCl}. *Geochim. et Cosmochim. Acta* 71(20), p. 4902-4919.
- Ducea M.N., McInnes B.I.A., Wyllie P.J. (1999) Experimental determination of compositional dependence of hydrous silicate melts on sulphate solubility. *Eur. J. Mineral.*, 11, p. 33-43.
- Eastoe C.J. (1978) A fluid inclusion study of the Panguna porphyry copper deposit, Bougainville, Papua New Guinea. *Economic Geology*, 73, p. 721–748.
- Edmonds M. (2015) Flotation of magmatic minerals. *Geology*, 43, 7, p. 655-656.
- Frezzotti M.L., Tecce F., Casagli A. (2012) Raman spectroscopy for fluid inclusion analysis. *Journ. of Geochim. Expl.*, 112, p. 1-20.
- Gallhofer D. (2015) Magmatic geochemistry and geochronology in relation to the geodynamic and metallogenic evolution of the Banat Region and the Apuseni Mountains of Romania. Diss. thesis ETH Zürich No. 22888, 145p.
- Gheorghită I. (1975) Mineralogic and petrographic study of the Moldova Nouă region Suvorov-Valea Mare zone. (In Romanian with extended English abstract). *Inst. Geol., Geofiz., Stud. Tehn. Econ., Ser. I., Min. -Petrogr.*, nr.11, 188p.
- Hack A.C., Mavrogenes J.A. (2006) A synthetic fluid inclusion study of copper solubility in hydrothermal brines from 525 to 725°C and 0.3 to 1.7 GPa. *Geochim. et Cosmochim. Acta*, 70, p. 3970-3985.
- Harris C.R., Pettke T., Heinrich C.A., Roșu E., Woodland S., Fry B. (2013) Tethyan mantle metasomatism creates subduction geochemical signatures in non-arc Cu–Au–Te mineralizing magmas, Apuseni Mountains Romania. *Earth and Planet. Sci. Lett.*, 366, p. 12-136.
- Haynes F.M., Sterner S.M., Bodnar R.J. (1988) Synthetic fluid inclusions in natural quartz. IV. Chemical analyses of fluid inclusions by SEM/EDA: Evaluation of method. *Geochim. et Cosmochim. Acta*, 52, p. 969-977.

- Heinrich C.A., Cousens D.R. (1989) Semi-quantitative electron microprobe analysis of fluid inclusion salts from the Mount Isa copper deposit Queensland, Australia. *Geochim. et Cosmochim. Acta*, 53, p. 21-28.
- Heinrich C.A., Halter W., Landtwing M.R., Pettke T. (2005) The formation of economic porphyry-gold deposits: constraints from microanalysis of fluid and melt inclusions. In: McDonald I., Boyce A.J., Buttler I.B., Herrington R.J., Polya D.A. (eds.) *Mineral Deposit and Earth evolution*. Geol. Soc. London, Spec. Publ. 248, p. 247-263.
- Henley R.W., Brink F.J., King P.L., Leys C., Ganguly J., Mernagh T., Middleton J., Renggli J.C., Sieber M., Troitzsch U., Turner M. (2017) High temperature gas-solid reactions in calc-silicate Cu-Au skarn formation; Ertsberg, Papua Province, Indonesia. *Contrib. Mineral. Petrol.*, 172:106. (<https://doi.org/10.1007/s00410-017-1413-6>)
- Hurai V., Huraiová M., Slobodník M., Thomas R. (2015) *Geofluids - Developments in Microthermometry, Spectroscopy, Thermodynamics, and Stable Isotopes*. Elsevier, 489p.
- Hollister V.F. (1975) An appraisal of the nature and source of porphyry copper deposits. *Min. Sci. Eng.*, 7, p. 225-233.
- Hovland M., Rueslåtten H., Johnsen H.K. (2014) Buried hydrothermal systems: the potential role of supercritical water," ScriW", in various geological processes and occurrences in the sub-surface. *Amer. Jour. of Analytical Chem.*, 5, p. 128-139.
- Ianovici V., Vlad Ş., Borcoş M., Boştinescu S. (1977) Alpine porphyry copper mineralization of West Romania. *Mineralium Deposita*, 12(3), p. 307-317. DOI:10.1007/bf00206169.
- Ilinca G., Berza T., Iancu V., Seghedi A. (2011) The late Cretaceous magmatic and metallogenetic belt and the alpine structures of the western south Carpathians. Field trip guide book. The 3rd Int. Symp. on the Geol. of the Black Sea Region, 1-10 oct. 2011, Bucharest, Romania.
- Ilinca G. (2012) Upper Cretaceous contact metamorphism and related mineralization in Romania. *Acta Mineralogica-Petrographica, Abstract Series, Szeged*, 7, p. 59-64.
- Knipping J.L., Bilenker L.D., Simon A.C., Reich M., Barro F., Deditius A.P., Wälle M. Heinrich C.A., Holtz F., Munizaga R. (2015) Trace elements in magnetite from massive iron oxide-apatite deposits indicate a combined formation by igneous and magmatic-hydrothermal processes. *Geochim. et Cosmochim. Acta*, 171, p. 15-38.
- Knipping J.L., Webster J.D., Simon A.C., Holtz F. (2019) Accumulation of magnetite by flotation on bubbles during decompression of silicate magmas. *Scientific Reports* 2019 March 7, 91, p. 3852.
- Koděra P., Heinrich C.A., Fallick A.E., Lexa J., Biroň A. (2014) Magmatic salt and vapor: Extreme fluids forming porphyry gold deposits in shallow subvolcanic settings. *Geology*, 42, 6, p. 495-498.
- Koděra P., Tacách Á., Racek M., Šimko F., Luptáková I., Váczi T., Antal P. (2017) Javorieite, KFeCl₃: a new mineral hosted by salt melt inclusions in porphyry gold systems. *Eur. J. Mineral.*, 6, p. 995-1004.
- Kontak D.J. (2004) Analysis of evaporate mounds as a complement to fluid-inclusion - thermometric data: case studies from granitic environments in Nova Scotia and Peru. *Canadian Mineralogist*, v. 42, p. 1315-1327.
- Kontak D.J. (2013) Fluid inclusion evaporate mound analysis: a rapid, efficient and informative means of determining fluid chemistry in hydrothermal systems. *Atlantic Geol.*, 49, 1, p. 34.
- Kotel'nikova Z.A., Kotel'nikov A.R. (2010) Experimental study of heterogeneous fluid equilibria in silicate-salt-water systems. *Geol. of Ore Dep.*, 52, 2, p. 154-166.
- Kotel'nikova Z.A., Kotel'nikov A.R. (2011) Na₂CO₃-bearing fluids: Experimental study at 700°C and under 1, 2, and 3kbar pressure using synthetic fluid inclusions in quartz. *Geol. of Ore Dep.*, 53, 2, p. 156-170.
- Kotel'nikova Z.A., Kotel'nikov A.R. (2016) Immiscibility in sulphide-bearing fluid systems at high temperatures and pressures. *Geochem. Internat.*, 48, 4, p. 381-389.
- Kouzmanov K., Pettke T., Heinrich C.A. (2010) Direct Analysis of Ore-Precipitating Fluids: Combined IR Microscopy and LA-ICP-MS Study of Fluid Inclusions in Opaque Ore Minerals. *Econ. Geol.*, 105, p. 351-373.
- Kouzmanov K., Pokrovsky G.S. (2012) Hydrothermal controls on metal distribution in porphyry Cu-Mo-Au systems. *Soc. Econ. Geol., Inc., Spec. Publ.*, 16, p. 573-618.
- Kozák J., Koděra P., Lexa J., Bakos F., Molnár L., Wälle M. (2017) Porphyry gold system of Beluj in the mantle of the Štiavica stratovolcano Slovakia. *Acta Geol., Slovaca*, 9, 1, p. 45-61.
- Lerchbaumer L., Audétat A. (2012) High Cu concentrations in vapor-type fluid inclusions: an artifact? *Geochim. et Cosmochim. Acta*, 88, p. 255-274.
- Li Y., Audétat A., Lerchbaumer L., Xiong X.L. (2009) Rapid Na, Cu exchange between synthetic fluid inclusions and external aqueous solutions: evidence from LA-ICP-MS analysis. *Geofluids*, 9, p. 321-329.
- Lowell, J.D., Guilbert, J.M. (1970) Lateral and vertical alteration-mineralization zoning in porphyry ore deposits: *Econ. Geol.*, v. 65, p. 373-408.
- Lowenstern J.B. (1993) Evidence for a copper-bearing fluid in magma erupted at the Valley of Ten Thousand Smokes, Alaska. *Contrib. Mineral. Petrol.*, 114, 3, p. 409- 421.
- Mavrogenes J., Bodnar R.R. (1994) Hydrogen movement into and out of fluid inclusions in quartz: Experimental evidence and geologic implications. *Geochim. et Cosmochim. Acta*, 58(1), p. 141-148.
- Mernagh T.P., Mavrogenes J. (2019) Significance of high temperature fluids and melts in the Grasberg porphyry copper-gold deposit. *Chem. Geol.*, 508, p. 210-224.
- Momma K. (2014) Clathrate compound of silica. *J. Phys.: Condens. Matter* 26 20141032013, 18p.

- Mungall J.E., Brenan J.M., Godel B., Barnes S.J., Gaillard F. (2015) Transport of metals and sulphur in magmas by flotation of sulphide melt on vapour bubbles. *Nat. Geosci.*, 8, p. 216-219.
- Nash T.J. (1976) Fluid inclusion petrology-data from porphyry copper deposits and applications to exploration. U.S. Geol. Survey, Prof. Paper, 907-D, 16 p.
- Pintea I. (1993) Microthermometry of the hydrosaline melt inclusions from copper - porphyry ore deposits Apuseni Mountains, Romania. *Arch. Mineral.* XLIX, p. 165-167, Warsaw, Poland.
- Pintea I. (1995) Fluid inclusion evidence for magmatic immiscibility between hydrous salt melt and silicate melt as primary source of ore metals in porphyry copper system from Apuseni Mountains, Romania. *Bol. Soc. Espagnola Mineralogia*, 18 - 1, p. 184-186, Barcelona *and* *Rom. Jour. of Mineralogy* 77/2, suppl. pages.
- Pintea I. (1996a) New aspects of fluid phase evolution during genesis of the porphyry copper ore deposits from South Apuseni as seen in fluid inclusions. *Ann. IGR.*, 69, Suppl. 1, 166, Bucharest.
- Pintea I. (1996b) Fluid inclusion study with special view on immiscibility of the fluid phases associated in porphyry copper genesis from Apuseni Mountains. PhD thesis, Bucharest Univ., 172 p (in Romanian, unpublished).
- Pintea I. (1997) The significance of the liquid homogenisation temperature in salt melt inclusions. A case study in Neogene porphyry copper ore deposits from Metaliferi Mountains western Romania. *ECROFI-XIV*, Nancy, France July 1-4, Abstr. Vol., p. 266.
- Pintea I. (2002) Occurrence and microthermometry of the globular sulfide melt inclusions from extrusive and intrusive volcanic rocks and related ore deposits from Alpine Carpathian chain Romania "Volcanic Systems - Geochemistry and Geophysics Monitoring" Workshop - Napoli, Italy. Short Course, *Proced.*, Abstr. vol., p. 177-180.
- Pintea I. (2009) Still problematic facts on the fate of brines in the Alpine porphyry copper systems in Romania. *ECROFI XX*, Granada, Spain, Abstr. vol., p. 187 - 188.
- Pintea I. (2010) Fluid and melt inclusions evidences for autometasomatism and remelting in the Alpine porphyry copper genesis from Romania. The 7th Nat. Symp. on Econ. Geol., "Mineral Resources of Carpathian area", 10 - 12 Sept. 2010, Baia Mare. *Romanian Journal of Mineral Deposits*, Vol. 84, Spec. issue, p. 15-18.
- Pintea. I. (2012) Fluid and melt inclusions: a precious tool in selective exploration strategy. *Rom. J. of Mineral Dep.*, 85, 1, p. 85-89.
- Pintea I. (2014) The magmatic immiscibility between silicate-, brine-, and Fe-S-O melts from the porphyry Cu-(Au)-(Mo) deposits in the Carpathians Romania: a review. *Rom. J. of Earth Sci.* 87, 1, online first, 32p.
- Pintea I. (2016) A self-perspective research topic revealed during the elaboration of the Atlas "Fluid and Melt Inclusions from Romania". *Rom. J. of Min. Dep.*, 89, 1-2, p. 1-6.
- Pintea I., Laczko A.A. (2005) Preliminary microthermometric data related to a complex magmatic-hydrothermal system from Sântimbru-Băi South-Harghita Mountains, Romania. *Geol. Soc. Romania meeting, Rosia Montana, Romania, Proceed.* Vol., p. 25-96.
- Pintea I., Nuțu-Dragomir M.-L., Udubașa S.S., Bîrgăoanu D., Iatan E.L., Berbelec I., Ciobotea-Barbu O.C. (2018) Hydrosilicate aqueous-, and vapor- "melt" inclusions in some specific rocks and minerals from Romania. *Rom. J. of Min. Dep.*, 91, 1-2, p. 13-18.
- Pintea I., Udubașa G., Nedelcu L. (1999) Evolution of fluid phases related to a new porphyry copper deposit in Romania: The Tibles massif. In: Stanley et al. (eds) *Mineral Deposits: Processes to Processing*, Balkema, Rotterdam, p. 83-85.
- Pintea I., Udubasa S.S., Nutu-Dragomir L. M., Iatan E.L., Berbelec I., Petrescu L., Ghinescu E. (2019) Clathrasil compound evidence in fluid and brine inclusions by microthermometry and Raman spectroscopy. *Goldschmidt Conference 2019, Barcelona, Spain, abstract online.*
- Pirajno F. (2009) *Hydrothermal processes and mineral systems*. Springer Science+Media B.V., 1273p.
- Pomârleanu V., Intorsureanu I. (1985) Salinity of fluid inclusions of porphyry copper ore deposits and their significance in geobarometry and prospecting the Lăpușnicu Mare ore deposit - Banat. *D.S. Inst. Geol. Geofiz.*, 70-71/2 (1983; 1984), p. 83-95.
- Ramboz C. (1979) A fluid inclusion study of the copper mineralization in Southwest Tintic district Utah. *Bull. Mineral.*, 102, p. 622-632.
- Redmond P.B., Einaudi M.T., Inan E.E., Landtwing M.R., Heinrich C.A. (2004) Copper deposition by fluid cooling in intrusion-centered systems: New insights from the Bingham porphyry ore deposit, Utah. *Geology*, 32, 3, p. 217-220.
- Renno A.D., Franz L., Witzke T., Herzig P.M. (2004) The coexistence of melts of hydrous copper chloride, sulphide and silicate compositions in a magnesiohastingsite cumulate, TUBA Seamount, Papua New Guinea. *The Canadian Mineralogist.*, 42, p. 1-16.
- Richards J.P. (2009) Postsubduction porphyry Cu-Au and epithermal Au deposits: Products of remelting of subduction-modified lithosphere. *Geology*, 37, p. 247-250.
- Roedder E. (1971) Fluid inclusion studies on the porphyry type ore deposits at Bingham Utah, Butte Montana and Climax Colorado. *Econ. Geol.*, 66, p. 98-120.
- Roedder E. (1984) Fluid inclusions. *Reviews in Mineralogy*, 12, 644 p.
- Roedder E., Bodnar R.J. (1980) Geologic pressure determinations from fluid inclusion studies. *Earth Planet. Sci., Ann. Rev.*, 8, p. 263-301.

- Roşu E., Seghedi I., Downes H., Alderton D.H.M., Szakács A., Péckaj Z., Panaiotu C., Panaiotu E.C., Nedelcu L. (2004) Extension-related Miocene calc-alkaline magmatism in the Apuseni Mountains, Romania: origin of magmas. *Schw. Miner. Petrogr. Mitt.* 84, p. 153-172.
- Sanchez-Lecumberri P., Steele-McInnis M., Bodnar R.J. (2012) A numerical model to estimate trapping conditions of fluid inclusions that homogenize by halite disappearance. *Geochim. et Cosmochim. Acta*, 92, p. 14-22.
- Seo J.H., Heinrich C.A. (2013) Selective copper diffusion into quartz-hosted vapour inclusions: evidence from other host minerals, driving forces and consequences for Cu-Au ore formation. *Geochim. et Cosmochim. Acta*, 113, p. 60-69.
- Sillitoe R.H. (2010) Porphyry copper systems. *Economic Geology*, v. 105, p. 3–41.
- Smirnov S.Z., Thomas V.G., Kamenetsky V.S., Kozmenko O.A. (2017) Hydrosilicate liquids in the system rare-metal granite-Na₂O-SiO₂-H₂O as accumulators of ore components at high pressure and temperature. *Petrology*, 25, 6, p. 625-635.
- Spencer E.T., Wilkinson J.J., Nolan J., Berry A.J. (2015) The control of post-entrapment diffusion on the solubility of chalcopyrite daughter crystals in natural quartz-hosted fluid inclusions. *Chem. Geol.*, 412, p. 15-25.
- Steele-MacInnis M., Sanchez-Lecumberri P., Bodnar J.R. (2012) HokieFlincs-H₂O-NaCl: a microsoft Excel spreadsheet for interpreting microthermometric data from fluid inclusions based on the PVTX properties of H₂O-NaCl. *Computers and Geosci.*, 49, p. 334-337.
- Stefanova E., Driesner T., Zajaz Z., Heinrich C.A., Petrov P., Vasiliev Z. (2014) Melt and fluid inclusions in hydrothermal veins: the magmatic to hydrothermal evolution of the Elatsite porphyry Cu-Au deposit, Bulgaria. *Econ. Geol.*, 109, p. 1359-1381.
- Sterner M.S., Bodnar R.J. (1987) Synthetic fluid inclusions. In *Hydrothermal experimental techniques* (Ulmer G.C., Barnes H.L., eds), p. p. 423-457.
- Thomas R., Davidson P. (2016) Revisiting complete miscibility between silicate melts and hydrous fluids, and the extreme enrichment of some elements in the supercritical state - Consequences for the formation of pegmatite and ore deposits. *Ore Geol. Rev.*, 72, p. 1088-1101.
- Tornos F., Velasco F., Hanchar J.M. (2016) Iron-rich melts, magmatic magnetite, and superheated hydrothermal systems: The El Laco deposit, Chile. *Geology*, 44, 6, p. 427-430.
- Tweedale F., Hanley J.J., Kontak D.J., Rogers N. (2015) Petrographic observations and evaporate mound analysis of quartz-hosted fluid inclusions hosted by granitoid samples from the South Mountain Batholith, Nova Scotia: An exploration tool for vectoring towards mineralised areas in intrusive rocks. In: Rogers N. (ed.) *TGI4 – Intrusion Related Mineralisation Project: New Vectors to Buried Porphyry-Style Mineralisation*. Geological Survey of Canada, Open File 7843, p. 79-99.
- Udubaşa G., Roşu E., Seghedi I., Ivăşcanu P.M. (2001) The “Golden Quadrangle” in the Metaliferi Mts., Romania: what does this really mean? *ABCD-GEODE Workshop, Vaţa Băi, Romania*. *Rom. J. Miner. Dep.*, 79, suppl 2, p. 24-34.
- Vlad S.N. (2011) Perspective targeting CuAuMo porphyries of Romanian Carpathians: blind porphyry mineralization and its variable distal expression as vein and skarns. *Cent. Eur. J. Geosci.*, 3(3), p. 318-335.
- Vlad Ş-N, Berza T. (2003) Banatitic magmatic and metallogenetic belt: metallogeny of the Romanian Carpathians segment. *Studia Universitatis Babeş-Bolyai, Geologia*, XLVIII, 1, 2003, p. 113-122.
- Weisbrod A. (1981) Fluid inclusions in shallow intrusives. In: Hollister L.S., Crawford M.L. (eds) *Mineral. Assoc. of Canada, Short course handbook 6*, p. 241-271.
- Wilkinson J.J., Nolan J., Rankin A.H. (1996) Silicothermal fluid: a novel medium for mass transport in the lithosphere. *Geology*, 24, p. 1059-1062.
- Wilkinson J.J., Vasyukova O., Laird J.S., Ryan C., Kamenetsky D. (2015) Hydrosilicate liquids: unconventional agents of metal transport in porphyry ore systems. *ECROFI, Leeds-UK, 27-29 June, 2015, Extended Abstracts Volume*, p. 116.
- Zimmerman A., Stein H.J., Hannah J.L., Koželi D., Bogdanov K., Berza T. (2008) Tectonic configuration of the Apuseni-Banat-Timok–Srednogorie belt, Balkans-South Carpathians, constrained by high precision Re–Os molybdenite ages. *Miner Deposita*, 43, p. 1-21.

SPHERULITES FROM LETEA BEACH RIDGE – DANUBE DELTA, PRELIMINARY DATA

Iulia NEGREA¹, Gheorghe C. POPESCU¹, Monica MACOVEI^{2*}, Eduard GHINESCU²

¹University of Bucharest, Faculty of Geology and Geophysics, Department of Mineralogy, 1, N. Bălcescu Blvd., Bucharest, Romania

²Geological Survey of Romania, 1, Caransebeş St., Bucharest, Romania

* *macoveimonica@yahoo.com*

Abstract. The sands that make up the Danube Delta and particularly Letea beach ridge are generated from detrital material transported both in the continental and maritime areas. In addition to those types of clasts, both industrial waste and meteoritic impact products have been identified. Surface samples from the sand deposited in the Letea beach ridge have been taken and analyzed in order to determine the origin of these sedimentary clasts, the present study is focused on the origin of some spheres that looked different from the rest of the material. The first identifications were made at the binocular magnifier, then spherulites of various sizes were analyzed, and chemistry and optical characters were identified. The conclusions of this preliminary study were clear about the existence of the two modes of generating spherulites: anthropic and cosmic activity.

Keywords: spherulites, microtektites, impactites, Danube Delta.

Introduction

Spherulites are a bundle, or a more or less completely spherical mass, of radiating fibrous crystals, often also showing concentric banding. Spherulites may be microscopic or be of several centimeters or more across. They occur as nodules in sedimentary rocks, but the term usually refers to spherulites in igneous rocks, where they are either dominantly glassy, devitrified, or hemicrystalline (Challinor, 1961).

The samples of sand (over 60) were taken from the surface sediments of Letea beach ridge, Danube Delta, in two phases: one campaign in 2012 and another in August 2013 (see localization in Fig. 1). The samples were collected separately and later divided into 4 or 5 granulometric classes (noted from S1 to S5). By incorporating into an acrylic resin, thin sections and polished sections were made for optical microscopy analysis.

During the observation under the binocular magnifier (Fig. 2 a-f) and the optical microscope (in both transmitted and reflected light) (Fig. 3, a-f), some spherical grains were identified. The structures were very unusual for some detrital sediments. They were mainly characterized by their lack of mechanical processing (a characteristic phenomenon for the sediment of the dunes) and a spherical external shape. Further analyzes have been conducted by the authors, both from a chemical and morphological point of view, and by comparison to the examples found in literature a new theory regarding their origin emerged: they might be the result of a newly formed material not far from the place where they were found. The energy needed for a material partial or total meltdown might be generated on meteoritic impact, and anthropic activity (metallurgical products).

1. Location and geological context

From a morphological point of view, the Danube Delta can be divided into two sectors: the river-delta to the west and the fluvial-maritime delta to the east. The present paper studies the area situated in the North-East, on the boundary between the two sectors - Letea beach ridge, a quasi-transversal barrier of the flow of the Danube with N-S orientation.

The landscape of the levee is generally characterized by the presence of constantly moving and changing sand dunes, the vegetation being insufficient for their complete fixation. The Letea's altitude varies as follows: out of a total area of 9250 ha, more than half - 5300 ha (57.3%) is located at 1-2 m above the sea level, 2870 ha (31.03%) is 2-3 m above the sea level and the rest of 1080 ha (11.67%) is over 3 m altitude; the maximum altitude is 12.4 m (maximum altitude at Danube Delta level). Due to this positive value altitude, the land surface of the Letea beach ridge is, in fact, a high marine plain (Vespremeanu, 2004).

The Danube Delta is made up of detrital deposits with varying thicknesses of up to 400 m. In most cases there is a "fining-up" deposit based on sandy deposits, sometimes rough, reaching to the gravel, and to the upper part, the size the fraction decreases to micrometers. The layout is not strictly, with climatic variations that come to complicate the storage and flow of aquifers in the area (Panin et al., 2004).



Fig. 1. Location of the investigated samples (P1/13-P51/13): left - a larger scale map, to show all the samples; right - a detail from the first map. Samples P1-P15 are located in the same area, in the sand dunes of Letea beach ridge (map on the right).

The heavy fraction consists of garnet, ilmenite, magnetite, zircon, rutile, titanite, monazite, epidote, staurolite, kyanite, tourmaline, apatite, amphiboles, sillimanite, pyroxenes, and chromite. The contents of ilmenite, zircon, magnetite, and rutile might be of economic interest if we weren't in a protected area. The distribution is unequal, and in other zones the contents are higher. In Caraorman the content varies between 20-150 kg/t and in Letea between 20-50 kg/t. Sărăturile and Chituc sand barriers contain major concentrations of 3-4 km long north of Sf. Gheorghe; they appear along the beach, especially in the area of sand dunes. In the Chituc area, accumulations of heavy minerals (29-36 kg/t) embroid the edge of the dry area. The external parts of the Caraorman and Sărăturile sandbanks contain 90% quartz. Basin bottom and sediments of the Danube Delta contain 2-12 kg/t of heavy minerals (Ianovici and Borcoș, 1983).

The beach ridges of the Danube Delta represent upper age seashores deposits (examples: Caraorman, Letea, Sărăturile, Chituc, etc.). The detrital material from which they are formed has two main sources: a part was brought by coastal sea currents and is represented by quartz sand (89-95% SiO₂ - sediments taken from the rivers of the Dnieper, Upper Bug, and Dnister), and another part is slightly finer and heavy minerals richer (2-3%), that was transported by the Danube (Gâștescu and Știucă, 2008).

2. Analytical methods

From the quantitative point of view, the largest part of the collected samples belongs to the light minerals: quartz and carbonates (most of the carbonates are of biotic origin) (Negrea et al., 2014).

The following laboratory analyses were applied: microscopical analysis in reflected and transmitted light, X-ray diffractometry as well as detailed analyzes on the scanning electron microscope (SEM) with EDS detector.

The first determinations were made by Carl Zeiss Jena binocular and Carl Zeiss Stemi 2000-C dissecting microscope. Photos have been taken with a Canon Powershot A640 attached to the Stemi 2000 (Fig. 2). For optical observations, a Carl Zeiss Jena Amplival microscope was used. Pictures of the polished section were taken with the Nikon Eclipse E - 400, 40 W, attached to a PANPHOT microscope (Fig. 3). Observations and photographs were made at the University of Bucharest - Faculty of Geology and Geophysics, as well as the X-ray diffraction analyses using a PANalytical X'Pert device.

Electronic microscopy analyzes have been conducted in the Microcosmos Laboratory of the Geological Institute of Romania using the Tabletop TM 3030 scanning microscope. The sample has been cleaned with ultrasounds and alcohol, and for an improved conductivity has been covered in silver.

3. Results

In the analyzed samples, some spherical shapes were identified (both in the observations made at the magnifier and in the following analyzes carried out on the thin and polished sections), that were discordant with the rest of the present granules from the same sample. They ranged from 90 – 300 μm in size.

The first major differentiation, based on optical properties, divided the spherulites into three classes: transparent, translucent, and opaque. Given the rather large compositional difference between the three classes, different origins can be assumed; it is unlikely that a single source would generate a similar structure of such different raw materials.

Detrital material transport in the sand is usually accomplished by saltation (especially in the case of so fine dust) under the influence of wind. As seen in Fig. 2 a, c, d, f, the surface of the granules is free of any impact or scratch marks (which demonstrates that these particles haven't undergone a long-term transport from the point of origin). On other examples (Fig. 2 b, e) the surface of the rounded granules is marked with transport traces. These observations lead to the conclusion of proximal origins for most of these spherulites. Clast's sphericity and surface smoothness necessarily suggest a melt-origin, so there may be two main sources of generation of these particles: anthropogenic (the particles are generated from

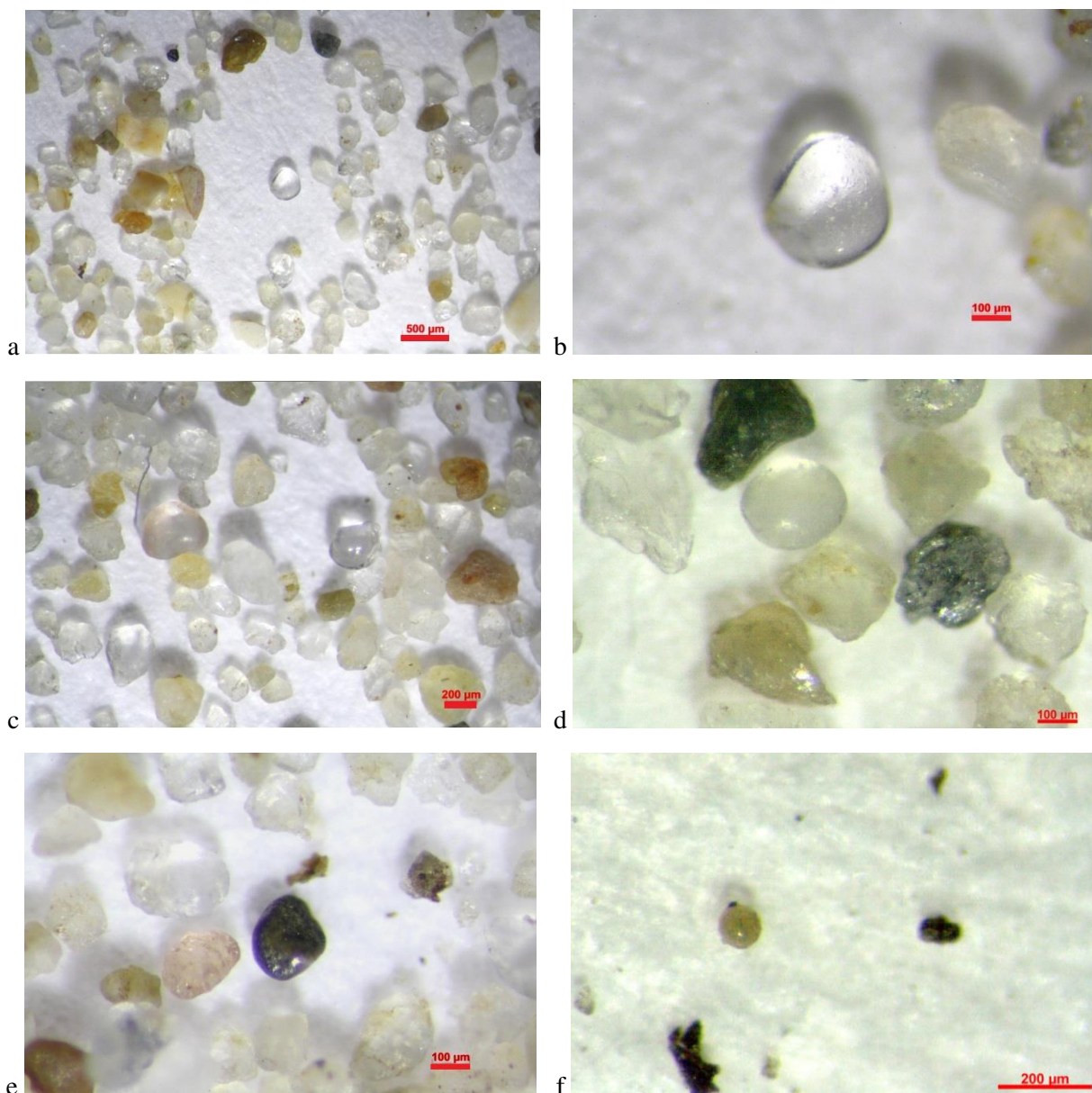


Fig. 2. Transparent spherulites (a, b, c, d), most likely coesite (in the central part of the photos, very rounded), opaque spherulite (e), translucent spherulites (f, g, h). Samples: a, b, c, e – P5; d – P4_S4; e –P49/13; f –P1_S; g – P10/13_S4.

industrial smoke emissions) and a natural one (in situ melting by meteoritic impact or lightning). Of course, the existence of transport traces does not exclude the possibility of an in-proximity generation of the material and short transport.

At impact, meteorites can generate recrystallized material that can be dispersed over very large distances (up to 100 km²). One of the most studied products of such impacts is tektite or microtektite (tektites that have one centimeter in size or right below this value). They are pure glass, called fulgurites, which are crystals that have undergone a melting after the action of lightning; these bulbous ones are rarely found, the usual form is the dendritically one.

Tektites are over a millimeter in size, therefore, at the level of the fraction presented in this paper, we will refer to microtektites (often preserved in marine sediments). It differs from volcanic products in that they are exclusively made of glass, without microlites or phenocrysts; the silica content exceeds 65% while isotope analysis (Taylor and Epstein, 1966) associates them with sedimentation rocks; the percentage of water is very low (below 0.02%); it forms structures in lechatelierite (molten glass). Some

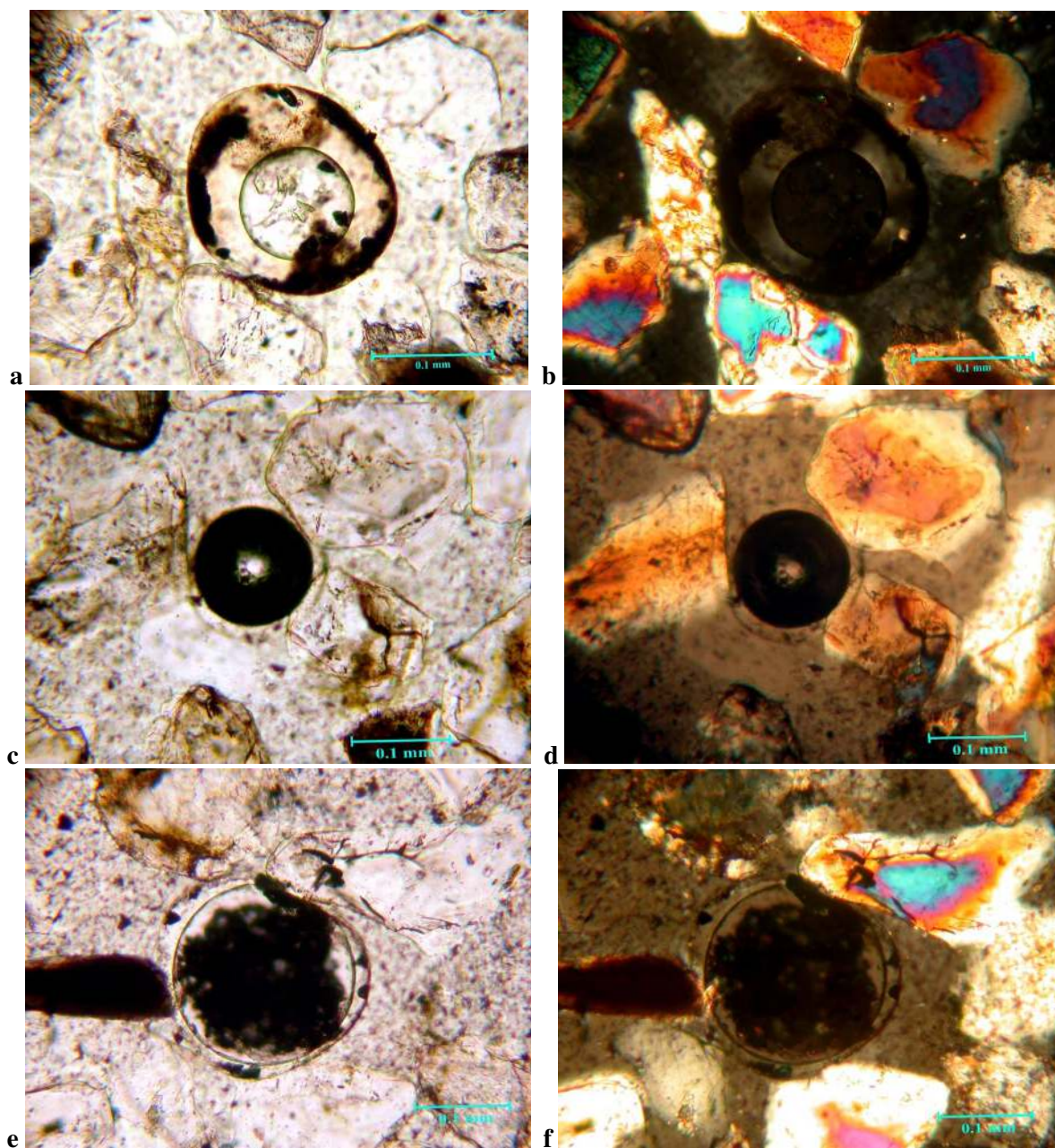


Fig. 3: Three spherulites from sample P5 in thin section (a, c, e: N//; b, d, f: N+): a, b – zoned concentric structure with opaque inclusions especially in the peripheric zone (optically corresponding to the silica); c, d – zoned structure with opaque median zone; e, f – zoned concentric structure with opaque minerals in the center part (a different rim can be noticed).

tektites/microtektites contain inclusions (quartz, apatite, zircon, and coesite) (Glass and Barlow, 1979). And microtektites usually appear spheroidal (French, 1998).

Microtektites have struck through their presence in thin sections (Fig. 3): perfectly round, isotropic granules, the result of melting. The images in the thin sections came to complement the information obtained from the physicochemical analyzes (XRD, SEM-EDS), finding various types of spherical crystals (from opaque to transparent, showing various inclusions).

These microtektites are composed of a quartz polymorph, coesite - identified by diffractometric analysis as a result of the existence of following lines – 3,098 (002); 3,432 (130) (111); 4,40 (021). The coesite forms at high pressures (2-3 GPa) and moderately elevated temperatures (150°C) or by a high impact force as the one generated by the meteoric impact. Its formation is determined by an impact force of 2 to 10 GPa, if there is a force bigger than that, stishovite is generated (Stöffler, 1971, Fig. 1; Grieve, 1990, p. 72; Grieve and Pesonen, 1992, in French, 1998).

The first natural occurrence of coesite was found by Chao et al. (1960) in Arizona, in a meteoritic crater. There is a restricted domain of pressure and temperature that can generate coesite in the eclogites (French, 1998). The closest source of metamorphic origin coesite would be in the Erzgebirge mountains in Germany, which would have assumed a fairly long transport that would certainly have left traces on the granules, especially that they are enclosed in metamorphic rocks (eclogite) and should first have been separated from the rest of the minerals and this, due to the low degree of stability, would have turned it into quartz as it happened with most of the rocks in that area, the coesite being seen as relics in the newly formed quartz (Massonne, 2001). Therefore, it is more plausible the in situ, recent, cosmic generation (as meteoritic impact) of this kind of grains.

Micro-spheres with a concentric morphology, consisting of opaque material or opaque and transparent mineral associations similar to Muong Nong (Glass and Barlow, 1979) have been identified.

Another possible origin of the spherulitic samples (Fig. 3) is the anthropogenic activity (industrial processes). At the TM3030 Tabletop Microscope have been analyzed two types of opaque spherules: quartz spherules, most likely similar to those presented in Fig. 2 and spherules with chromium (Fig. 4).

The presence of chromium has been identified in some of these spheres, associated with carbon, oxygen, chlorine, silicon, calcium, and oxygen (Fig. 4, Table 1). The calcium may be provided by the surrounding biogenic material (very present into the rest of the sample), while the silicon and oxygen seem to form some quartz inclusions (see Fig.4c – the distribution map of the elements). As regarding the carbon, oxygen, and chlorine, they are the compounds of the epoxy resin that includes the analyzed grains. The presence of chromium induces indubitably the acceptance of an anthropogenic origin; these microspherules originate probably from some industrial furnace – maybe from Galați or from Tulcea (the former factory of special alloys). There have been also identified some similar rounded clasts that contained tellurium and tungsten.

These products can have a negative effect on the environment, both through the entrainment of the component metals in the water circuit and through the wearing of the particle by the wind (Vlase et al., 2012).

4. Conclusions.

An important factor in determining the origin of the spherulites was the fact that most of them did not show traces of transport on their surface (which denotes that they are formed in situ or at a very short distance from the place of sampling or in situ formation of the material). In the case of opaque granules consisting of metal (as in the case of the grain in Fig. 4) it can be seen that they are relatively recently formed, because there are no mechanical traces (transport over long distances) or chemical alterations on their surface and, in particular, superficial cracks are not filled with subsequent precipitations.

In the sampling area, meteoritic fragments have not been noticed, but it is explainable because most of them are completely melted and vaporized by the impact (especially the smaller ones) and due to their metallic composition (in majority iron and nickel) even the remaining tend to be rapidly weather (in the Danube area the air humidity is elevated) (French, 1998).

Regarding all the presented aspects we can conclude that these spherical clasts are most of them, microtektites. They can be also traces of industrial activity.

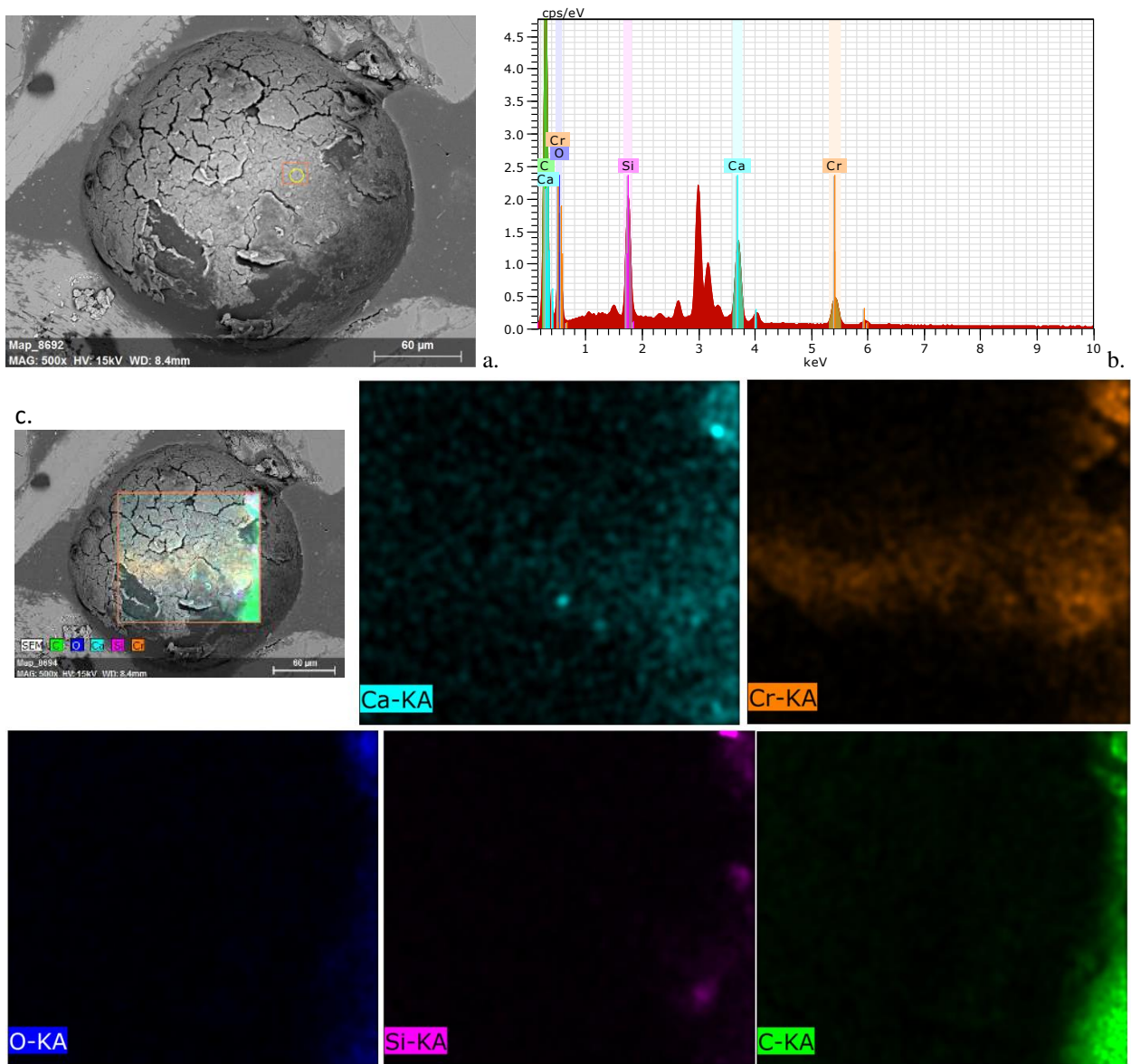


Fig. 4: Product of anthropogenic activity, probably industrial waste (sample P1): Electron microscope analysis - TM3030 Tabletop Microscope (see Table 1) of a rounded grain composed mostly of pure chromium with some superficial deposits of silica carbonate (used in industry): a. General image of the concerning spherule (with the measuring point marked by a yellow circle); b. the elements detected by the analysis; c. Elemental Mapping_881: PMImage size: 480 x 360Mag:600xHV:15.0kV.

Table 1. Electron microscope analysis - TM3030 Tabletop Microscope of the rounded grain in Fig. 4.

Element	AN	Series	unn. C	norm. C	Atom. C	Error
			[wt.%]	[wt.%]	[at.%]	[%]
Carbon	6	K-series	37.97	51.16	68.67	5.5
Oxygen	8	K-series	14.77	19.90	20.05	2.7
Chromium	24	K-series	12.14	16.36	5.07	0.4
Silicon	14	K-series	4.54	6.12	3.51	0.2
Calcium	20	K-series	3.42	4.61	1.85	0.1
Chlorine	17	K-series	1.37	1.85	0.84	0.1
Total:			74.22	100.00	100.00	

References:

- Challinor, J. (1961) A Dictionary of Geology. Univ. of Wales Press, 235 p., Cardiff.
- Chao E.C.T., Shoemaker E.M., Madsen B.M. (1960) First Natural Occurrence of Coesite. *Science*, vol.132, Issue 3421, p. 220–222.
- French B.M. (1998) *Traces of Catastrophe: A Handbook of Shock-Metamorphic Effects in Terrestrial Meteorite Impact Structures*. Lunar and Planetary Institute, 120 p., Houston.
- Gâștescu P., Știucă R. (2008) Danube Delta – biosphere reserve (in Romanian). Ed. CD Press, 400 p., Bucharest.
- Glass B.P., Barlow R.A. (1979) Mineral inclusions in Muong Nong type indochinites: implications concerning parent material and process of formation. *Meteoritics*, vol. 14, No. 1, p. 55-67.
- Ianovici V., Borocoș M. (1983) Romania. In: *Mineral deposits of Europe, Volume 2: Southeast Europe*, Londra, 142 p.
- Massonne H.-J. (2001) First find of coesite in the ultrahigh-pressure metamorphic area of the central Erzgebirge, Germany. *Eur. J. Mineralogy*, 13 (3), p. 565–570.
- Negrea I., Dimofte D., Popescu Gh.C. (2014) Preliminary data regarding sands heavy minerals from the Levee Letea (Danube Delta). *Romanian Journal of Mineral Deposits*, vol. 87, No. 2, Bucharest, p. 91-97.
- Panin N., Ion G., Ion E. (2004) The Danube Delta-Chronology of Lobes and Rates of Sediment Deposition. *Geo-Eco-Marina 9-10/2003-2004, Proceedings of Euro-EcoGeoCentre-Romania*, p. 36-40.
- Taylor H.P. Jr., Epstein S. (1966) Oxygen Isotope Studies of Ivory Coast Tektites and Impactite Glass from the Bosumtwi Crater, Ghana. *Science*, vol. 153, Issue 3732, p. 173-175.
- Vespremeanu E. (2004) Morphology of the relief of the Danube Delta in the last 40 years (in Romanian). *Studii și cercetări de oceanografie costieră (revista științelor litorale)*, vol. 1, Ed. Universității, Bucharest, p. 31-66.
- Vlase T., Vlase G., Doca N. (2012) *Inorganic Pollutants: Sources, Analyzes, Decrease (in Romanian)*. Ed. Mirton, 150 p., Timișoara.

CONTRIBUTIONS TO THE MINERALOGY OF THE „PURPLE” METAMORPHIC ROCKS FROM THE NORTH-WEST FLANK OF VÂLCAN MOUNTAINS

Robert SZABO^{1,2}, Gheorghe C. POPESCU¹, Eduard GHINESCU²

¹ University of Bucharest, 1, Nicolae Balcescu Blv., 010041 Bucharest, Romania;

² Geological Institute of Romania, 1, Caransebes Str., 012271 Bucharest, Romania.

*robert.szabo@yahoo.com, **gheorghec.popescu@yahoo.com, *** ghinescu.edi@gmail.com

Abstract: The Vâlcan Mountains are located in the central part of the South Carpathians, Romania. The studied area consists of formations belonging to the Danubian and Getic napes. Three types of metamorphic rocks were observed in the area, differing by the rest of the rocks found in the region, due to their red-purple color. The analyses were done so far only on two of the three types and showed that the specific color of the rocks is due to the presence of iron oxides and titanium oxides. The mineralogical analysis identified as color grains of hematite, ilmenite and minerals of the magnetite - ulvöspinel solid solution series. Ulvöspinel was mentioned for the first time in the studied area along with monazite. Accompanying minerals are feldspars, quartz, titanite, apatite and zircon, the feldspar being the main host for the color nuclei. From the petrographic point of view, the purple rock could be defined as a gneiss.

Keywords: Iron oxides, titanium oxides, apatite, zircon, ulvöspinel, monazite, metamorphism

1. Geographical data of the studied area.

From the geographical point of view, the Vâlcan Mountains are located in the western South Carpathians, in the south-west region of Hunedoara County, Romania.

The studied area is situated on the northern slopes of Vâlcan Mountains attributed to the upper basin of the Jiul de Vest river from the springs of this river in the west where the Vâlcan Mountains meet the Retezat Mountains stretching downward, along the river. The researched area is situated between Câmpu Mielului as the eastern limit and Scorota Brook as the western limit. The area lies on the right bank of Jiul de Vest river. The research stretched beyond the designated area, all the way to the Oslîța – Oslea ridge, in the west, where the Vâlcan Mountains ends. In this region occurrences of red-purple rocks were observed.

2. Geological settings.

Studies on the region were done along the time starting from the end of the 19th century all the way to the modern times. The first Romanian and foreign scientists, considered as pioneers in studying the region, are B. Inkey (1891), E. de Martonne (1906), L. Mrazec (1891-1899), Gh. Munteanu Murgoci (1898), G. Manolescu (1937, 1940) and others (M. Baron, 1998).

The geology of the studied area as described by modern researches consists of formations belonging to the Danubian and Getic napes (Figure 1). The structures of the Getic realm appear in form of „blocks” originating from the mega Getic block, which was fragmented after the collision with the Danubian block (Popescu, 1981; Popescu et.al., 1998). A regional metamorphism of a medium grade with non-homogeneous pressure consisting mainly of medium- and low-grade metamorphic structures is characteristic.

From the geological point of view, the northern flank of the Vâlcan Mountains belongs to the Danubian domain. Also the Getic – Supragetic nappe system is encountered along with the presence of some formations of the ophiolite – bearing Severin Nappe placed structurally between the Getic and the Danubian napes (Kräutner et. al., 1981).

The Danubian was first named by Gh. Munteanu Murgoci in 1910 and considered as autochthonous. New studies showed that the Danubian is built on a nappe system, representing the lowest part of the nappe pile in the South Carpathians.

The Danubian nappe system has been divided in two parts: the Upper Danubian and the Lower Danubian (Berza and Seghedi, 1983). The two subdivisions are separated by a major thrust plane and differ in their Mesozoic covers (Stănoiu, 1973; Kräutner et.al., 1981). The Lower Danubian has two nappes differentiated: The Lainici and the Schela – Petreanu nappes (Kräutner et.al., 1981, 1988; Berza et.al., 1994). The pre-Alpine thrusts of the Lower Danubian nappes are of Variscan age and consist of Retezat-Parâng unit resting always structurally upon the Vâlcan –Pilugu unit.

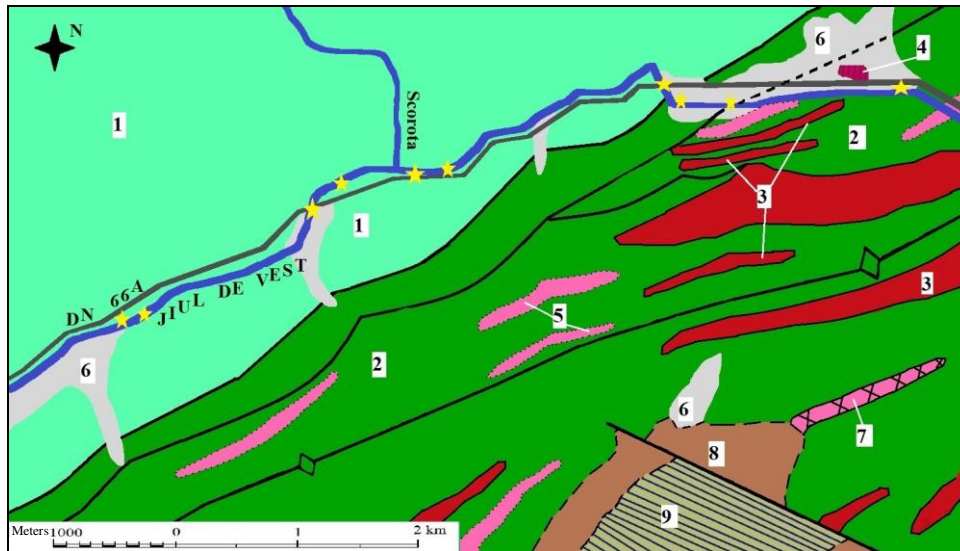


Fig. 1. Geological map of Câmpu Mielului - Scorota area (compiled after Berza et al., 1984), from the West Jiu upper basin. Legend: 1 – Middle Jurassic limestones; 2 – Upper Precambrian age pre-alpine unit of Retezat - Parâng with amphibolite gneiss and amphibolite +/- garnets; 3 – Minor granitic intrusions; 4 – The Severin unit with serpentinised peridotites; 5 – Upper Precambrian with micaceous gneisses; 6 – River deposits and pluvial deposits from Holocene period; 7 – Porphyritic microgranite of inferior Palaeozoic age; 8 – Metapelite, metapsammite of Coadă Oslei; 9 – limestones and crystalline dolomites of carboniferous age. The places from where the samples were collected are underlined on the map with a yellow star.

The lithology of the Danubian basement is represented by rock formations grouped as follows: the Lainici – Păiuș metasedimentary group and its intrusive in the Vâlcăni-Pilugu Variscan unit and the Drăgășan metavolcanic group with its intrusives in the Retezat-Parâng Variscan unit, both being of late precambrian age as recent studies have shown (Liégeois et al., 1996).

The Lainici - Păiuș group have been described by Manolescu since 1937 and updated with recent studies. It is composed mainly of quartzites, biotite gneisses, marbles and graphitic gneisses with minor amphibolites. Also migmatic zones can be observed in the proximity to the studied area. A major characteristic feature is the abundance of dykes or bodies of leucogranitoid intrusions in the metasediments.

The metasediments and the leucogranitic dykes were intruded by large elongated plutons. This geological unit appears in small places on the north side of Vâlcăni Mountains, but does not affect the samples taken for studies.

The Drăgășan group is encountered on the northern flank of the Vâlcăni mountains, following from west to east the alignment: Oslea – Oslita – Șiglău Mare – Negrele, situated on the right bank of the Jiul de Vest river. It is composed of banded amphibolites and ultramafic bodies, augen gneisses, biotite gneisses and rare marbles. This group was intruded by the Retezat-Parâng and Culmea Cernei plutons. The Retezat pluton is composed of granodiorites and tonalites with some quartz diorites at its periphery (Liégeois et al., 1996).

3. Methods of research.

The studies were made on eight rock samples collected from the field, both from Jiul de Vest river bank and from two tributaries of the main river: the Gârbovul brook and the Valea Jidanului brook. From these rocks thin and polished sections were made and they were studied under the optical microscope.

Thin and polished sections were analyzed using three polarized microscopes: Leitz Wetzlar (from the Mineralogy laboratory at the University of Bucharest), Optika B-150 POL (personal equipment) and Zeiss Microscope (from the Geological Institute of Romania). The photos of these sections were taken with a PANPHOT microscope equipped with Nikon Eclipse camera, E-400 lenses.

The minerals were also investigated using scanning electron microscopy (SEM), combined with energy dispersion spectroscopy (SEM-EDS). The electron microscope analyses were performed using a Zeiss Merlin GEMINI II, SEM-EDS (Scanning Electron Microscope – Energy Dispersive Spectrometer, Geological Institute of Romania) instrument with a working regime up to 300 nA, with a 30KV acceleration factor. We also used scanning electron microscopy (SEM), combined with energy dispersion

spectroscopy (SEM–EDS) performed with a Hitachi TM 3030 Plus Tabletop SEM equipped with a Bruker Quantax X Flash 6/10 detector.

4. Results and discussions.

Three types of metamorphic rocks were observed in the area, differing from the rest of the rocks found in the region, due to their red-purple color. Two of these rocks were studied and for the third the study is under way. Eight specimens were collected, differing in size, from small grains having 7-8 cm diameter to large samples even with 35 to 40 cm in diameter, weighing from a few grams to several kilograms. Some of these samples can be observed in Plate I, Image A.

Mainly iron oxides and titanium oxides were discovered along with apatite, zircon and a mineral containing Rare Earth Elements (REE) (*i.e. monazite*). The minerals identified are presented in the followings.

Magnetite, $\text{Fe}^{2+}\text{Fe}_2^{3+}\text{O}_4$ (Plate II, Images A and B). This mineral is primary and is being altered to hematite and goethite. A few relict grains could have been observed in polished sections in which it can be observed the degradation and transformation of magnetite. It is isotropic and has a grey color with brownish tint in reflected light.

Table 1. The chemical composition of magnetite, determined by SEM-EDS analysis.

Element	C norm. (Wt. %)	C Atom. (At. %)	C Error (%)
Oxygen	28.35	58.00	3.4
Iron	71.65	42.00	2.1
Total	100.00	100.00	

Ilmenite, $\text{Fe}^{2+}\text{TiO}_3$. Its formation is linked to the intrusive basic rocks and his association with magnetite was observed in our studied rocks too. It can be found as thick tabular crystals, with dominant base, to rhombohedral ones; in nature large crystals up to 25 cm can be found. It has an iron-black color and is grey with a brownish-pink tint in reflected light. In the case of these purple rocks ilmenite is formed due to high grade metamorphism. It is associated with magnetite, hematite, rutile, ulvöspinel, apatite, titanite, hematite, quartz. All the minerals mentioned in the literature as usually associated with ilmenite have been found in the composition of the purple rock.

Table 2. The chemical composition of ilmenite, determined by SEM-EDS analysis.

Element	C norm. (Wt. %)	C Atom. (At. %)	C Error (%)
Oxygen	41.09	69.11	8.7
Titanium	31.35	17.62	0.9
Iron	27.55	13.27	0.8
Total:	100.00	100.00	

Hematite, $\alpha\text{-Fe}_2\text{O}_3$ (Plate I, Image C). This mineral is formed by the alteration of magnetite as observed in our specimens and is dispersed as fine grains in the mass of the rock. It has an iridescent tarnish, dull to bright red color, and in reflected light is white to grey-white, with a bluish tint, having deep blood-red internal reflections.

Table 3. The chemical composition of hematite, determined by SEM-EDS analysis.

Element	C norm. (Wt. %)	C Atom. (At. %)	C Error (%)
Oxygen	31.89	62.04	3.7
Iron	68.11	37.96	1.8
Total	100.00	100.00	

Ulvöspinel, $\text{TiFe}_2^{2+}\text{O}_4$ (Plate II, Image C). It is a new discovery for the studied area. It has not been mentioned yet before in this area, being a rare mineral. It forms a fine network along {100} in magnetite or in ilmenite. His color is black, brown to reddish brown in reflected light. It is isotropic. In our samples it is associated with magnetite, ilmenite, biotite, plagioclase and apatite.

In our research this mineral is linked both to the remnants of magnetite but also to the existence of ilmenite as mentioned in the literature. The preliminary chemical analyses (Table 4) showed the presence of some minor elements in it structure, such as aluminum, silicon and potassium. The presence

of these elements is linked to the matrix of the rock which consists of plagioclase and quartz. Eliminating these elements, the percentage of iron titanium and oxygen is exactly as the one presented in literature for this mineral.

Table 4. The chemical composition of ulvöspinel, determined by SEM-EDS analysis.

Element	C norm. (Wt. %)	C Atom. (At. %)	C Error (%)
Oxygen	31.04	58.61	
Aluminum	1.21	1.36	0.03
Silicon	2.14	2.31	0.03
Potassium	0.75	0.58	0.02
Titanium	23.03	14.53	0.08
Iron	41.82	22.62	0.11
Total:	100.00	100.00	

Goethite, α -Fe³⁺O(OH) (Plate I, Image B). It is common and along with hematite and magnetite forms the main iron minerals that were identified in the studied rocks. It is a secondary mineral and it is formed by the alteration of hematite, process observed in our samples also. It presents a yellowish to reddish brown color in massive aggregates, and it is also banded as described by Ramdohr (1980).

Table 5. The chemical composition of goethite, determined by SEM-EDS analysis.

Element	C norm. (Wt. %)	C Atom. (At. %)	C Error (%)
Oxygen	35.64	65.91	4.5
Iron	64.36	34.09	1.8
Total	100.00	100.00	

Anatase, TiO₂ (Plate I, Image D). It is a common titanium oxide alongside goethite and magnetite, being responsible for the purple color of the rock. In our rocks this mineral is not secondary, it has a high frequency of occurrence next to hematite and goethite. Usually is transparent when light colored, to nearly opaque when deeply colored. Pyramidal crystals may appear opaque because of the total reflection of light. It has various colors: brown, pale yellow or reddish brown, indigo, black, pale green, pale lilac and grey, rarely nearly colorless. In transmitted light it is brownish yellow or yellow-brown.

Table 6. The chemical composition of anatase, determined by SEM-EDS analysis.

Element	C norm. (Wt. %)	C Atom. (At. %)
Oxygen	44.79	70.83
Titanium	55.21	29.17
Total	100.00	100.00

Titanite, CaTiSiO₅. It is a mineral of the monoclinic system. It can be sometimes metamict. It is compact, massive, transparent to opaque, presenting a wide range of color from black, brown, grey, to green, yellow and red. In thin section it is either colorless to yellow or brown. It is associated with: albite, apatite, monazite, magnetite, ilmenite and calcite. All the accompanying minerals mentioned before have been found in our studied samples.

Table 7. The chemical composition of titanite, determined by SEM-EDS analysis.

Element	C norm. (Wt. %)	C Atom. (At. %)	C Error (%)
Oxygen	37.48	58.95	5.3
Silicon	16.47	14.76	0.7
Titanium	25.64	13.47	0.7
Calcium	20.41	12.81	0.6
Total	100.00	100.00	

Fluorapatite, Ca₅(PO₄)₃F (Plate I, Image F). It is hexagonal or monoclinic and can be found in nature as prismatic hexagonal crystals even up to 2 m. It has been described along the time in complex tabular to discoidal crystals typically with many forms: granular, globular to reniform, nodular and

massive. Transparent to translucent. The color of this mineral can be sea-green, violet, purple, blue, pink, yellow, brown, white and colorless.

In the macroscopic samples, fluorapatite appears pale green in color. In thin section is colorless or faintly tinted with greenish shades.

Table 8. The chemical composition of fluorapatite, determined by SEM-EDS analysis.

Element	Wt. %	Wt. % Sigma	Atomic %	Oxide	Oxide % Sigma
Oxygen	39.36		58.73		
Flourine	3.04	0.09	3.82		0.09
Phosphorus	18.46	0.05	14.23	P ₂ O ₅	0.12
Calcium	38.36	0.08	22.85	CaO	0.11
Total:	100.00		100.00		

Monazite, (Ce, La, Nd, Th) PO₄ (Plate II, Images E and F). This mineral is also a new mention for the studied area. It is monoclinic, usually not very big, being observed at the electronic microscope on veins next to flourapatite. According to literature it occurs as long prismatic crystals, or grains, to 15 μm which is the case for our study too. The chemical composition of the monazite can be seen in Table 9. It has cerium and neodymium as rare earth elements in its formula.

In this study the monazite is the cerium first member of the monazite group. Is a rare mineral that usually occurs as an accessory in granites, gneisses, aplites and pegmatites. It can also be found as rounded grains in the sand from the decomposition of the rocks mentioned before.

Table 9. The chemical composition of monazite, determined by SEM-EDS analysis.

Element	C norm. (Wt. %)	C Atom. (At. %)	C Error (%)
Oxygen	32.58	68.28	2.8
Phosphorus	17.33	18.75	0.4
Cerium	28.70	6.87	0.5
Neodymium	20.28	4.71	0.4
Total	100.00	100.00	

Zircon, ZrSiO₄. It belongs to the tetragonal system. It may be metamict. Most commonly as tabular to prismatic crystals, with square cross sections, or as irregular grains, massive. Transparent to opaque. It has a very diverse range of color like reddish brown, yellow, green, blue and grey or colorless. In thin section is colorless to pale brown.

Table 10. The chemical composition of zircon, determined by SEM-EDS analysis.

Element	C norm. (Wt. %)	C Atom. (At. %)	C Error (%)
Oxygen	34.07	65.35	5.4
Silicon	16.50	18.02	0.7
Zircon	49.43	16.63	1.8
Total	100.00	100.00	

Conclusions

The two purple rocks found in the northern flank of Vâlcan Mountains have a diverse mineralogy, being of interest due to the association of the minerals found in this type of rocks. The main matrix of the purple rock is made of plagioclase and with quartz crystals, however the quartz is not found in a very large amount. These criteria led us to the opinion that this is a type of gneiss.

The minerals identified are high temperature minerals formed usually at early stages of mineralization and also they are found in depths. They are characterized by stability, they present relatively high specific gravity and chemically resistant, that is why some of these minerals are also found in sands along riverbeds. The ulvöspinel is a new mention for the studied area and this part of the Carpathian Mountains. Another spinel newly mentioned in previous researches, was cuprospinel found on the northern slopes of Vâlcan Mountains (Szabo et. al., 2017).

The formation of these red-purple rocks can be linked to the existence of the plutonic intrusions and also linked to the metamorphic processes, all of these contributed to the alteration of magnetite to hematite. The metamorphism could also be the one responsible for the dispersed grains of hematite in the mass of the rock.

The grains of hematite with goethite and anatase, encountered in our samples, are responsible for the presence of the red-purple color of the rock. These rocks are found in place, they have an autochthonous character, however they are not found in abundance. A new mineral has been found for the studied area, ulvöspinel, that accompanies magnetite and ilmenite, both found in the studied samples. This is only the second mention of ulvöspinel in Romania, the other mention being in Almaş-Sălişte magmatites. (Udubaşa et. al., 2002).

Monazite-(Ce) is also a first mention for the studied area. This mineral is rare but it has been mentioned at the Răscoala Valley from the Sebeş Mountains as the nearest place to the studied area and also in other parts of Romania (Udubaşa et. al., 2002). Monazite is found accompanying fluorapatite grains.

Fluorapatite in this case is the fourth mineral from the constitution of these rocks after hematite, goethite and anatase. As relict minerals magnetite, titanite, ilmenite and zircon have been identified in the studied rock sections and represent components of the primary granitoid pluton.

Acknowledgements

The authors wish to express their gratitude for guidance and support given in the laboratory by Dr. Delia-Georgeta Dumitraş from the Geological Institute of Romania – National Museum of Geology. We also would like to thank Dr. Nicolae Călin and technician Carmen Călinoiu for their support given in the laboratory during the process of preparing the thin and polished sections.

References

- Baron M., (1998) Cărbune și societate în Valea Jiului: perioada interbelică. Editura Universitas, Petroșani, 431 p.
- Berza T., Seghedi A., (1983) The crystalline basement of the Danubian Units in the central South Carpathians. *An. Inst. Geol. Geof.*, LXI, p. 15-22.
- Berza T., Pop G., Seghedi A., Iancu V., Hîrtopanu I., Hîrtopanu P., Năstăseanu S., Moisescu V. (1984) Geological Map of Romania, Scale 1:50.000, Mount Oslea Sheet, 123b, edited by the Geological Institute of Romania.
- Berza T., Seghedi A., Pop L., Szasz L., Hîrtopanu I., Săbău G., Moisescu V., Popescu Gh. (1986) Geological map of Romania, Scale 1:50.000, Lupeni Sheet, 106c, edited by the Geological Institute of Romania.
- Kräutner, H.G., Năstăseanu, S., Berza, T., Stănoiu, I., Iancu V. (1981) Metamorphosed Paleozoic in the South Carpathians and its relation with the pre-paleozoic basement. Guide to excursion A, Carp. Balk. Geol. Assoc. Congr. XII, București.
- Liégeois J.P., Berza T., Tatu M., Duchesne J.C. (1996) The Neoproterozoic Pan-African basement from the Alpine Lower Danubian nappe system (South Carpathians, Romania). *Precambrian Research* (Elsevier) 80, p. 281-301.
- Manolescu G. (1937) Étude géologique et pétrographique dans les Munții Vulcan (Carpatés Méridionales). *An. Inst. Geol. Rom.*, Vol. XVIII, Imprimeria Națională, București;
- Murgoci, G.M. (1905) Sur l'existence d'une grande nappe de recouvrement dans les Karpathes Méridionales. *C. R. Acad. Paris* (31 Juillet, 1905). Published also in *Bul. Soc. Șt. București*, XVI (1907), nr. 1-2, p. 50-52.
- Popescu C.Gh. (1981) Dispersia metalogenezei prealpine din Carpații Meridionali cu referire specială asupra metalogenezei manganifere. *Lucrările Sesiunii Științifice „Grigore Cobalcescu”* 24-25 octombrie 1981, p. 119 -125.
- Popescu C.Gh., Buia Gr., Rădulescu M. (1998) Metalogeny of Romania: Plate tectonics models. *Actas X Congreso Latinoamericano de geologia y VI Congreso Nacional de Geologia Economica*, vol. III, Buenos Aires, Argentina, 8-13 noviembre 1998, p. 186 – 192.
- Ramdohr P. (1980) *The ore minerals and their intergrowth*. 2nd Edition, Pergamon Press, 1269 p.
- Szabo R., Popescu C.Gh. (2017) Preliminary data on secondary copper minerals from the Șiglău-Uricani perimeter, Vîlcan Mountains, Romania. *Romanian Journal of Mineral Deposits*, Vol. 90, No. 1-2, București, p. 19-25.
- Stănoiu, I., (1973) Zona Mehedinți – Retezat, o unitate paleogeografică și tectonică distinctă a Carpaților Meridionali. *D.S. Inst. Geol.*, LIX/5, p. 127-171;
- Udubaşa G., Đuđa R., Szakáll S., Kvasnytsya V., Koszowska E., Novák M. (2002) Minerals of the Carpathians. Sándor Szakáll (ed.), *Granit Prague*, 479 p.

Plate I

Photographs of the purple rock as found in nature (Image A). Thin section microphotographs of magnetite (Mag), Hematite (Hm) and Goethite (Gt) with some fine micro-veins of quartz (Image B). Backscattered electron images from C to F of: dispersed grains of hematite (Hm) with quartz (Qtz) grains and plagioclase (Plag) as the main matrix of the rock (Image C); anatase (Anat) surrounded by quartz (Qtz) and dispersed grains of hematite (Hm) enveloped in the plagioclase matrix of the rock (Image D); zircon (Zr) with quartz (Qtz) and Plagioclase (Plag) (Image E); fluorapatite (Fap) in quartz (Qtz) and plagioclase (Plag) matrix, with dispersed grains of hematite (Hm).

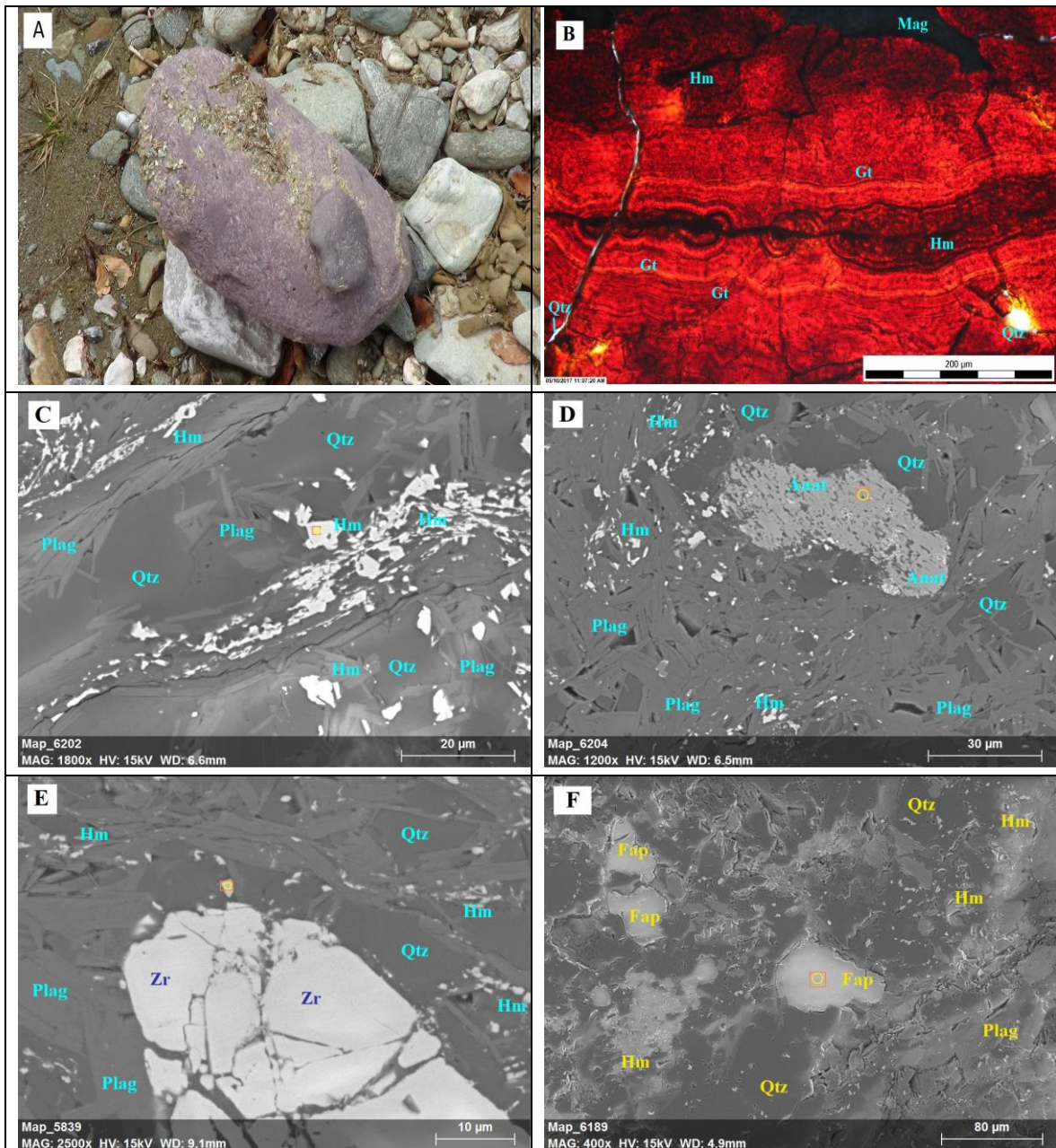
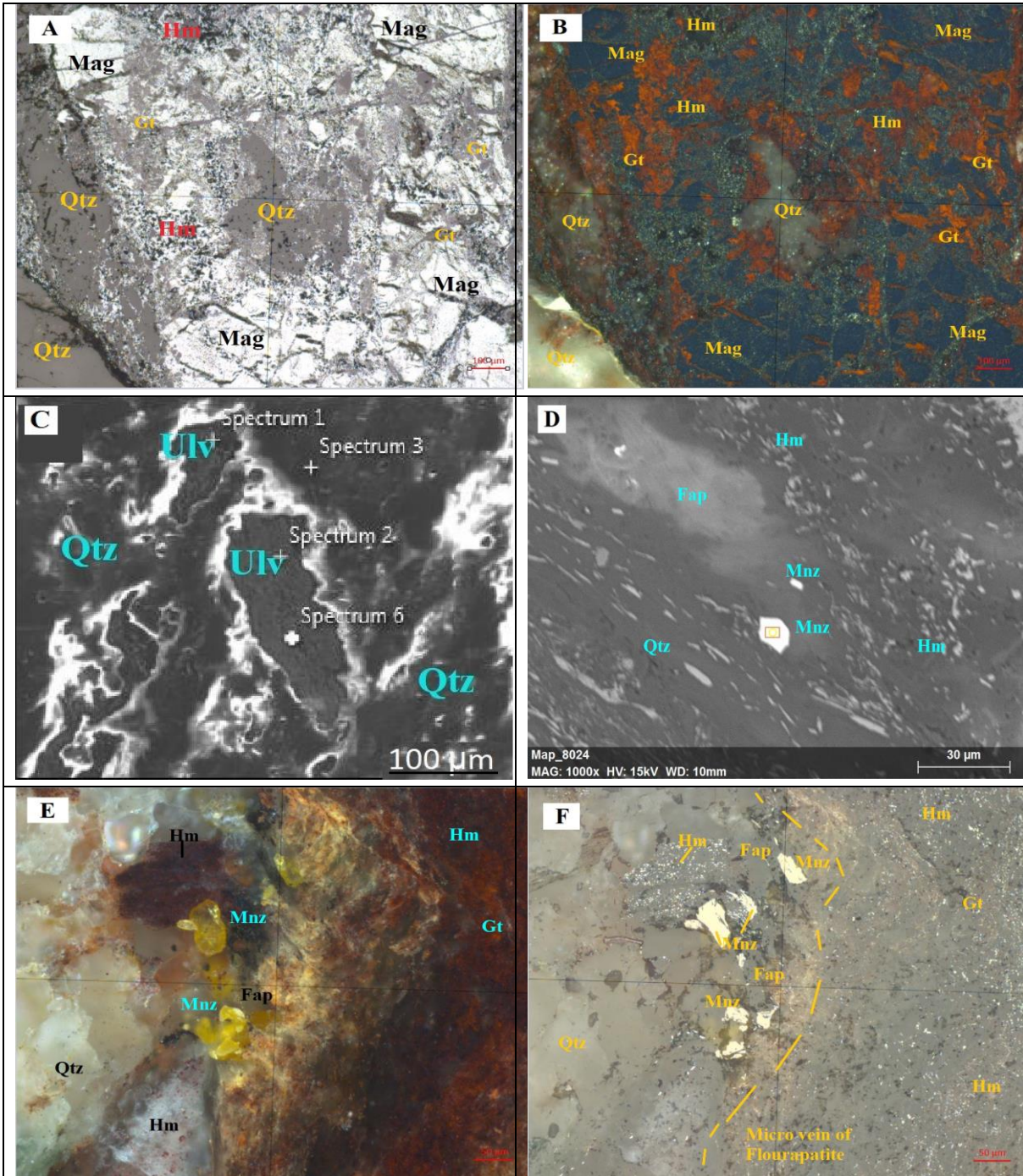


Plate II

A and B are polished section images in reflected light (N// and N+, respectively), showing a zoned magnetite (Mag) crystal, altered to hematite (Hm) and Goethite (Gt) with quartz (Qtz). Images C and D present backscattered electron images of: C - ulvöspinel (Ulv); D - monazite (Mnz) grains along with fluorapatite (Fap), quartz (Qtz) and dispersed grains of hematite (Hm). Images E and F are from polished sections in reflected light (N+ and N//, respectively) of monazite (Mnz) grains situated on a micro-vein with fluorapatite (Fap), hematite (Hm), goethite (Gt) and quartz grains (Qtz).



THE QUANTITATIVE AND QUALITATIVE PRELIMINARY EVALUATION FOR THE HEAVY MINERALS OF THE SAND QUATERNARY DEPOSITS FROM THE SOUTHEASTERN IRAQ REGION.

Safaa Abdulhadi Khudhair ALSHAWI*, Gheorghe C. POPESCU**, Daniela DIMOFTE***, Antonela NEACȘU****

University of Bucharest, Faculty of Geology and Geophysics, Department of Mineralogy.

*safaahadi70@gmail.com; **gheorghec.popescu@yahoo.com; ***danidimofte@gmail.com;

****antonelaneacsu@gmail.com

Abstract. The paper deals with the study of heavy minerals in 11 samples from 11 excavated pits in the quaternary deposits from the southeastern region of Iraq, covering 3500 km² and an average depth of 6 m, to find their concentration in the sand deposits, their distribution into sediments, and their sources and origins. The results showed that there is a difference in the concentration of heavy minerals in the modeling sites, but the qualitative composition is similar, consisting of *anatase, ilmenite, hematite, magnetite, goethite, garnet, zircon, tourmaline, rutile, hornblende, and pyroxene*. So, the origin of the rock source of heavy minerals belongs to felsic igneous rocks, metamorphic (schist and gneiss), and older sedimentary rocks. Their source area is represented by the north and north-east zones of Iraq, from where Tigris and Al-Ghraf Rivers transported sediments. This area hosts the BaiHassan (Pliocene-Pleistocene) formation deposited in the fluvial environment, Perispiki Red Beds including quartzite, shale, conglomerate, and basalt, Chalki volcanics consisting of basalt flows with tuff intercalations (Devonian age), and an intrusive complex (Cretaceous age) consisting of syenite, granodiorite, gabbro, peridotite, and pyroxenite. The estimated reserve of heavy minerals representing *the industrial bed* is of 43,568,000 tons, with an average thickness of 3.2 m, and a volume of 11,200,000 m³.

Keywords. Chalki volcanics, assessment, heavy minerals, Quaternary sediments, alluvial fans.

Introduction

The study area lies between the Tigris and Euphrates Rivers, and is basically a flat terrain with gentle slope, from northwest to southeast towards the Persian Gulf. It is mainly covered by different types of Quaternary sediments.

The main Pleistocene sediments are represented by alluvial fans and fluvial sediments. The Pleistocene – Early Holocene Units include sheet run-off with secondary gypsum and slope sediments. The Holocene Units include sediments of different origins, such as fluvial, lacustrine, marine, estuarine, aeolian, and also anthropogenic (Fig. 1).

1. Samples and techniques

Eleven samples were collected from 11 excavations using a drilling Bohlen excavator. 75 g of each sample were treated with 10% HCl to remove carbonate materials until any trace of carbonates disappears (no effervescence appears when treating the sample with acid) then the sample is dried at 40°C and weighted. The samples were washed with distilled water to remove the clay materials, heated again in the oven at 40°C, then sieved by screens of size range 0.250-0.063 mm and weighted, followed by the separation of the heavy minerals from the light minerals using bromoform (the preparation of samples for the separation of heavy minerals with heavy fluids was performed based on the Australian standards AS 2884, AS 2884.3 -1984 and AS 4350.2-1999). These standards establish a method to determine the content of heavy minerals and free quartz from the concentrated mineral sand samples. Then the grains of heavy minerals were mounted on a glass slide using Canada balsam. Binocular and polarizing microscopes were used to identify each mineral. About 300 grains have been counted by the Fleet method and the percentage of the heavy mineral was also calculated (Fleet, 1926).

2. Work procedures

2.1. Data and Software

ERDAS Imagine V.9.1, and ArcGIS V.9.3 software were used to perform data analysis.

2.2. Pre-processing

The ETM data subset using the area of interest files (AOI) was corrected according to WGS84 datum and UTM N38 projection using the nearest neighbor resembling. The processing also was carried out on the high-resolution satellite images.

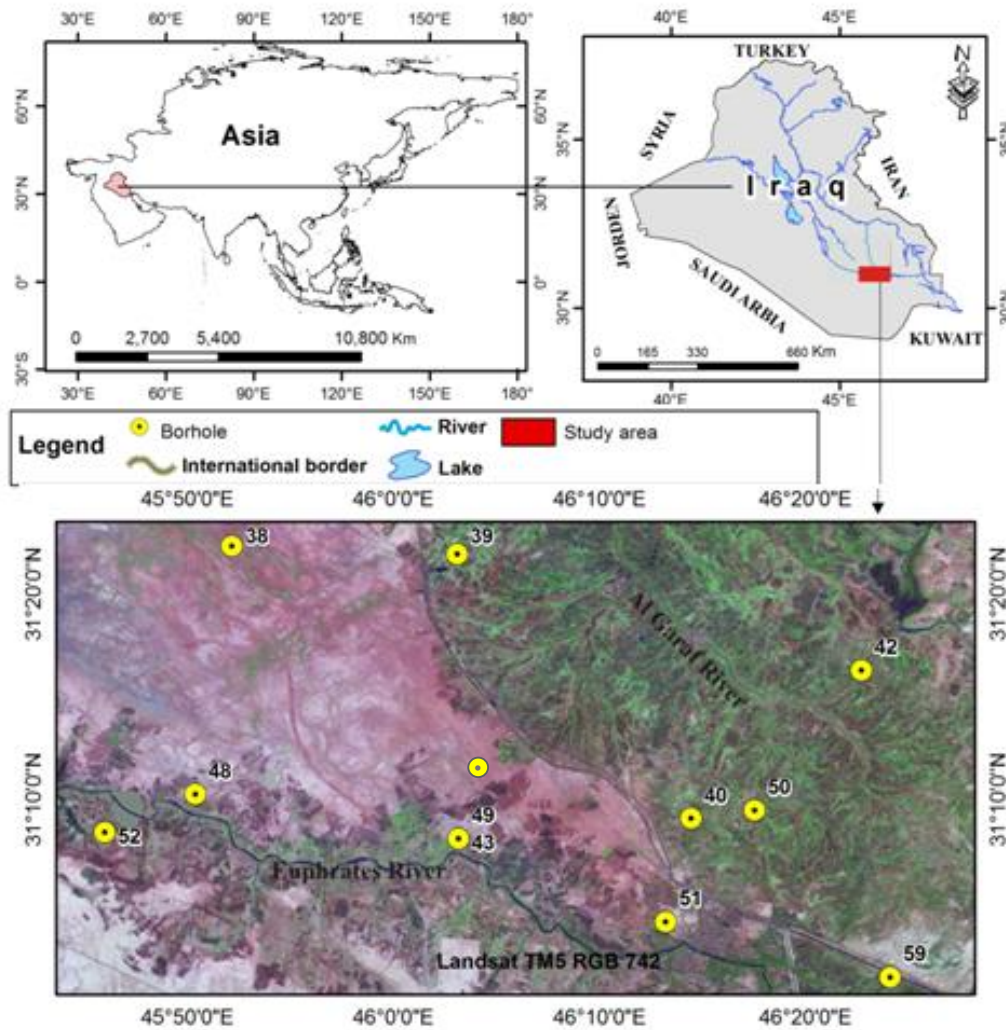


Fig. 1. Location of the study area.

2.3 Laboratory works

- Grain size analysis

Grain size analysis is an analytical technique used in Earth sciences and implemented as a routine laboratory study. It is a sedimentological analysis carried out to determine the grain size of the unconsolidated sedimentary deposit. The main goal of this procedure is to determine the type of environment and energy associated with the transport mechanism at the time of deposition; this is done by inference from the grain sizes of the sediment analyzed and their distributions. The granulometry is a basic analytical technique with wide applications within the Earth sciences. The grain size ranges define the limits of the classes that are given names in the **Wentworth scale** (or Udden–Wentworth scale) used in the United States. The Krumbein *phi* (ϕ) scale, a modification of the Wentworth scale created by W. C. Krumbein in 1937, is a logarithmic scale computed by the equation:

$$\phi = -\text{Log}_2 D/D_0$$

Where: ϕ is the Krumbein *phi* scale,

D is the diameter of the particle or grain in millimeters (Krumbein and Monk's equation, from PetroWiki - https://petrowiki.org/Estimating_permeability_based_on_grain_size)

D_0 is a reference diameter, equal to 1 mm (to make the equation dimensionally consistent)

This equation can be rearranged to find diameter using ϕ : $D = D_0 \times 2^{-\phi}$ (Gilbert, 2017).

The detrital grains are sorted according to their size, density, and shape through different mechanisms: erosion, transport, and deposition. During erosion, transport, and deposition, the absolute and relative abundance of heavy mineral species in sediments may change (Flores and Shideler, 1978; Komar and Wang, 1984; Frihy et al., 1995).

- Morphometric analysis

The morphometric analysis, together with grain size analysis, follow the description of the texture of the sedimentary rocks and complete their petrographic characterization. The categories with a morphology of grains and crystals fundamentally different by their nature are appreciated by distinct terms and separate methodologies. Their study represents, in most cases, a statistic examination of a big number of individuals and leads to the reconstruction of their origin and genesis from clastic or unconsolidated deposits (rudite, psammite, and pelite).

- Mineralogic analysis

Regardless of the manufacturing company, the microscopes used for the study of heavy minerals are of two types: microscopes which are used only in reflected light, and mixed microscopes, that can be used for observations in both reflected and transmitted light. By using the Fleet method (Fleet, 1926) on 200-300 grains, we calculate the number of granules per metal and divide it to the total number to find the ratio of the metal.

- XRD analysis

This investigation is used to define the mineralogic composition (in favorable circumstances).

3. Results

3.1. Grain size

After the volumetric analysis, by using sieves suitable to work with Wentworth coefficients, we find that the ranges of particle sizes of sand are particularly in the size of the sieve for 500-250 μm , i.e. medium sand (Fig. 2). This indicates that the sample is in the range of poorly sorted – sediments, usually deposited quickly.

A poorly sorted sediment means a mixture of coarse sand, fine sand, and gravel accumulation which indicates powerful currents. Always powerful currents are loading bigger granules along with micro grains creating poorly sorted sand (Komer, 1985).

3.2. Morphometric analysis

The morphometric analysis, together with grain size analysis, follow the description of the sedimentary rock texture and complete its petrographic characterization. The categories with a morphology of grains and crystals fundamentally different by their nature are appreciated by distinct terms and separate methodologies.

The morphometric analysis of minerals indicates that sphericity and roundness have different values depending on the mineral species, as follows:

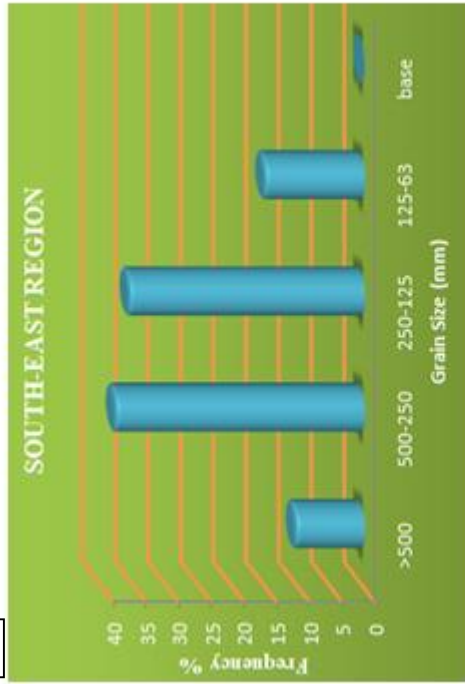
- Garnet has the spherical index values ranging from 0.3 to 0.5, while the roundness index varies between 0.3 and 0.7,
- Rutile has spherical index values ranging from 0.5 to 0.9, while the roundness index ranges from 0.1 to 0.7,
- Zircon has spherical index values ranging from 0.5 to 0.7, while the roundness index ranges from 0.1 to 0.7 (Fig. 3.A),
- Opaque minerals have the spherical index values ranging from 0.7 to 0.9, while the roundness index ranging between 0.1 and 0.7 (Fig. 3.B).

The particles transported by the currents of the predominant water in the region get many distortions in the morphology of the transferred part, so we find that the number of spherical particles is higher than the rest. Therefore, minerals with high erosion resistance have spherical forms (zircon, rutile, tourmaline). The predominance of ultra-stable minerals indicates the recycling of these minerals. The distribution of heavy minerals in the studied area environments shows selective deposition of these minerals with respect to their densities, sorting, and transport processes prior to their final deposition.

3.3. Heavy minerals analysis

According to Table 1 and Figure 4, ilmenite has a maximum percentage value of 7.215% in the pit no. 59 and a minimum value of 1.229% in the pit 52; anatase has a minimum value 1.09% in the pit no. 39 and a maximum value of 4.9% in the pit no. 52. Zircon values range from a minimum of 15.00% in the borehole no. 39 to a maximum of 26.04% in the borehole no. 43 near the Euphrates River. There are different types of zircon in sandstones, being the best source indicator and one of the most resistant minerals of all the heavy minerals (Pettijohn, 1975). The euhedral form of zircon suggests that the sediments were partly derived from acid igneous rocks (Permian and Triassic). Rutile is characterized by the highest value in the pit no. 51 (25.92%) and the lowest value (16.2%) in the pit no. 43.

A.



B.

Wentworth Size Class	Mm Scale	Phi Scale
Pebbles	256 to 4	-8 to -2
Gravel	4 to 2	-2 to -1
Very coarse and Coarse sand	2 to 0.5	-1 to 1
Medium sand	0.5 to 0.25	1 to 2
Fine and Very fine sand	0.25 to 0.06	2 to 4
Silt	0.06 to 0.004	4 to 8
Clay	<0.004	>8.00

C.

Diameter (phi units)	Description
$\sigma_1 < 0.35$	very well sorted
$0.35 < \sigma_1 < 0.50$	well sorted
$0.50 < \sigma_1 < 1.00$	moderately sorted
$1.00 < \sigma_1 < 2.00$	poorly sorted
$2.00 < \sigma_1 < 4.00$	very poorly sorted
$4.00 < \sigma_1$	extremely poorly sorted

Fig. 2. A. Grain sizes of the study area. **B.** Diagram showing the different ranges of particle sizes, based on the Udden-Wentworth and ϕ grain sizes for clastic sediments (Wentworth, 1922; Krumbein and Sloss, 1963 – in Gilbert, 2017). **C.** results and description of sorted sediments (Gilbert, 2017).

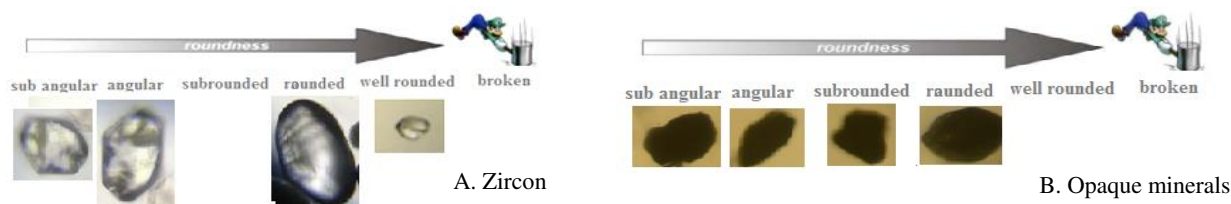


Fig. 3. Morphometry of zircon (A) and opaque minerals (B).

Garnet is characterized by high values, as in the pit no. 39, where is 25.36%. The lowest value, 9.37%, is recorded in the pit 50. Rutile, garnet, and epidote are indicators of the metamorphic provenance. The presence of rutile is characteristic of high-grade schist. Zircon, rutile, and tourmaline show an acid igneous source. The current beddings observed in the research area are formed due to the water transport of the particles by the Euphrates and Al-Ghraf rivers, and less to the wind transport. The highest value for the pyroxene is 10.83% in the pit 59, the lowest value is 4.41% in the pit 52. Most of the pyroxenes are corroded, have denticulate outlines, parallel to the c-axis, and have skeletal textures. The percentage of biotite is between 0.0-4.91%. The highest value for the biotite is found in the pit no. 39. Staurolite recorded the highest value in pit no. 51, which is 4.69%. These analyses indicate that the sedimentation basin is broad and contains deposits from the Permian age (Ga'ara formation) to Jurassic (Amij and Hussainiyat formations) and Cretaceous (Rutbah and Omar formations). All these geological formations that cross the Euphrates river, end in Shatt al-Arab, in the southern part of Iraq. In addition, there are sediments transported by the Tigris river from the main sources (Lesser Zab, Greater Zab, Diyala, and Al-Khabour rivers) in the north-east and north-west of Iraq, crossing the igneous and metamorphic rocks. Another way of transport is represented by the Euphrates river, which transports sediments from the main source (Turkey) through Syria. According to Fig. 4, the distribution of heavy minerals in the studied area reveals the presence of rutile, 21%, garnet, 20%, zircon, 19%, and opaque minerals, consisting of ilmenite, 4%, anatase, 3%, hematite, 1%, magnetite, 2%, and goethite, 1%. Also present are hornblende, 7%, pyroxenes, 8%, tourmaline, 7%, epidote, 2%, biotite, 2%, and staurolite, 1%.

a. Microscopic analysis

Three types of investigations have been performed. A binocular microscope has been used to determine the roundness (rounded and subrounded) and the mineralogical composition, which consists of rutile, zircon, tourmaline, hornblende, and magnetite. Transmitted light microscopy revealed the presence of rutile, zircon, and tourmaline (Plate I, photos no. 1-8). In reflected light microscopy, anatase, ilmenite, magnetite, rutile, and garnet can be observed (Plate II, photos no. 9-16).

b. X-ray analysis

By using the Bruker's X-ray Diffraction D8-Discover instrument, 4 samples have been analyzed. Heavy minerals were found in all the analyzed granulometric fractions (very fine sand, fine sand, and medium sand; Table 2). In the very fine sand, a large and diversified quantity of heavy minerals was identified. The X-ray diffraction on the 0.125-0.063 mm fraction highlights the presence of the heavy minerals as rutile, zircon, garnet, hematite, and hornblende.

4. Qualitative and quantitative assessment

For calculating the reserves of heavy minerals from the investigated area, we used the data from eleven pits excavated in the investigated area (Fig. 5).

• Qualitative assessment

The analysis of the pits showed a few layers of sands containing a large quantity of heavy minerals. They are distinctive and clear, depending on the field description. We used the results of morphometric, mineralogical and XRD analyses to indicate the percentages of the heavy minerals.

▪ Physical specifications

In the investigated area, the color of the sands is grayish-brown or gray, and occasionally brown-gray to grayish. Pale to white sand layers also appear in the sequence. Sands are generally fine or medium-grain. Massive layers are also observed. The bulk density interval is between 3.0 and 5.3 g/cm³ and the average is 3.89 g/cm³.

Table 1. Heavy minerals percentages in the boreholes from the study area.

Heavy minerals	Percentages in the boreholes (%)										
	B.H.38	B.H.39	B.H. 40	B.H42	B.H.43	B.H.48	B.H.49	B.H.50	B.H.51	B.52	B.H.59
Ilmenite	2.127	2.614	3.627	4.42	4.0275	4.473	4.164	5.68	5.256	1.229	7.215
Anatase	2.836	1.09	2.418	3.56	2.685	2.982	3.123	2.272	4.088	4.916	4.329
Hematite	1.418	1.162	0.806	2.99	0.895	0.994	1.457	1.704	1.6352	6.3015	2.1645
Magnetite	0.709	0.290	1.209	0.07	1.3425	1.491	1.46	1.704	1.168	1.8435	2.1645
Goethite	2.12	2.615	1.006	1.14	1.992	0	3.12	0.98	1.709	1.049	0.43
Epidote	1.78	3.78	3.04	2.41	2.21	0.92	1.76	0.25	1.04	2.59	2.06
Hornblende	5.06	3.96	7.67	7.39	6.73	5.06	2.21	9.48	1.34	9.45	15.05
Pyroxene	9.01	7.86	6.06	7.05	7.36	9.45	10.22	11.88	4.75	4.41	10.83
Zircon	17.24	15	20.89	17.98	26.04	20.74	18.39	19.06	16.98	18.39	18.87
Rutile	25.24	24.9	18.94	20.93	16.2	24.01	20.39	21.01	25.92	20.26	17.22
Tourmaline	3.94	2.09	8.09	9.41	4.31	7.98	4.59	16.02	8.62	3.9	4.88
Garnet	20.46	25.36	20.92	20.05	22.76	20.45	27.37	9.37	23.83	20.49	13.93
Staurolite	0.24	1.23	2.63	1.01	0.99	1.96	0.79	0.75	4.69	1.1	0.66
Chlorite	2.89	3.919	0.51	0.41	1.3	0	0.75	0.17	0.42	0.77	0.44
Biotite	1.19	4.91	2.99	2.78	1.29	1.05	1.92	2.59	0	0	2.19

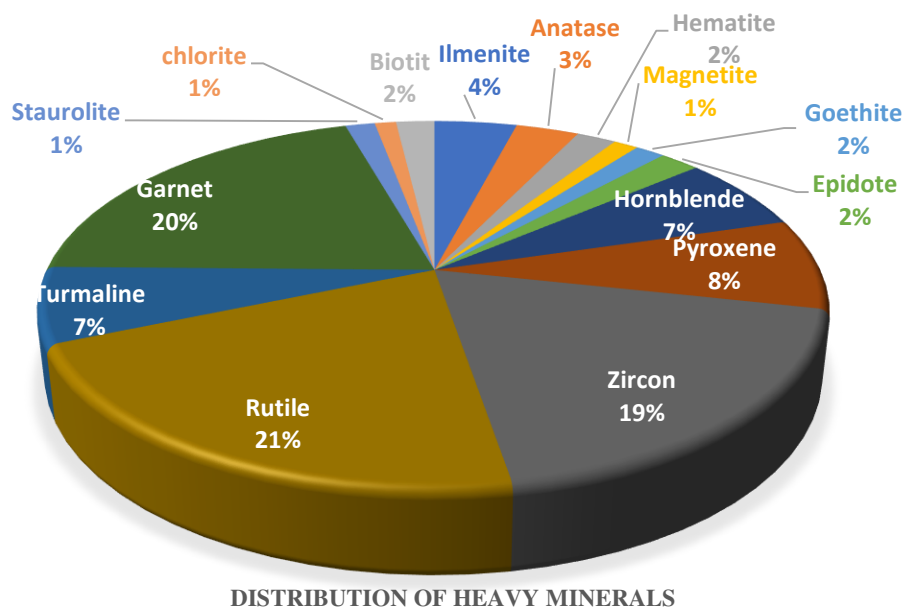


Fig. 4. Distribution of heavy minerals in the studied area.

Table 2. Frequency of heavy minerals from samples analyzed by X-ray diffraction.

pit no.				pit no.					
40	43	51	52	Heavy minerals		40	43	51	52
+	+	+		Rutile	Hematite		+		
+	+			Zircon	Magnetite				+
		+		Garnet	Epidote				+
+	+	+	+	Hornblende	Pyroxene			+	
					Anatase				+

- **Quantitative assessment**

- Estimated Reserve

In this study, the reserve has been calculated by the surface of the area multiplied by the average thickness of the studied sections - GIS Method.

Technically, we draw a polygon that represents the study area in relation to the data taken from the field, arranged in an Excel table. ETM data subset using the area of interest files (AOI) was corrected according to WGS84 datum and UTM N 38 projection using the nearest neighbor resampling. Geological reserves of the beds were estimated according to the geological data and laboratory test results, generally depending on density and surface area (Table 3).

a) Estimated Reserve (in cubic meters)

The estimated reserve calculated in cubic meters is as follows: the area of the estimated reserve multiplied by the average thickness.

The area = **3,500,000 m²**.

The average thickness = 3.2 m.

Estimated Reserve (cubic meters) = 3,500,000 m² × 3.2 m = 11,200,000 m³.

b) Estimated Reserve (in tons)

The estimated reserve calculated in tons is as follows: the volume of the estimated reserve multiplied by the average of the total density.

The average of the total density = 3.89 g/cm³.

Reserve (tons) = area (m²) × average thickness (m) × bulk density (g/cm³)

Estimated Reserve (tons) = 11,200,000 m³ × 3.89 g/cm³ = 43,568,000 tons.

Table 3. Thicknesses of the heavy minerals sand beds.

No.	Pits no.	Depth (m)	Thickness of sand deposits (m)
1	38	5.5	3
2	39	6	4.7
3	40	5	4.4
8	50	6.1	3.3
9	51	5	1.5
11	52	4.5	3.5

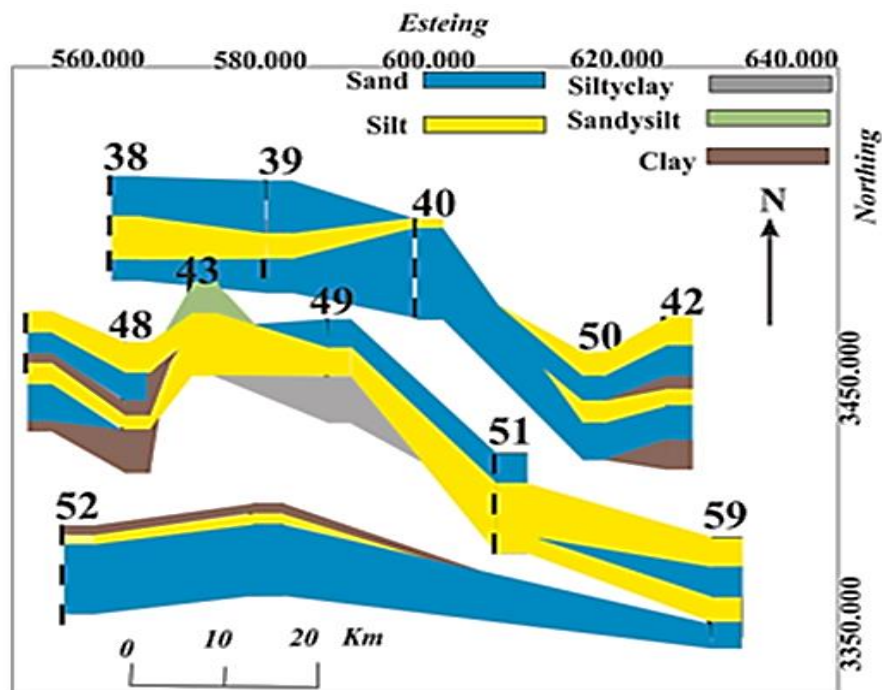


Fig. 5. The lateral and vertical change of layers for all the pits of the research area (drawing in software system Coral DRAWX4).

5. Conclusions

The obtained results revealed that the origin rocks of the heavy minerals belong to felsic igneous rocks, metamorphic (schist and gneiss) and older sedimentary rocks, due to the presence of certain minerals. Their source areas are in the north and north-east of Iraq, from where Tigris and AL-Gharraf rivers transported the sediments. There are several formations in the zone as BaiHassan formation (Pliocene-Pleistocene), deposited in fluvial environment, Perispiki Red Beds, including quartzite, shale, conglomerate, and basalt, Chalki volcanics, consisting of basalt flows with tuff intercalations (Devonian age), and the intrusive complex (Cretaceous age) with syenite, granodiorite, gabbro, peridotite, and pyroxenite. A poorly sorted sediment (a mix of gravel, coarse and fine sand) has resulted due to the strong waves and currents.

The mineralogical analysis highlighted the presence of rutile (21%), garnet (20%), and zircon (19%), as well as opaque minerals, consisting of ilmenite (4%), anatase (3%), hematite (2%) magnetite (1%), and goethite (1%). In addition, hornblende (7%), pyroxenes (8%), tourmaline (7%), epidote (2%), biotite (2%), and staurolite (1%) were found.

XRD analysis confirmed the presence of rutile, zircon, garnet, hematite, magnetite, epidote, hornblende, pyroxene, and anatase.

The location of the heavy mineral beds has been defined by excavating 11 pits disposed as a net of 15 x 15 km, within an area of 3,500 km². ***The estimated reserve of heavy minerals representing the industrial bed is of about 43,568,000 tons, calculated to a thickness of 3.2 m, and a volume of 11,200,000 m³.***

References

- Fleet W.F. (1926) Petrological Notes on the Old Red Sandstone of the West Midlands. Geological Magazine 63, p. 505-516.
- Flores R.M., Shideler G.L. (1978) Factors controlling heavy mineral variations on the South Texas outer continental shelf, Gulf of Mexico. Journal of Sedimentary Petrology 48, p. 269–280.
- Frihy O.E., Lotfy M.F., Komar P. (1995) Spatial variations in heavy minerals and patterns of sediment sorting along the Nile delta, Egypt. Sedimentary Geology 97, p. 33–41.
- Gilbert A.S. (Ed.) (2017) Encyclopedia of Geoarchaeology. Encyclopedia of Earth Science Series XXIX, 1046 p.
- Komar P.D., Wang C. (1984) Process of selective grain transport and the formation of placers on beaches. J. Geol., 92, p. 637 – 655.
- Komar P.D. (1985) The hydraulic interpretation of turbidities from their grain sizes and sedimentary structures. Sedimentology 32, p. 395–407.
- Pettijohn F.J. (1975) Sedimentary Rocks. 2nd Edition, Harper and Row Publishers, New York, 628 p.

Plate I.

Microphotographs at the binocular microscope (photos 1-4) and in transmitted light (photos 5-8).



Photo 1: 1. garnet, 2. tourmaline, 3. rutile, 4. magnetite; width of field: 500µm.



Photo 2: 1. zircon, 2. rutile, 3. hematite, 4. garnet; width of field: 500µm.

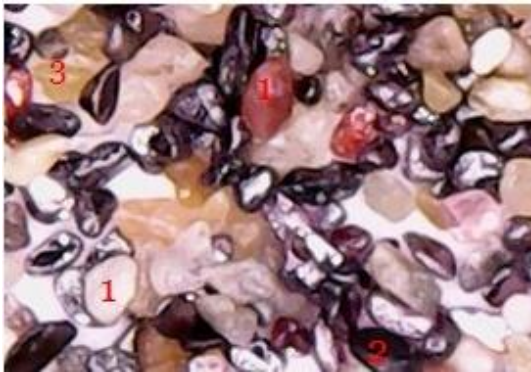


Photo 3: 1. hornblende, 2. garnet, 3. rutile, 4. zircon; width of field: 500µm.



Photo 4: 1. garnet, 2. rutile, 3. zircon; width of field: 500µm.

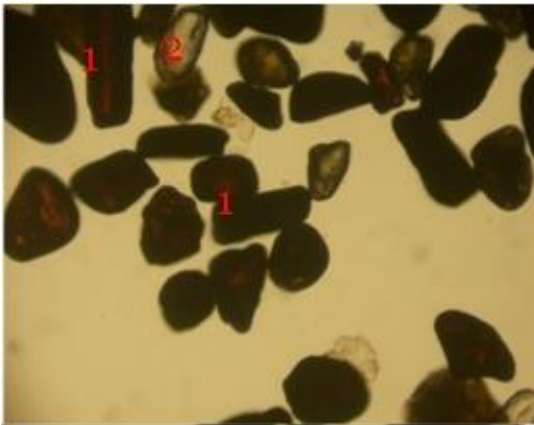


Photo 5: 1. rutile, 2. zircon; x35, N//.

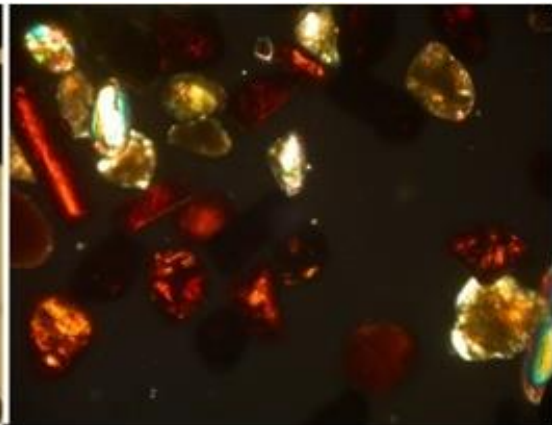


Photo 6: Same view as in photo 5, with N+.

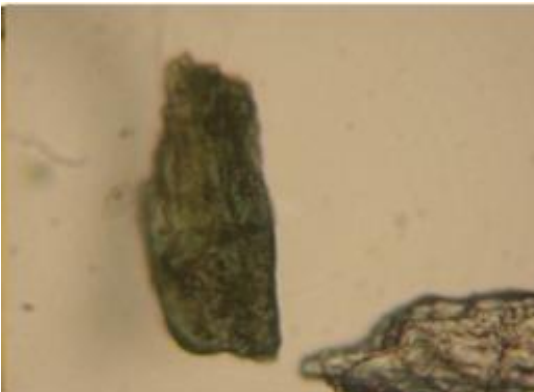


Photo 7: Tourmaline; x 40, N//.

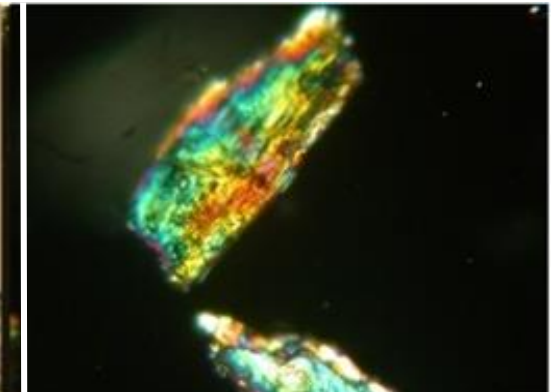


Photo 8: Same view as in photo 7, with N+.

Plate II.

Reflected light microphotographs.



Photo 9: 1. ilmenite, 2. anatase; 35x, N//.



Photo 10: Same view as in photo 9, with N+.

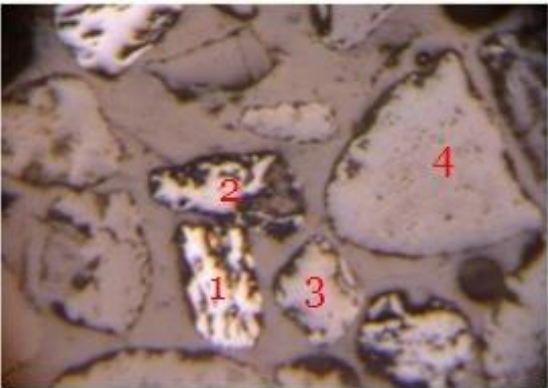


Photo 11: 1. rutile, 2. magnetite, 3. garnet, 4. anatase; 35x, N//.



Photo 12: Same view as in photo 11, with N+.

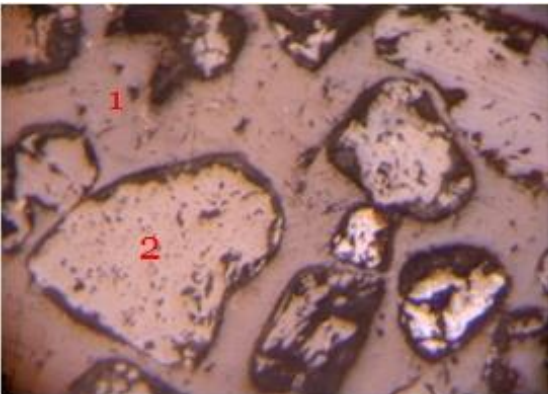


Photo 13: 1. magnetite, 2. anatase; 35x, N//.



Photo 14: Same view as in photo 13, with N+.

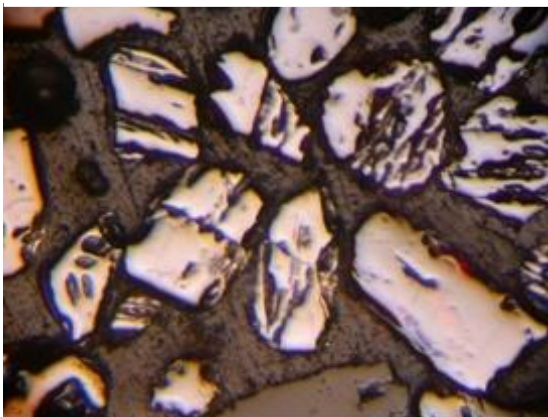


Photo 15: Rutile; x35, N//.



Photo 16: Same view as in photo 15, with N+.

OVERVIEW OF HEAVY MINERALS STUDY IN THE SOUTH AND SOUTHWEST OF IRAQ

Safaa Abdulhadi Khudhair ALSHAWI*, Gheorghe C. POPESCU**, Daniela DIMOFTE***

University of Bucharest, Faculty of Geology and Geophysics, Dept. of Mineralogy, Bucharest, Romania.

*safaahadi70@gmail.com; **gheorghec.popescu@yahoo.com; danidimofte@gmail.com***

Abstract. The research deals with the study of heavy minerals in 110 samples from 110 holes in the south and southwest region of Iraq, consisting of Holocene sediments (quaternary sediments). The aim was to find the concentration and the distribution of the heavy minerals in the sand deposits, in addition to the knowledge of their sources and origins. The results showed that there is a difference in the concentrations of heavy minerals in the modeling sites but similar in quality. The sediments are composed of dark heavy minerals (ilmenite, hematite, magnetite, anatase), garnet, zircon, tourmaline, rutile, hornblende, amphibole, and quartz. These minerals are attributed to metamorphic rocks (gneiss and schist), igneous, and sedimentary rocks. The study revealed the presence of heavy minerals in the Quaternary sediments. The most important is the sand, which is transported by the dominant air streams in the desert environment, coming from the Arab shield as well as the sand formed on the account of the geological formations degradation in the southwest and northwest of Iraq. The climate had variations during different geological periods, so during the Pleistocene - Pliocene period, the climate was semi-humid and varied in Holocene to semi-arid and arid, while in present the dominant climate is arid.

Keywords: heavy minerals, sand, zircon, Arab Shield.

1. Introduction.

Quaternary sediments spread over the whole studied area due to the wind direction, generally NW-SE. 110 samples were chosen from longitudinal sand dunes, barchans, dome dunes, and the fluvial plane of Samawa, Qadissiya, Nasiriyah, Najaf, Karbala, Hilla, and AL-Basra valleys, in order to study the heavy minerals in terms of grain size and from the chemical point of view. Heavy minerals were identified in the fraction 0.250-0.063 mm.

1.1. Location.

The study area is in the south and southwest part of Iraq, within the Al-Basra, Nasiriyah, Samawa and Qadissiya, Najaf, Karbala, Hilla governorates, as shown in Fig. 1. It covers an area of 70000 km² and is limited by the following coordinates: 44°09'- 47°40' longitude and 33°20'- 30°01' latitude.

2. Geological setting.

The research area is situated in the stable platform in the southern part of the western desert, where terrigenous and carbonate sediments of the Miocene period are mostly covered by Paleocene to Holocene sediments. Upper Miocene Dibdibba sediments (Pliocene-Pleistocene) appear in the southern part of the desert, while residual and terrace deposits are restricted to the western side of the alluvial plain (Al-Ani, 1979). The stratigraphic units are described, according to Buday (1980), Jassim and Goff (2006), as pre-Quaternary units and Quaternary deposits.

3. Materials and methods.

We have analyzed 110 samples from the research area, regarding the grain size (laser grain size), mineralogy (optic microscope observations, X-ray diffraction) and chemistry (XRF analyses).

Each sample was treated with sodium polyphosphate to disperse the particles. Then the sample (with sodium polyphosphate) was measured using a Horiba LA-950 grain size device (Sedimentology laboratory, Bucharest University). 1g of each sample was ground to a fine powder and then analyzed using an analytical XPert diffractometer to identify the minerals from each sample. Also, 1g from each sample was analyzed using an X-ray fluorescence Horiba XGT-7000 device for the determination of the element concentrations in the samples. The samples were embedded in epoxy resin, polished, and then analyzed with an optic microscope.

4. Results.

4.1. Grain size analysis.

The grain size analysis of 13 samples revealed similarities between them. The samples are considered fine-grained sand and medium-grained sand. The details are presented in Figs. 2, 3, and Table 1.

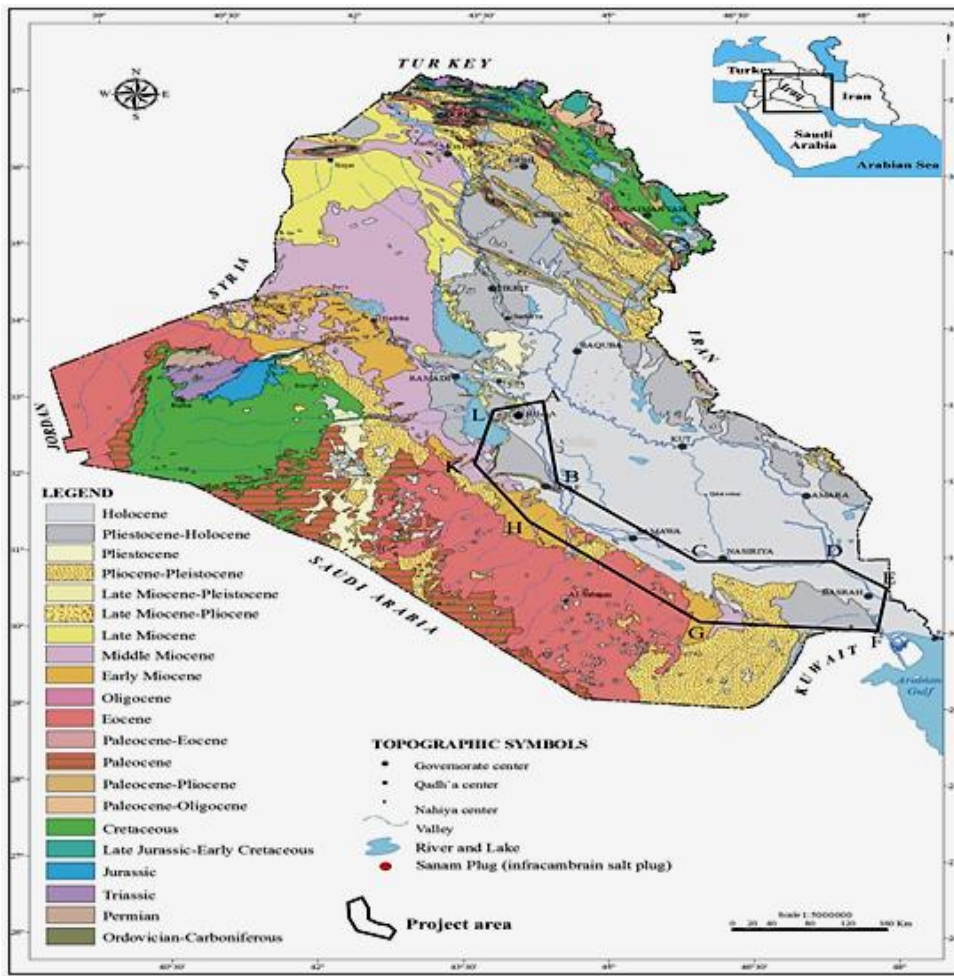


Fig. 1. Location map of the investigated area (Jassim and Gof, 2006).

According to the Table 1, the Mean (X) grain size after the Folk method is 1.479 ϕ that means the sample is medium sand. The dominant Kurtosis (K) characteristic is mesokurtic, the dominant Skewness (SK) corresponds to symmetrical, and Sorting (σ) to well sorted, all that signifying a long distance transport.

4.2. X-ray diffraction.

The samples were separated on grain size fractions. We analyzed every grain size fraction from each sample in order to identify the abundance of the heavy minerals. Heavy minerals were found in all the analyzed grain size fractions (very fine sand, fine sand, and medium sand) (Table 2). A large quantity of heavy minerals was found in the very fine sand fraction, where we could identify a high variability of them. Using X-ray diffraction on the fine fraction (63-125 μm), rutile, pyrope, spinel, zircon, ilmenite, and muscovite were identified.

4.3. Microscope analysis.

The microscopic observations consisted of three types of investigation: binocular magnifier, transmitted light and reflected light microscopy. The binocular microscope has been used to determine the roundness (rounded and sub-rounded, angular and sub-angular) and the shape of the granules: isometric, tabular, lamellar, cylindrical. The mineralogical composition consists of quartz, feldspar, carbonates, and heavy minerals (e.g. garnet, amphibole, zircon, and Fe and Ti oxides) (Plate I).

The microscopic observations in transmitted light (Plate II) allowed the identification of the clastic quartz grains, which in most of the cases have a wavy extinction, and the presence of the amphibole, biotite, and zircon, as well as rutile included in quartz.

Using the reflected light microscopy (Plate III) we identified two TiO_2 polymorphic minerals (rutile and anatase) as well as ilmenite, sometimes transformed in rutile, magnetite, and goethite. Note that anatase was often recognized under the microscope thanks to the whitish internal reflexes. Chromite was rarely observed.

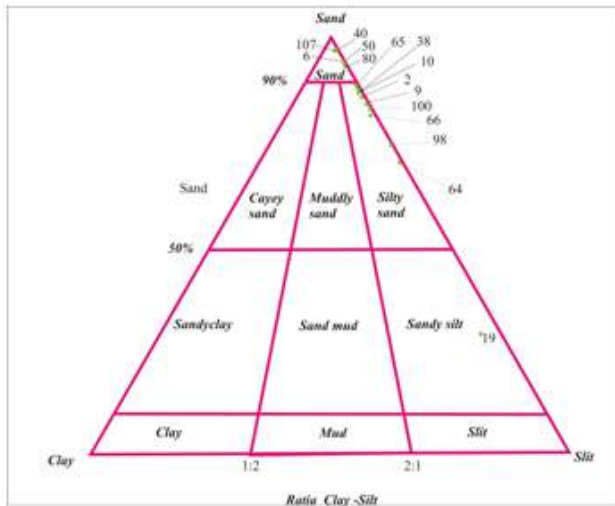


Fig. 2. Folk classification.

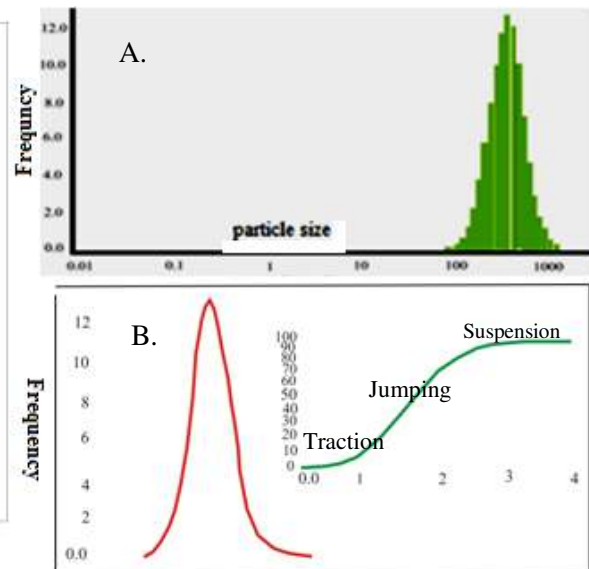


Fig. 3. A. granulometric distribution, and B. cumulative curve.

Table 1. Results of samples analysis by using Horiba LA-950 X-ray analyzer.

SAMPLE STATISTICS						
SAMPLE IDENTITY: H40			ANALYST & DATE: DD. 04.03.2015			
SAMPLE TYPE: Unimodal, Moderately Well Sorted			TEXTURAL GROUP: Sand			
SEDIMENT NAME: Moderately Well Sorted Medium Sand						
	μm	ϕ	GRAIN SIZE DISTRIBUTION			
MODE 1:	369,2	1,441	GRAVEL: 0,0%	COARSE SAND: 20,6%		
MODE 2:			SAND: 100,0%	MEDIUM SAND: 58,2%		
MODE 3:			MUD: 0,0%	FINE SAND: 19,0%		
D_{10} :	204,4	0,686		V FINE SAND: 1,1%		
MEDIAN or D_{50} :	361,6	1,467	V COARSE GRAVEL: 0,0%	V COARSE SILT: 0,0%		
D_{90} :	621,6	2,291	COARSE GRAVEL: 0,0%	COARSE SILT: 0,0%		
(D_{90} / D_{10}) :	3,041	3,339	MEDIUM GRAVEL: 0,0%	MEDIUM SILT: 0,0%		
$(D_{90} - D_{10})$:	417,2	1,605	FINE GRAVEL: 0,0%	FINE SILT: 0,0%		
(D_{75} / D_{25}) :	1,777	1,780	V FINE GRAVEL: 0,0%	V FINE SILT: 0,0%		
$(D_{75} - D_{25})$:	209,3	0,830	V COARSE SAND: 1,1%	CLAY: 0,0%		
	METHOD OF MOMENTS			FOLK & WARD METHOD		
	Arithmetic	Geometric	Logarithmic	Geometric	Logarithmic	Description
MEAN (\bar{x}):	395,1	358,5	1,480	358,7	1,479	Medium Sand
SORTING (σ):	179,3	1,548	0,631	1,642	0,625	Moderately Well So
SKEWNESS (SA):	1,371	-0,072	0,072	-0,021	0,021	Symmetrical
KURTOSIS (K):	5,889	3,144	3,144	1,032	1,032	Mesokurtic

Table 2. XRD results on the 63-125 μm fraction.

Samples	Enstatite	Lepidocrocite	Ilmenite	Muscovite	Pyrope	Rutile	Zircon	Samples	Epidote	Muscovite	Olivine	Rutile	Spinel	Titanite	Zircon
H93-1		+		+		+		H29-2			+				+
H59-1					+	+		H15-2		+					+
H89-2	+		+	+	+	+		H15-1						+	+
H103-2							+	H29-1				+	+		+
H89-3							+	H25-1	+	+					

4.4. X-ray fluorescence.

X-ray fluorescence was performed on polished sections, 10-11 points being measured on every section, for more reliable results. The geochemical similarities between the samples can be observed in Table 3. The elements with high concentration are Si, Fe, Ca, and K.

Table 3. X-ray fluorescence analyses (%) on polished section.

Sample No.H25												
Point	Mg	Al	Si	S	Cl	K	Ca	Ti	Mn	Fe	Sr	Zr
P1	0.47		46.83	1.40	1.20	2.19	34.19	0.96	0.16	12.27	0.32	
P2	0.94		44.32	2.07	1.31	2.38	38.69	0.77	0.33	8.92	0.28	
P3	12.05		46.36	0.61	0.87	1.67	28.33	0.72	0.15	8.98	0.26	
P4	1.02		42.38	0.81	1.46	2.21	37.55	1.16	0.17	12.94	0.31	
P5	1.30		60.40	0.37	0.76	1.73	22.25	0.69	0.23	11.80	0.22	0.25
P6	4.02	4.94	47.14	1.42	1.76	1.96	26.33	0.79	0.15	11.17	0.31	
P7	4.75	3.28	32.51	1.89	1.55	2.34	39.79	1.51	0.16	11.81	0.40	
P8	4.24	3.52	37.01	0.43	0.98	2.18	39.03	0.78	0.2	11.34	0.29	
P9	1.25		52.07	1.09	1.51	1.64	31.10	0.87	0.15	10.07	0.26	
P10	3.56	3.65	39.27	0.49	1.03	1.83	37.09	1.36	0.18	11.23	0.30	
P11	4.10	2.91	41.57	0.75	1.16	1.82	37.92	0.69	0.15	8.67	0.26	
total	37.7	18.30	489.86	11.33	13.59	21.95	372.27	10.30	2.03	119.2	3.21	0.25
rata	3.427	3.66	44.50	1.03	1.235	1.9955	33.84	0.94	0.18	10.836	0.292	0.25

Conclusions.

Samples from Quaternary deposits are similar from the standpoints of grain size and mineralogy. The samples are fine-medium sand and moderately well sorted. More heavy minerals were found in the fine fraction (63-125 μm). Skewness on sorting give us information about the type of sand (fluvial and aeolian) and the transport (on long distance) of the sand deposits. The mixed character of the source is observed, with the domination of the fluvial sand. Regarding the mineralogy of the samples, a notable variation of heavy minerals was observed, dominated by the presence of the iron and titanium oxides. The heavy minerals were transported from the source by the dominant airstreams in the desert environment, coming from the Arab shield, as well as the sand, transferred from the geological formations in the southwest and northwest of Iraq.

References.

- Al-Ani R.A. (1979) Sedimentology and geomorphology of sandstones of Najaf-Samawa- Nasriya area. M.Sc. thesis, University of Baghdad, Iraq, 202 p.
- Buday T. (1980) The regional geology of Iraq, stratigraphy and paleogeography. I. Daral Kutid Pub. House, Mousel, Iraq, 445 p.
- Jassim S.Z., Goff J.C. (2006) Geology of Iraq. Dolin, Prague and Moravian Museum, Brno, Czech Republic, 341 p.

Plate I.

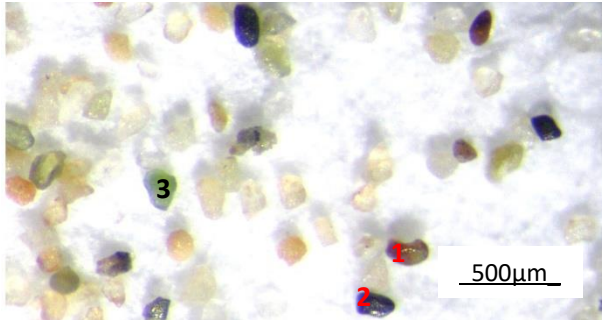
Binocular microscope images.



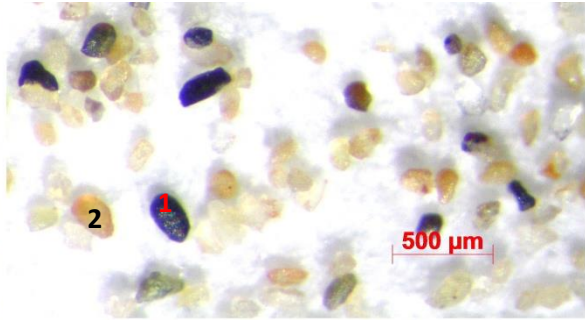
1. crystal of gypsum, 2. zircon.



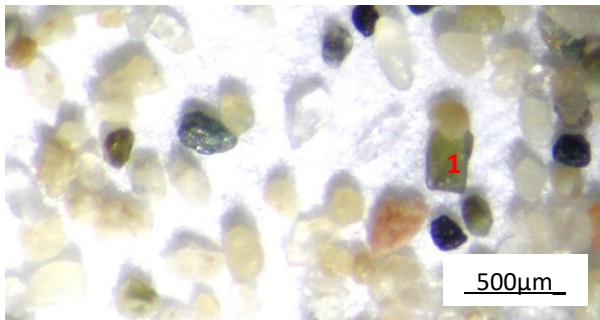
1. epidote, 2. ilmenite, 3. green garnet.



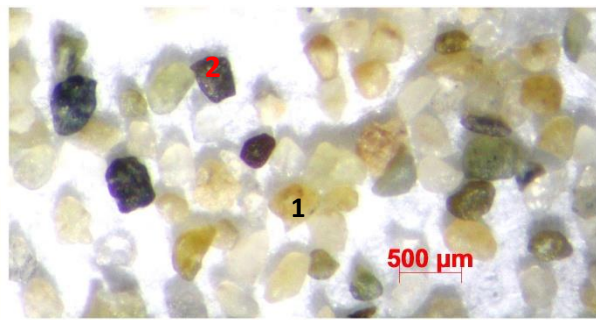
1. rutile, 2. zircon. 3. garnet.



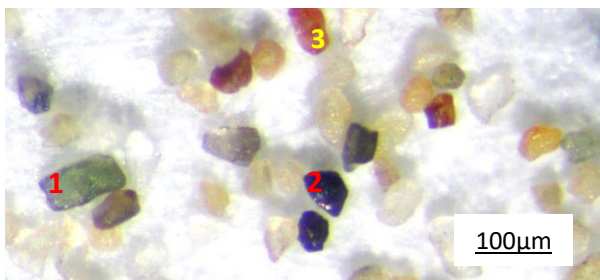
1. zircon, 2. rutile.



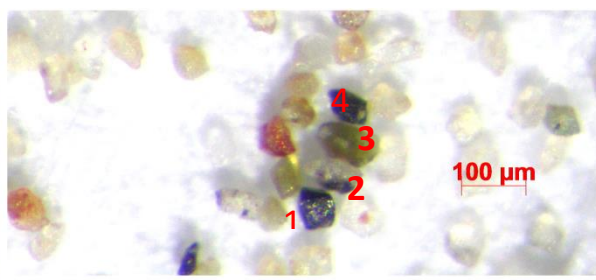
1. amphibole



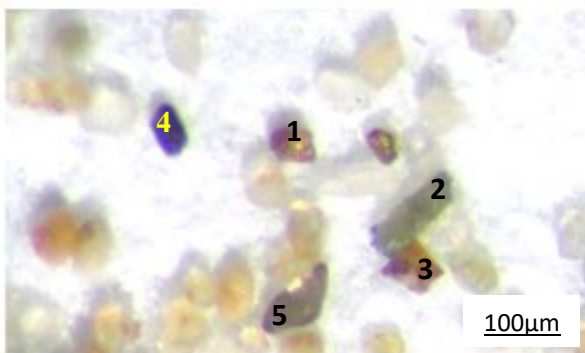
1. epidote, 2. hematite.



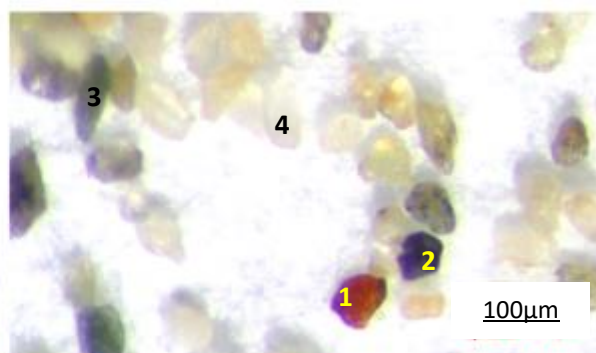
1. hornblende, 2. zircon, 3. rutile.



1. zircon, 2. garnet, 3. anatase, 4. hematite.



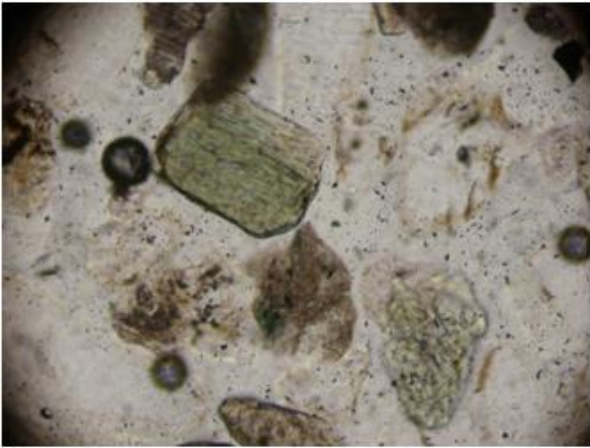
1. garnet, 2. hornblende, 3. garnet, 4. magnetite, 5. quartz.



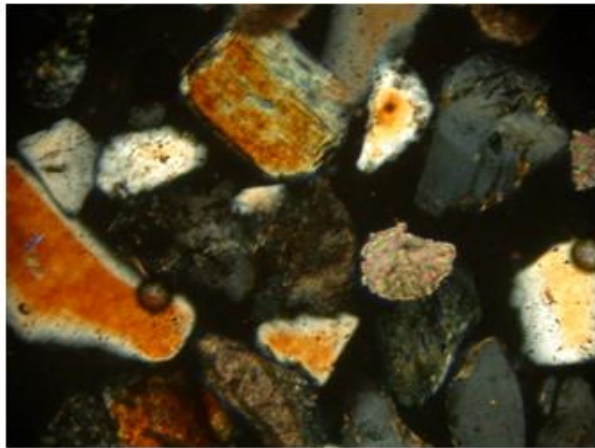
1. garnet, 2. hematite, 3. hornblende, 4. quartz.

Plate II.

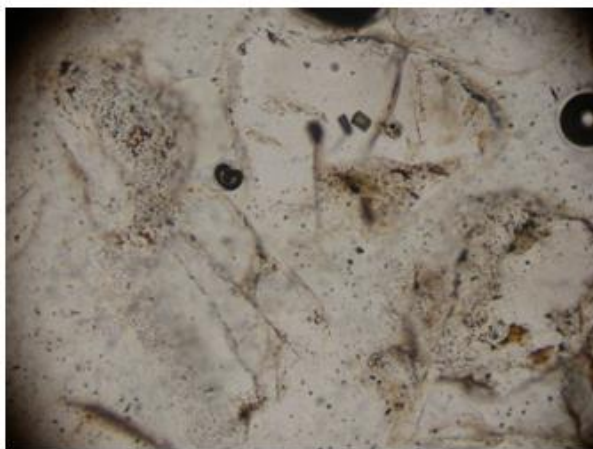
Microscopic images in transmitted light with N// and N+.



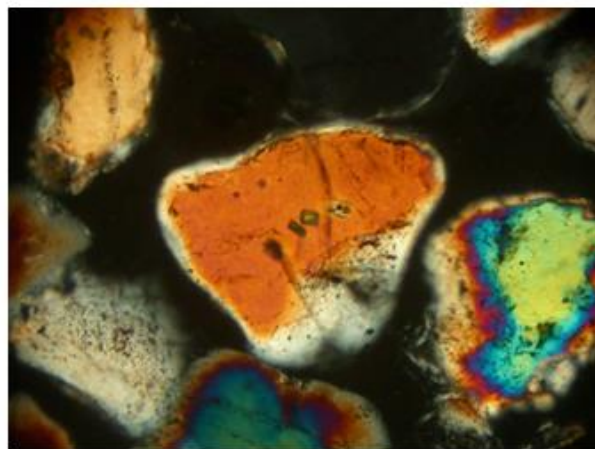
Amphibole; 35x, N//.



Same view, with N+.



Zircon inclusions in quartz; 35x, N//.



Same view, with N+.



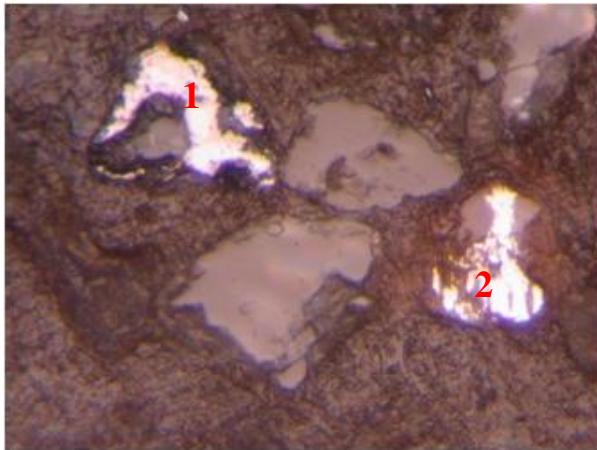
Biotite in quartz; 35x, N//.



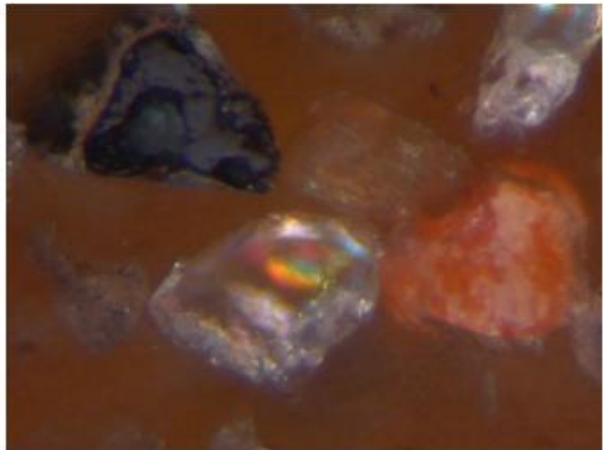
Same view, with N+.

Plate III.

Microscopic images in reflected light with N// and N+.



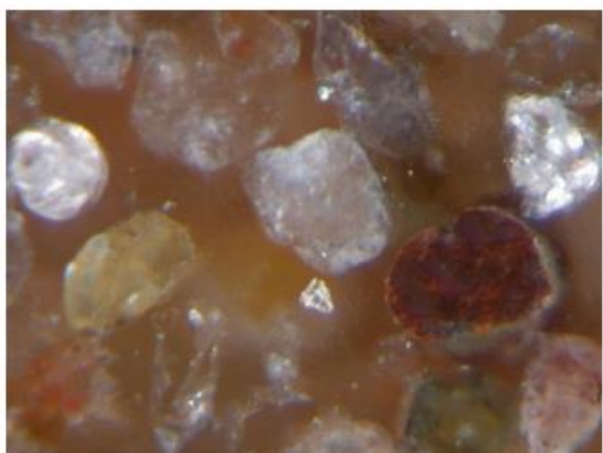
1. magnetite, 2. rutile; 60x, N//.



Same view, with N+.



1. anatase, 2. rutile; 60x, N//.



Same view, with N+.



Ilmenite; 60x, N//.



Same view, with N+.

